On the Divergence Constraint in Mixed Finite Element Methods for Incompressible Flows*

Volker John[†]
Alexander Linke[‡]
Christian Merdon[‡]
Michael Neilan[§]
Leo G. Rebholz[¶]

Abstract. The divergence constraint of the incompressible Navier–Stokes equations is revisited in the mixed finite element framework. While many stable and convergent mixed elements have been developed throughout the past four decades, most classical methods relax the divergence constraint and only enforce the condition discretely. As a result, these methods introduce a pressure-dependent consistency error which can potentially pollute the computed velocity. These methods are not robust in the sense that a contribution from the right-hand side, which influences only the pressure in the continuous equations, impacts both velocity and pressure in the discrete equations. This article reviews the theory and practical implications of relaxing the divergence constraint. Several approaches for improving the discrete mass balance or even for computing divergence-free solutions will be discussed: grad-div stabilization, higher order mixed methods derived on the basis of an exact de Rham complex, H(div)-conforming finite elements, and mixed methods with an appropriate reconstruction of the test functions. Numerical examples illustrate both the potential effects of using nonrobust discretizations and the improvements obtained by utilizing pressure-robust discretizations.

Key words. incompressible Navier–Stokes and Stokes equations, divergence-free properties, mixed finite elements, pressure-robust discretization

AMS subject classifications. $65N30,\,76M10$

DOI. 10.1137/15M1047696

Contents

The Navier-Stokes and the Stokes Equations, Goals, and Contents of the Review 493

^{*}Received by the editors November 9, 2015; accepted for publication (in revised form) August 1, 2016; published electronically August 7, 2017.

http://www.siam.org/journals/sirev/59-3/M104769.html

Funding: The work of the third author was supported in the framework of the project "Macroscopic Modeling of Transport and Reaction Processes Magnesium-Air-Batteries" (grant 03EK3027D) under the research initiative "Energy Storage" of the German Federal government. The work of the fourth author was partially supported by National Science Foundation grant DMS-1417980 and the Alfred Sloan Foundation. The work of the fifth author was partially supported by U.S. Army grant 65294-MA and National Science Foundation grant DMS-1522191.

[†]Weierstrass Institute for Applied Analysis and Stochastics, 10117 Berlin, Germany, and Freie Universität Berlin, Department of Mathematics and Computer Science, 14195 Berlin, Germany (john@wias-berlin.de).

[‡]Weierstrass Institute for Applied Analysis and Stochastics, 10117 Berlin, Germany (alexander. linke@wias-berlin.de, Christian.Merdon@wias-berlin.de).

[§]Department of Mathematics, University of Pittsburgh, Pittsburgh, PA (neilan@pitt.edu).

[¶]Department of Mathematical Sciences, Clemson University, Clemson, SC (rebholz@clemson.edu).

		DIVERGENCE-FREE CONSTRAINT IN MIXED METHODS	493			
	1.1 1.2 1.3 1.4	Examples That Demonstrate Difficulties of Standard Mixed Methods . Goals of the Review				
2	Variational Formulation, Helmholtz-Hodge Decomposition, and an Invariance Property 50					
3	The	Lack of Pressure-Robustness for Standard Mixed Methods	503			
4		Stability and Accuracy of Pressure-Robust Mixed Methods for the Stokes Equations	507 507 510 512 516			
5	5.1 5.2 5.3	Grad-div Stabilization	521 524 528			
6	Nur	merical Studies	528			
7	Out	look	540			
References						

I. The Navier–Stokes and the Stokes Equations, Goals, and Contents of the Review. The Navier–Stokes equations are a fundamental model of incompressible Newtonian flows. They are used to model flows in pipes and channels, flows around objects such as the wing of a plane, and weather and climate, to name just a few. Developed in the mid-19th century, these equations have garnered great interest from mathematicians, engineers, and scientists. In their simplest form, and assuming constant fluid density, the equations are given in a domain $\Omega \subset \mathbb{R}^d$, $d \in \{2,3\}$, and a time interval $(0,T), T < \infty$, by

(1.1a)
$$\partial_t \mathbf{u} - \nu \Delta \mathbf{u} + (\mathbf{u} \cdot \nabla) \mathbf{u} + \nabla p = \mathbf{f},$$
(1.1b)
$$\nabla \cdot \mathbf{u} = 0,$$

where \boldsymbol{u} denotes the velocity of the fluid, p denotes the pressure, and ν is the kinematic viscosity. The nonlinear term $\boldsymbol{u} \cdot \nabla \boldsymbol{u} = (\boldsymbol{u} \cdot \nabla) \boldsymbol{u}$ represents the inertial force, while the term with the Laplace operator $\Delta \boldsymbol{u} := \sum_{i=1}^d \partial_{ii} \boldsymbol{u}$ encodes the viscous effects of the fluid. The given function \boldsymbol{f} takes into account external forces, e.g., gravity, buoyancy, and centrifugal forces, and the divergence constraint $\nabla \cdot \boldsymbol{u} = 0$ represents the incompressibility of the fluid, or equivalently in this setting, the conservation of mass.

The fact that the Navier–Stokes equations are a constrained system of partial differential equations poses fundamental mathematical and numerical difficulties. A basic model for studying the impact of the divergence constraint is that of the steady-state (scaled) Stokes equations, given by

$$(1.2a) -\nu \Delta \boldsymbol{u} + \nabla p = \boldsymbol{f},$$

$$-\nabla \cdot \boldsymbol{u} = g,$$

(1.2c)
$$u|_{\partial\Omega} = 0$$
,

with the last equation representing no-slip boundary conditions. The divergence constraint $-\nabla \cdot \boldsymbol{u} = g$ originates, e.g., from transforming inhomogeneous Dirichlet boundary conditions to no-slip boundary conditions. One notes immediately that the analysis of the Stokes equations is simpler than that of the Navier–Stokes equations, since the Stokes equations form a linear system and are not time-dependent.

A main goal of this review is to highlight and elaborate a type of nonrobustness of many standard mixed finite element methods for the Stokes and Navier–Stokes equations. This nonrobustness is connected to the discretization of the divergence constraint (and not to the nonlinearity nor to dominating convection). The intended type of robustness is called pressure-robustness, which means that some mixed methods are robust with respect to large and complicated pressures and some are not. To avoid technicalities which do not concern the divergence constraint and its discretization, the numerical analysis presented in this article is limited to the Stokes equations. However, it is directly relevant to more complex systems, and the fundamental ideas presented herein for the Stokes equations are extendable. The numerical studies consider the Stokes and Navier–Stokes equations, and also multiphysics systems.

1.1. Examples That Demonstrate Difficulties of Standard Mixed Methods.

In what follows, three simple numerical examples are presented which illustrate the lack of pressure-robustness in the numerical simulation of incompressible flow problems with standard finite element methods. All simulations were performed on uniformly refined grids using classical pairs of mixed finite elements: the mini element proposed in [4], the Taylor–Hood element from [41], and the nonconforming Crouzeix–Raviart element [26].

Example 1.1. No-flow problem for the Stokes equations. Consider the Stokes equations with $\nu=1$ in $\Omega=(0,1)^2$, no-slip boundary conditions, the right-hand side $\mathbf{f}=(0,\operatorname{Ra}(1-y+3y^2))^T$, where $\operatorname{Ra}>0$ is a parameter, and g=0. One finds that $\mathbf{u}=\mathbf{0},\ p=\operatorname{Ra}(y^3-y^2/2+y-7/12)$ is the solution of this equation. Changing the parameter Ra in the right-hand side changes only the pressure. On the other hand, applying standard mixed finite element methods, one can also see an influence of this parameter on the discrete velocity; see Figure 1.1. For all considered pairs of finite element spaces, the Taylor–Hood space $\mathcal{P}_2/\mathcal{P}_1$, the mini element (not shown for the sake of brevity), and the nonconforming Crouzeix–Raviart space, the discrete velocity is far from being equal to zero, even for $\operatorname{Ra}=1$.

The impact on the discrete velocity of a term which only influences the pressure in the continuous case is one type of nonrobustness which is studied here. By the construction of this example, this lack of robustness cannot be due to dominating convection or to the nonlinearity of the problem. It is clarified in this review that this lack of robustness is connected with the discretization of the divergence-free constraint in mixed finite element methods. Based on a careful study of this issue, a remedy which removes this instability for the Crouzeix–Raviart pair of finite element spaces

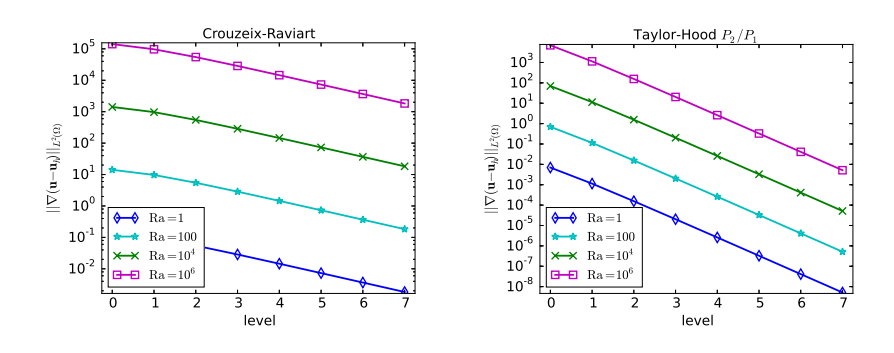


Fig. 1.1 Example 1.1. Velocity errors in the no-flow problem for the Stokes equations.

was proposed in [51]. The underlying idea of this remedy is explained in section 5.2 and the result of its application is shown in Example 6.1.

Example 1.2. Stationary vortex. Consider the Navier–Stokes equations (1.1) with $\nu = 1$ in $\Omega = (-1, 1)^2$ with the prescribed solution

$$\boldsymbol{u} = \begin{pmatrix} -y \\ x \end{pmatrix}, \quad p = \operatorname{Re}\left(\frac{x^2 + y^2}{2} - \frac{1}{3}\right), \quad \operatorname{Re} > 0,$$

and with Dirichlet boundary conditions. The flow field has the form of a vortex and a direct calculation shows that f = 0. Clearly, $\partial_t u = 0$ and $\Delta u = 0$. Hence, there is a balance of the nonlinear term of the Navier–Stokes equations and the pressure gradient.

In standard finite element error estimates, some norm of the solution appears on the right-hand side. In this example, one could think that the velocity errors are uniformly bounded since the velocity does not depend on Re. Instead, one observes in Figure 1.2 that the errors are proportional to Re, i.e., the velocity error has the same scaling as the pressure.

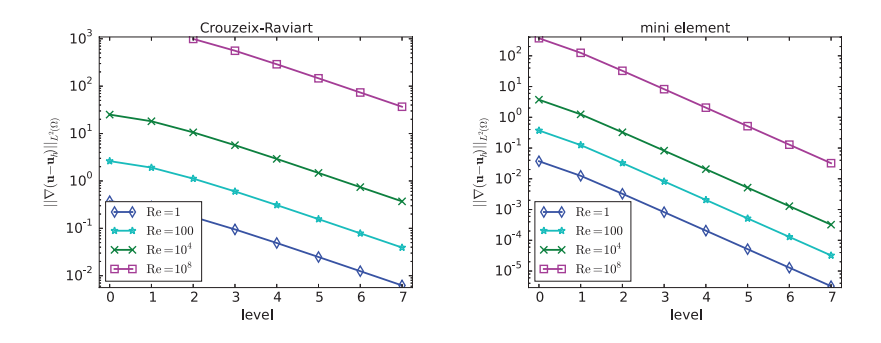


Fig. 1.2 Example 1.2. Velocity errors for the stationary vortex.

This example shows that there is a negative impact of the pressure on the discrete velocity. This influence is also a kind of non-pressure-robustness which by construction is not due to dominating convection. A remedy in the case of the Crouzeix–Raviart

finite element pair was proposed in [51]; see section 5.2 for the basic idea and Example 6.1 for numerical results.

Example 1.3. Flow with Coriolis force. In some applications, such as meteorology, the Coriolis force acting on the flow field is of the utmost importance. The Coriolis force is modeled with the additional term $2\boldsymbol{w}\times\boldsymbol{u}$ on the left-hand side of the moment balance of the Navier–Stokes equations (1.1), where \boldsymbol{w} is the vector of angular momentum.

Consider a flow field which is two-dimensional, that is, assume $\mathbf{u} = (u_1, u_2, 0)$, $\mathbf{w} = y(0, 0, \omega/2)^T$, $\omega \in \mathbb{R}$, and assume that none of the functions of the problem depends on the third coordinate. Then one obtains a two-dimensional model, similar to the Navier–Stokes equations. In this model, the left-hand side of (1.1) contains the additional term $\omega y(-u_2, u_1)^T$. The y-dependence of the Coriolis force models in meteorology a latitude-dependence in a so-called β -plane approximation [67]. Here, a part of the Earth's surface is approximated by a tangent plane and vertical velocities are neglected.

This problem is considered for the Navier–Stokes equations in $\Omega=(0,10)\times(0,1)$ with $\nu=1$ and the prescribed solution

$$oldsymbol{u} = egin{pmatrix} 1 \\ 0 \end{pmatrix}, \quad p = \omega \left(-rac{y^2}{2} + rac{1}{6}
ight) \quad \Longrightarrow \quad oldsymbol{f} = oldsymbol{0},$$

and with Dirichlet boundary conditions. In meteorology, this situation would model a constant ocean current from west to east. For this solution, the first three terms of the momentum balance of the Navier–Stokes equations (1.1) vanish, while ∇p is balanced by the additional Coriolis force $2\boldsymbol{w}\times\boldsymbol{u}$.

Once again this is a problem where in the continuous setting the velocity does not depend on the parameter ω , but the pressure does. The numerical results presented in Figure 1.3 show that this property is not inherited by standard pairs of mixed finite elements. The discrete velocity depends on ω and the error scales linearly with this parameter, i.e., it scales the same way as the pressure.

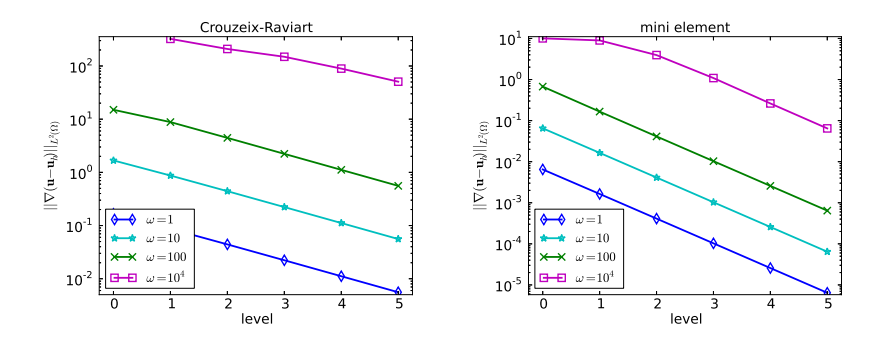


Fig. 1.3 Example 1.3. Velocity errors for the flow with Coriolis force.

1.2. Goals of the Review. A pressure-robust method in the sense studied in this review is a method for which modifications of the continuous problem that only affect the pressure lead to changes in the discrete solution that only affect the discrete pressure. Otherwise, the method is said to be non-pressure-robust. In Examples 1.1–1.3

it was shown that for non-pressure-robust methods there might be a large impact on the discrete velocity from modifications that only affect the pressure in the continuous equations.

Two fundamental observations concerning the Stokes (1.2) and Navier–Stokes equations (1.1) can be made immediately:

1. For solutions to exist, the divergence operator must possess a certain surjectivity property, the fundamental inf-sup compatibility condition: There exists a constant β such that

(1.3)
$$\inf_{q \in L_0^2(\Omega) \setminus \{0\}} \sup_{\boldsymbol{v} \in \boldsymbol{H}_0^1(\Omega) \setminus \{\boldsymbol{0}\}} \frac{(\nabla \cdot \boldsymbol{v}, q)}{\|\nabla \boldsymbol{v}\|_{L^2(\Omega)} \|q\|_{L^2(\Omega)}} \ge \beta > 0.$$

Otherwise, the constraint $-\nabla \cdot \boldsymbol{u} = q$ cannot hold.

2. A fundamental invariance property holds: Changing the external force by a gradient field changes only the pressure solution, and not the velocity; in symbols,

(1.4)
$$f \to f + \nabla \psi \implies (u, p) \to (u, p + \psi),$$

since the additional force field $\nabla \phi$ is balanced by the pressure gradient, and the no-slip boundary conditions do not involve the pressure.

These issues not only affect the continuous equations, but also their discretizations. In this review, the effect of the second observation on mixed finite element discretizations will be elaborated upon. Discretizations that contain a stabilization with respect to the discrete inf-sup condition, e.g., the pressure-stabilized Petrov–Galerkin (PSPG) method [42], are not considered in this review.

The significance of the first observation is well known and forms a cornerstone of numerical analysis for the Stokes and Navier—Stokes equations. It comprises the fundamental finding that numerical schemes for approximating the Stokes and Navier—Stokes equations should satisfy a certain compatibility criterion between the discrete velocity and pressure spaces, in order to fulfill an appropriate surjectivity of the discrete divergence operator: the so-called discrete inf-sup stability. The need for discrete inf-sup stability results from the fact that the discrete velocity trial functions are constrained. The great practical value of discrete inf-sup stability is that it provides a recipe for the construction of well-posed discretization schemes, whose solutions have (asymptotically) optimal convergence rates.

The significance of the second observation for the discretization of the Navier–Stokes equations has only recently begun to be realized [35]. As is explained in detail in section 4.2, the discrete divergence constraint induces a discrete rotation operator via the velocity test functions, since divergence-free vector test functions have a vector potential. Therefore, in every mixed finite element discretization for the Stokes problem (1.2) a discrete vorticity equation is hidden. For discretization schemes satisfying (1.4) it holds exactly that $\nabla \times \nabla \psi \equiv 0$ for any differentiable ψ . However, classical mixed methods, which satisfy the discrete inf-sup condition, satisfy $\nabla \times \nabla \psi \equiv 0$ only approximately, up to some order of accuracy. In addition, (1.4) can be explained using the Helmholtz–Hodge projection (see section 2), which is mathematically more rigorous.

The violation of (1.4) by a discretization might have severe consequences.

• As is discussed in section 3, the violation of (1.4) results in finite element error bounds for the velocity which depend on the pressure. Thus, large pressures may lead to large velocity errors, which has already been observed

- in Examples 1.1–1.3. Indeed, there are important applications, e.g., natural convection problems, where the pressure is larger than the velocity by orders of magnitude. In such situations, one cannot expect to compute accurate velocity fields with classical mixed methods, at least for low order methods.
- In the case $\nabla \cdot \boldsymbol{u} = 0$, one often expects in applications that the discrete computed velocity field is also divergence-free. Otherwise, the conservation of mass is violated. A violation of this conservation law is not tolerable in many applications.

It turns out that so-called divergence-free mixed methods, i.e., methods whose discrete velocity u_h is in a sufficiently strong sense divergence-free (or in the general case $\nabla \cdot u_h = g$ in a sufficiently strong sense), satisfy (1.4) and thus belong to the class of pressure-robust methods.

Another main goal is to review the construction of pressure-robust mixed methods that satisfy simultaneously the discrete inf-sup stability and (1.4). In the last decade, tremendous progress has been made in approaching this goal, though seemingly it was believed for more than thirty years that it would be (practically) impossible to construct such schemes. Indeed, the first pressure-robust mixed method on three-dimensional tetrahedral grids was published only recently in 2005 [80]. Pressure-robust mixed methods in two dimensions reach back to 1983 [75], although they were rarely used in practice. Nowadays, three different approaches exist for the construction of pressure-robust mixed methods.

- The first approach, which is the most classical, constructs divergence-free mixed Galerkin schemes such that the discrete velocity is H^1 -conforming and divergence-free. Here, novel ideas from the finite element exterior calculus have delivered a tremendous breakthrough; see section 4.3.
- The second approach is due to recent discontinuous Galerkin (DG) methods. Here, novel mixed schemes for (1.2) look for divergence-free, H(div)-conforming velocities; see section 4.4. This regularity suffices to assure (1.4). Due to the relaxation of the H^1 -conformity of the velocity, the tangential velocity components are discretized in the DG framework.
- The third approach is very recent and is based on the observation that velocity trial and velocity test functions play a different role in order to guarantee discrete inf-sup stability and (1.4); see section 5.2. Therefore, the resulting schemes are not of Galerkin type. For (1.2) a variational crime in the right-hand side of the momentum balance is applied, in order to replace discretely divergence-free velocity test functions by divergence-free ones. In the case of the Navier–Stokes equations, the variational crime must also be applied to the test function of the convective term, and if a Coriolis force term is present, also to this term.

In addition, an approach for improving the pressure-robustness of classical mixed methods, the so-called grad-div stabilization, is presented in section 5.1.

1.3. Outline of the Review. An outline of this review article is now given, followed by a list of notation. To focus on the goals of the review and to avoid technical details, the review will concentrate on the Stokes equations (1.2).

Section 2 recalls the variational formulation of the Stokes equations and presents the fundamental associated results. The momentum balance is discussed in detail, as is the invariance property that "changes to the irrotational part of the forcing only affect the pressure and do not alter the velocity." The standard mixed finite element method for Stokes is given in section 3, along with results for well-posedness

under an inf-sup condition and a general error estimate. It is discussed that common element choices only enforce the divergence constraint discretely, and that this leads to pressure-dependent error estimates for the velocity.

Section 4 discusses pressure-robust mixed finite element methods for the Stokes equations. In particular, it is shown that for special element choices, the divergence constraint is enforced exactly and the velocity error does not depend on the pressure. Such methods are deemed pressure-robust mixed methods in this article, as this property does not hold in most commonly used elements. Discrete invariance properties which are analogues of those found at the continuous level are also discussed, and it is shown that they hold for pressure-robust mixed methods. A detailed description is then given of the de Rham complex, which is a tool to develop pressure-robust mixed methods. The section is concluded with a discussion of (nonconforming) H(div) mixed methods and how they can be used in a pressure-robust way.

The focus of section 5 is on techniques that improve, or even fix, standard (non-pressure-robust) mixed methods. The topics discussed are grad-div stabilization and appropriate modification of test functions, which all serve the purpose of reducing or eliminating the pressure from the velocity error. Moreover, a kind of postprocessing approach is discussed that produces divergence-free H(div)-conforming velocities from discretely divergence-free velocity fields. Such postprocessing is related to the discussed modification of test functions, and it is interesting for the discretization of tracers described by convection-diffusion equations; see, e.g., [33]. Results and discussion for several numerical studies presented are given in section 6. The aim of this section is to show the types of problems for which the methods discussed in this article can make a significant improvement in solution accuracy, as well as problems where they do not make a difference.

1.4. Nomenclature. Throughout this review, standard notation will be used for function spaces.

velocity-velocity bilinear form	$b(\cdot,\cdot)$	velocity-pressure bilinear form
Fortin operator constant	C_P	constant in Poincaré's estimate
vector curl operator	div	divergence operator
gradient operator	β	continuous inf-sup constant
discrete inf-sup constant	Ra	Rayleigh number
triangulation of Ω	Re	Reynolds number
set of edges of \mathcal{T}_h	γ	parameter in grad-div
		stabilization
mesh cell of \mathcal{T}_h	ν	kinematic viscosity
mesh cell of \mathcal{E}_h	f	body force
right-hand side of continuity	h	maximal value of h_T for given
equation		mesh
diameter of T	\mathbf{n}	outward unit normal to $\partial\Omega$
outward unit normal to T	$\mathbb{P}(\cdot)$	Helmholtz-Hodge projector
pressure	p_h	finite element pressure
space of globally continuous	${m \mathcal{P}}_k$	space of globally continuous
scalar-valued piecewise		vector-valued piecewise
polynomials of degree not		polynomials of degree not
exceeding k		exceeding k
velocity	\boldsymbol{u}_h	finite element velocity
set of vertices of \mathfrak{T}_h	\boldsymbol{W}_h	nonconforming finite element
		velocity space
velocity space, $\boldsymbol{H}_0^1(\Omega)$	\boldsymbol{X}_h	conforming finite element
		velocity space
	Fortin operator constant vector curl operator gradient operator discrete inf-sup constant triangulation of Ω set of edges of \mathcal{T}_h mesh cell of \mathcal{E}_h right-hand side of continuity equation diameter of T outward unit normal to T pressure space of globally continuous scalar-valued piecewise polynomials of degree not exceeding k velocity set of vertices of \mathcal{T}_h	Fortin operator constant vector curl operator div gradient operator β div gradient operator β discrete inf-sup constant Ra triangulation of Ω Re set of edges of \mathfrak{I}_h γ mesh cell of \mathfrak{E}_h f right-hand side of continuity equation diameter of T noutward unit normal to T pressure space of globally continuous scalar-valued piecewise polynomials of degree not exceeding k velocity \mathbf{I}_h

$oldsymbol{X}_{ ext{div}}$	subspace of X , containing the weakly divergence-free	$oldsymbol{X}_{h, ext{div}}$	space of discretely divergence-free functions
	functions		
$\boldsymbol{X}_{h,\mathrm{div}}(g)$	manifold of functions with	Y	pressure space, $L_0^2(\Omega)$
	divergence equal to g		
Y_h	finite element pressure space	π_F	Fortin operator
π	L^2 -projection to some space	Ω	domain
ω	vorticity	$\partial\Omega$	boundary of Ω
$ abla \cdot_h$	discrete divergence operator	$\left[\left \cdot\right \right]_{\tau}$	jump across edges/faces in two
			or three dimensions

2. Variational Formulation, Helmholtz-Hodge Decomposition, and an Invariance Property. In this section, the variational formulation of the Stokes problem is introduced, and the Helmholtz projector is discussed and its significance is emphasized for the (Navier-)Stokes momentum balance. The Helmholtz projector is of central importance for understanding the results obtained with mixed finite element methods, yet is generally not emphasized in the numerical analysis literature, or only in a posteriori error control [1, 21].

Let Ω be a bounded domain with polyhedral and Lipschitz continuous boundary and let $\mathbf{f} \in \mathbf{L}^2(\Omega)$ and $g \in L^2(\Omega)$. A weak solution to the incompressible Stokes equations (1.2) is defined as a pair $(\mathbf{u}, p) \in \mathbf{X} \times Y := \mathbf{H}_0^1(\Omega) \cap L_0^2(\Omega)$ satisfying

(2.1a)
$$a(\boldsymbol{u}, \boldsymbol{v}) + b(\boldsymbol{v}, p) = (\boldsymbol{f}, \boldsymbol{v}) \quad \forall \boldsymbol{v} \in \boldsymbol{X},$$

$$(2.1b) b(\boldsymbol{u}, q) = (q, q) \forall q \in Y,$$

where $L_0^2(\Omega)$ is the space of square integrable functions with vanishing mean. The bilinear forms are given by $a(\boldsymbol{w}, \boldsymbol{v}) = \nu(\nabla \boldsymbol{w}, \nabla \boldsymbol{v})$ and $b(\boldsymbol{v}, q) = -(\nabla \cdot \boldsymbol{v}, q)$, and (\cdot, \cdot) denotes the L^2 inner product over Ω . Note that vector-valued functions and vector-valued function spaces are denoted in boldface, e.g., $\boldsymbol{H}_0^1(\Omega) = (H_0^1(\Omega))^d$.

To analyze (2.1), the following partial integration formula for the divergence is recalled which allows the introduction of a distributional divergence and a weak divergence.

LEMMA 2.1. For all $\psi \in H^1(\Omega)$ and $\mathbf{w} \in \mathbf{H}^1(\Omega)$ there holds

$$\int_{\Omega} \psi \nabla \cdot \boldsymbol{w} \, d\boldsymbol{x} = - \int_{\Omega} \nabla \psi \cdot \boldsymbol{w} \, d\boldsymbol{x} + \int_{\partial \Omega} \psi \boldsymbol{w} \cdot \boldsymbol{n} \, d\mathbf{s}.$$

The surface integral is understood as a duality pairing between the spaces $H^{\frac{1}{2}}(\partial\Omega)$ and $H^{-\frac{1}{2}}(\partial\Omega)$.

Proof. For smooth functions $\psi \in C^{\infty}(\Omega)$ and $\boldsymbol{w} \in \boldsymbol{C}^{\infty}(\Omega)$, the proof is a direct consequence of the vector calculus identity $\nabla \cdot (\psi \boldsymbol{w}) = \psi \nabla \cdot \boldsymbol{w} + \nabla \psi \cdot \boldsymbol{w}$ and the divergence theorem (integration by parts of the divergence term). Using the density of $C^{\infty}(\Omega)$ and $\boldsymbol{C}^{\infty}(\Omega)$ in $H^{1}(\Omega)$ and $\boldsymbol{H}^{1}(\Omega)$, respectively, gives the statement of the lemma.

This lemma motivates the introduction of the notion of a distributional divergence.

Definition 2.2. For a vector field $\mathbf{w} \in \mathbf{L}^1(\Omega)$ the mapping $C_0^{\infty}(\Omega) \to \mathbb{R}$ given by

$$\psi \mapsto -\int_{\Omega} \nabla \psi \cdot \boldsymbol{w} \, d\boldsymbol{x}$$

is called the distributional divergence of w.

The weak divergence is defined in the usual way of defining weak derivatives.

DEFINITION 2.3. If for a vector field $\mathbf{w} \in \mathbf{L}^p(\Omega)$ with $p \geq 1$ there exists a function $\rho \in L^1_{loc}(\Omega)$ such that the distributional divergence can be represented in the form

$$-\int_{\Omega} \nabla \psi \cdot \boldsymbol{w} \, d\boldsymbol{x} = \int_{\Omega} \psi \rho \, d\boldsymbol{x} \quad \forall \ \psi \in C_0^{\infty}(\Omega),$$

the function ρ is called the weak divergence of \mathbf{w} , abbreviated as $\rho := \nabla \cdot \mathbf{w}$. In particular, for divergence-free vector fields \mathbf{w} there holds

(2.2)
$$\int_{\Omega} \nabla \psi \cdot \boldsymbol{w} \, d\boldsymbol{x} = 0 \quad \forall \ \psi \in C_0^{\infty}(\Omega).$$

Remark 2.4. Loosely speaking, divergence-free vector fields are characterized by the fact that they are orthogonal in the $L^2(\Omega)$ scalar product to all gradient fields (with compact support). Classical mixed methods, whose construction is guided by the discrete inf-sup condition (3.2), usually violate this essential property. Its violation might lead to the lack of pressure-robustness as demonstrated in Examples 1.1–1.3.

Considering in the divergence constraint (2.1b) a test function $q \in Y \cap C_0^{\infty}(\Omega)$, one obtains with the divergence theorem

$$\int_{\Omega} \nabla q \cdot \boldsymbol{u} \, d\boldsymbol{x} = \int_{\Omega} qg \, d\boldsymbol{x}.$$

Following Definition 2.3, -g is the weak divergence of \boldsymbol{u} . This statement can be made more precise. Since \boldsymbol{u} satisfies no-slip boundary conditions, one finds by the divergence theorem that $0 = \int_{\partial\Omega} \boldsymbol{u} \cdot \mathbf{n} \ d\mathbf{s} = \int_{\Omega} \nabla \cdot \boldsymbol{u} \ d\boldsymbol{x}$. Combining this identity with $\boldsymbol{u} \in \boldsymbol{H}^1(\Omega)$ implies that $\nabla \cdot \boldsymbol{u} \in Y$. Hence, one can choose $q = \nabla \cdot \boldsymbol{u} - g$ in (2.1b), such that

Thus, $\nabla \cdot \boldsymbol{u} = -q$ in the sense of $L^2(\Omega)$.

Definition 2.5. The Hilbert space of vector fields that possess a weak divergence is defined by

(2.4)
$$\boldsymbol{H}(\operatorname{div},\Omega) := \{ \boldsymbol{w} \in \boldsymbol{L}^2(\Omega) : \nabla \cdot \boldsymbol{w} \in L^2(\Omega) \}.$$

Here, $\nabla \cdot \boldsymbol{w}$ is understood in the sense of Definition 2.3.

Note that Lemma 2.1 is valid also for functions $\mathbf{w} \in \mathbf{H}(\text{div}, \Omega)$.

These definitions and lemmas allow us to prove the Helmholtz–Hodge decomposition, a fundamental result for understanding the lack of pressure-robustness in classical mixed methods.

LEMMA 2.6 (Helmholtz-Hodge decomposition). Let Ω be a connected domain. For every vector field $\mathbf{f} \in \mathbf{L}^2(\Omega)$, there exist a vector field $\mathbf{f}_0 \in \mathbf{H}(\operatorname{div}, \Omega)$ and a scalar function $\phi \in H^1(\Omega)/\mathbb{R}$ with

- 1. $\mathbf{f} = \mathbf{f}_0 + \nabla \phi$,
- $2. \ \nabla \cdot \boldsymbol{f}_0 = 0,$
- 3. $(\boldsymbol{f}_0, \nabla \psi) = 0$ for all $\psi \in H^1(\Omega)$.

The decomposition is unique.

Proof. The following Neumann problem is well posed [36, p. 40]: find $\phi \in H^1(\Omega)/\mathbb{R}$ such that

(2.5)
$$(\nabla \phi, \nabla \psi) = (\mathbf{f}, \nabla \psi) \quad \forall \ \psi \in H^1(\Omega)/\mathbb{R}.$$

Since $\mathbf{f} \in \mathbf{L}^2(\Omega)$ and $\phi \in H^1(\Omega)$, it follows that $\mathbf{f}_0 := \mathbf{f} - \nabla \phi$ is in $\mathbf{L}^2(\Omega)$. By construction, it holds that

$$(2.6) (f_0, \nabla \psi) = 0 \forall \ \psi \in H^1(\Omega)/\mathbb{R}.$$

Since $C_0^{\infty}(\Omega)/\mathbb{R} \subset H^1(\Omega)/\mathbb{R}$, it follows that \boldsymbol{f}_0 is weakly divergence-free in the sense of Definition 2.3. In particular, $\nabla \cdot \boldsymbol{f}_0 = 0 \in L^2(\Omega)$ so that $\boldsymbol{f}_0 \in \boldsymbol{H}(\operatorname{div},\Omega)$. Equation (2.6) gives the third property stated in the lemma. With a proof by contradiction, the uniqueness of the decomposition follows in a straightforward manner using the third property.

DEFINITION 2.7 (Helmholtz-Hodge projector). The function $f_0 =: \mathbb{P}(f)$ is called the Helmholtz-Hodge projector of f.

Using the Helmholtz–Hodge projector, the following existence, uniqueness, and stability estimates can be derived.

LEMMA 2.8. Let $\mathbf{f} \in \mathbf{L}^2(\Omega)$ and $g \in Y$. Then the Stokes problem (2.1) has a unique solution for which the following stability estimates hold:

(2.7a)
$$\|\nabla u\|_{L^{2}(\Omega)} \leq \frac{C_{P}}{\nu} \|\mathbb{P}(f)\|_{L^{2}(\Omega)} + \frac{1}{\beta} \|g\|_{L^{2}(\Omega)},$$

(2.7b)
$$||p||_{L^{2}(\Omega)} \leq \frac{C_{P}}{\beta} ||f||_{L^{2}(\Omega)} + \frac{\nu}{\beta^{2}} ||g||_{L^{2}(\Omega)},$$

where β is the inf-sup constant defined in (1.3).

Proof. Assume that there is a velocity solution $u \in X$. Define the divergence-free subspace

$$X_{\text{div}} := \{ \boldsymbol{v} \in \boldsymbol{X} : b(\boldsymbol{v}, q) = 0 \ \forall \ q \in Y \}.$$

Then \boldsymbol{u} can be orthogonally decomposed $\boldsymbol{u}=\boldsymbol{u}^0+\boldsymbol{u}^\perp$ with respect to the scalar product $a(\cdot,\cdot)$ with $\boldsymbol{u}^0\in\boldsymbol{X}_{\mathrm{div}}$ and $\boldsymbol{u}^\perp\in\boldsymbol{X}_{\mathrm{div}}^\perp$. It will be shown that both parts of this decomposition exist and are uniquely defined. Hence, \boldsymbol{u} also exists and is unique.

Due to the continuous inf-sup condition, the divergence operator is bijective from $\boldsymbol{X}_{\mathrm{div}}^{\perp}$ to Y. Thus, there exists a unique $\boldsymbol{w}^{\perp} \in \boldsymbol{X}_{\mathrm{div}}^{\perp}$ with $-\nabla \cdot \boldsymbol{w}^{\perp} = g$ and $\|\nabla \boldsymbol{w}^{\perp}\|_{L^{2}(\Omega)} \leq \frac{1}{\beta} \|g\|_{L^{2}(\Omega)}$. Since $\nabla \cdot \boldsymbol{u} = \nabla \cdot \boldsymbol{u}^{\perp}$, condition (2.1b) enforces $\boldsymbol{u}^{\perp} = \boldsymbol{w}^{\perp}$. Consequently, \boldsymbol{u}^{\perp} is uniquely given and

(2.8)
$$\|\nabla u^{\perp}\|_{L^{2}(\Omega)} \leq \frac{1}{\beta} \|g\|_{L^{2}(\Omega)}.$$

The divergence-free part u^0 is determined by testing (2.1a) with an arbitrary divergence-free function $v^0 \in X_{\text{div}}$. One obtains, using on the left-hand side the a-orthogonality and on the right-hand side the L^2 -orthogonality against X_{div} ,

$$(2.9) a(\boldsymbol{u}, \boldsymbol{v}^0) + b(p, \boldsymbol{v}^0) = (\boldsymbol{f}, \boldsymbol{v}^0) \iff a(\boldsymbol{u}^0, \boldsymbol{v}^0) = (\mathbb{P}(\boldsymbol{f}), \boldsymbol{v}^0).$$

Applying the Lax-Milgram theorem, it follows that u^0 is uniquely defined due to the coercivity of $a(\cdot,\cdot)$. The Cauchy-Schwarz inequality and Poincaré's inequality for

 $\boldsymbol{v}^0 = \boldsymbol{u}^0$ yield

$$\nu \|\nabla \boldsymbol{u}^0\|_{L^2(\Omega)}^2 \leq \|\mathbb{P}(\boldsymbol{f})\|_{L^2(\Omega)} \|\boldsymbol{u}^0\|_{L^2(\Omega)} \leq C_P \|\mathbb{P}(\boldsymbol{f})\|_{L^2(\Omega)} \|\nabla \boldsymbol{u}^0\|_{L^2(\Omega)}.$$

Division by $\|\nabla u^0\|_{L^2(\Omega)}$, the decomposition of u, and estimate (2.8) give (2.7a).

The pressure p is now obtained by testing (2.1a) with arbitrary functions $v^{\perp} \in X_{\text{div}}^{\perp}$, yielding

$$(2.10) \quad a(\boldsymbol{u}, \boldsymbol{v}^{\perp}) + b(p, \boldsymbol{v}^{\perp}) = (\boldsymbol{f}, \boldsymbol{v}^{\perp}) \quad \Longleftrightarrow \quad (p, \nabla \cdot \boldsymbol{v}^{\perp}) = -(\boldsymbol{f}, \boldsymbol{v}^{\perp}) + a(\boldsymbol{u}^{\perp}, \boldsymbol{v}^{\perp}).$$

Again, since $\nabla \cdot : \boldsymbol{X}_{\text{div}}^{\perp} \to Y$ is a bijection, p is uniquely determined by (2.10). For proving the stability estimate of the pressure, one chooses the unique $\boldsymbol{v}_p \in \boldsymbol{X}_{\text{div}}^{\perp}$ such that $\nabla \cdot \boldsymbol{v}_p = p$ and $\|\nabla \boldsymbol{v}_p\|_{L^2(\Omega)} \leq \frac{1}{\beta} \|p\|_{L^2(\Omega)}$ hold. Inserting \boldsymbol{v}_p into (2.10), and using the Cauchy–Schwarz and Poincaré estimates and (2.8), yields

$$||p||_{L^{2}(\Omega)}^{2} \leq C_{P} ||\mathbf{f}||_{L^{2}(\Omega)} ||\nabla \mathbf{v}_{p}||_{L^{2}(\Omega)} + \nu ||\nabla \mathbf{u}^{\perp}||_{L^{2}(\Omega)} ||\nabla \mathbf{v}_{p}||_{L^{2}(\Omega)}$$

$$\leq \frac{C_{P}}{\beta} ||\mathbf{f}||_{L^{2}(\Omega)} ||p||_{L^{2}(\Omega)} + \frac{\nu}{\beta^{2}} ||g||_{L^{2}(\Omega)} ||p||_{L^{2}(\Omega)},$$

which proves (2.7b).

The Helmholtz–Hodge projector allows us to justify the fundamental invariance property (1.4) in a mathematically rigorous way. First, the following corollary is proved.

COROLLARY 2.9. The Helmholtz projector $\mathbb{P}(\nabla \phi)$ of a gradient field $\nabla \phi$ with $\phi \in H^1(\Omega)/\mathbb{R}$ vanishes, i.e., $\mathbb{P}(\nabla \phi) = \mathbf{0}$.

Proof. Taking $f = \nabla \phi$, it follows from the first property given in Lemma 2.6 and the uniqueness of the Helmholtz–Hodge decomposition that $f_0 = \mathbf{0}$ and consequently $\mathbb{P}(f) = \mathbb{P}(\nabla \phi) = \mathbf{0}$.

LEMMA 2.10. Let $\mathbf{f} \in \mathbf{L}^2(\Omega)$; then it holds for the Stokes problem (2.1) that changing the right-hand side by $\mathbf{f} \to \mathbf{f} + \nabla \psi$, with $\psi \in H^1(\Omega)/\mathbb{R}$, leads to a change in the solution by $(\mathbf{u}, p) \to (\mathbf{u}, p + \psi)$.

Proof. Let the Stokes solutions for the forcings \boldsymbol{f} and $\boldsymbol{f} + \nabla \psi$ be denoted by (\boldsymbol{u},p) and $(\boldsymbol{u}_{\psi},p_{\psi})$, respectively. Both solutions are decomposed, $\boldsymbol{u} = \boldsymbol{u}^0 + \boldsymbol{u}^{\perp}$ and $\boldsymbol{u}_{\psi} = \boldsymbol{u}_{\psi}^0 + \boldsymbol{u}_{\psi}^{\perp}$ with \boldsymbol{u}^0 , $\boldsymbol{u}_{\psi}^0 \in \boldsymbol{X}_{\text{div}}$ and \boldsymbol{u}^{\perp} , $\boldsymbol{u}_{\psi}^{\perp} \in \boldsymbol{X}_{\text{div}}^{\perp}$. Since (2.1b) is satisfied in both cases, it follows that $b(\boldsymbol{u}^{\perp} - \boldsymbol{u}_{\psi}^{\perp}, q) = 0$ for all $q \in Y$ such that from the continuous inf-sup condition (1.3) it follows that $\boldsymbol{u}^{\perp} = \boldsymbol{u}_{\psi}^{\perp}$. The divergence-free parts \boldsymbol{u}^0 and \boldsymbol{u}_{ψ}^0 are determined by (2.9) and they are equal, since it holds that $\mathbb{P}(\boldsymbol{f} + \nabla \psi) = \mathbb{P}(\boldsymbol{f})$ according to Corollary 2.9. Using $\boldsymbol{u}^{\perp} = \boldsymbol{u}_{\psi}^{\perp}$, (2.10) for (\boldsymbol{u}, p) , and integration by parts gives the following pressure equation for the forcing:

$$(p_{\psi}, \nabla \cdot \boldsymbol{v}^{\perp}) = -(\boldsymbol{f} + \nabla \psi, \boldsymbol{v}^{\perp}) + a(\boldsymbol{u}^{\perp}, \boldsymbol{v}^{\perp}) = (p + \psi, \nabla \cdot \boldsymbol{v}^{\perp}) \quad \forall \ \boldsymbol{v}^{\perp} \in \boldsymbol{X}_{\mathrm{div}}^{\perp}.$$

Therefore, the fundamental invariance property (1.4) holds.

3. The Lack of Pressure-Robustness for Standard Mixed Methods. This section presents the basic finite element formulation for the Stokes problem and the error analysis for the velocity error $\|\nabla(u-u_h)\|_{L^2(\Omega)}$. In particular, it is pointed out why the pressure cannot be removed from the a priori velocity error bound for standard mixed methods.

A finite element method poses the variational formulation (2.1) on a pair of finitedimensional spaces consisting of piecewise polynomials. In particular, if $X_h \times Y_h \subset$ $X \times Y$ denotes a pair of conforming piecewise polynomial spaces with respect to a partition \mathcal{T}_h of Ω (parameterized by h), then a Galerkin finite element method for the Stokes equations seeks $(\boldsymbol{u}_h, p_h) \in \boldsymbol{X}_h \times Y_h$ such that

(3.1a)
$$a(\boldsymbol{u}_h, \boldsymbol{v}_h) + b(\boldsymbol{v}_h, p_h) = (\boldsymbol{f}, \boldsymbol{v}_h) \qquad \forall \ \boldsymbol{v}_h \in \boldsymbol{X}_h,$$
(3.1b)
$$b(\boldsymbol{u}_h, q_h) = (g, q_h) \qquad \forall \ q_h \in Y_h.$$

$$(3.1b) b(\mathbf{u}_h, q_h) = (g, q_h) \forall q_h \in Y_h.$$

The discrete problem (3.1) is an example of a mixed finite element method in which two finite element spaces are present in the formulation. In such methods, the finite element spaces X_h and Y_h must be compatible in order to guarantee the existence and uniqueness of a solution as well as convergence, as the discretization parameter tends to zero. In the case of the Stokes (and Navier–Stokes) equations, the compatibility requirement is a surjective property of the divergence operator. In particular, a necessary condition for the existence and stability of a solution of problem (3.1) is the discrete inf-sup condition

(3.2)
$$\inf_{q_h \in Y_h \setminus \{0\}} \sup_{\boldsymbol{v}_h \in \boldsymbol{X}_h \setminus \{\boldsymbol{0}\}} \frac{(\nabla \cdot \boldsymbol{v}_h, q_h)}{\|\nabla \boldsymbol{v}_h\|_{L^2(\Omega)} \|q_h\|_{L^2(\Omega)}} \ge \beta_h > 0.$$

For stability and optimal order convergence, it is required that $\beta_h \geq \beta_0 > 0$ as $h \to 0^+$. Setting $v_h = u_h$ in (3.1a) and $q_h = -p_h$ in (3.1b) and adding the two equations gives

$$\nu \|\nabla \boldsymbol{u}_h\|_{L^2(\Omega)}^2 = (\boldsymbol{f}, \boldsymbol{u}_h) - (g, p_h),$$

which implies that zero data $f \equiv 0$ and g = 0 yield a zero solution $u_h \equiv 0$. Since the problem is linear, uniqueness of the discrete velocity solution is guaranteed, independent of the choice of finite element spaces. With uniqueness of the velocity established, the uniqueness of the pressure follows immediately by assuming two solutions and inserting the corresponding finite element problems into the discrete inf-sup condition (3.2). The existence of solutions follows from the uniqueness, since the problem is linear and finite-dimensional.

The discrete divergence operator $\nabla \cdot_h : \mathbf{X}_h \to Y_h$ is defined with the help of the L^2 -projection

$$(\nabla \cdot_h \boldsymbol{v}_h, q_h) = (\nabla \cdot \boldsymbol{v}_h, q_h) \quad \forall \ q_h \in Y_h.$$

Condition (3.2) implies that this operator is surjective from X_h onto Y_h , with a bounded right-inverse. Many finite element pairs have been developed that satisfy the discrete inf-sup condition (3.2) with $\beta_h \geq \beta_0 > 0$ as $h \to 0^+$. A popular example is the family of Taylor-Hood finite element pairs $\mathcal{P}_k/\mathcal{P}_{k-1}$, $k \geq 2$. In the mini element [4] it is $Y_h = \mathcal{P}_1$, and the velocity space consists of continuous linear functions that are enriched with local bubble functions to satisfy (3.2). An enrichment of the velocity space with bubble functions for the same reason is also used for the Bernardi-Raugel element [14], where the base polynomial spaces are \mathcal{P}_2 for the velocity and discontinuous piecewise linears for the pressure. A first order variant in the same paper is based on piecewise constant pressures and \mathcal{P}_1 for the velocity enriched by normal-weighted face bubbles.

In the finite element problem, the divergence-free condition is enforced only by (3.1b). Note that the pairs of spaces just mentioned satisfy $\nabla \cdot_h \mathbf{X}_h = Y_h$ but lack the inclusion $\nabla \cdot \boldsymbol{X}_h \not\subset Y_h$. If $\nabla \cdot \boldsymbol{X}_h \not\subset Y_h$, it cannot be expected that $\|\nabla \cdot \boldsymbol{u}_h\|_{L^2(\Omega)} = 0$. In fact, it is known that this quantity can become quite large in simulations with common element choices such as the Taylor–Hood pair $\mathcal{P}_2/\mathcal{P}_1$; see [22].

To derive finite element error estimates, under the assumptions that the discrete inf-sup condition (3.2) holds for the pair $\boldsymbol{X}_h \times Y_h$ and that $\nabla \cdot \boldsymbol{X}_h \not\subset Y_h$, consider the manifold

(3.3)
$$X_{h,\text{div}}(g) := \{ v_h \in X_h : (\nabla \cdot v_h, q_h) = (g, q_h) \ \forall \ q_h \in Y_h \}.$$

In the case g=0, the abbreviation $X_{h,\mathrm{div}}=X_{h,\mathrm{div}}(0)$ will be used, i.e., $X_{h,\mathrm{div}}$ is the space of discretely divergence-free functions, which is the kernel of the discrete divergence operator. Note that, because of $\nabla \cdot X_h \not\subset Y_h$, functions from $X_{h,\mathrm{div}}$ are generally not divergence-free in the sense of $L^2(\Omega)$ and hence it follows that $X_{h,\mathrm{div}} \not\subset X_{\mathrm{div}}$. Since $X_{h,\mathrm{div}} \subset X_h \subset X$, test functions from $X_{h,\mathrm{div}}$ can be used as test functions in the continuous problem (2.1a) as well as in the finite element problem (3.1). Taking such test functions, $q_h=0$, and subtracting both equations gives the error equation

(3.4)
$$a(\boldsymbol{u} - \boldsymbol{u}_h, \boldsymbol{v}_h) + b(\boldsymbol{v}_h, p - p_h) = 0 \quad \forall \ \boldsymbol{v}_h \in \boldsymbol{X}_{h, \text{div}}.$$

Because of the special choice of test function there holds $b(\boldsymbol{v}_h, p_h) = 0$, and therefore the discrete pressure can be removed from the error equation. However, since $\boldsymbol{X}_{h,\text{div}} \not\subset \boldsymbol{X}_{\text{div}}$, the continuous pressure does not vanish in general. At this point it is not possible to remove the dependency of the velocity error on the pressure. The best that can be done is to add $b(\boldsymbol{v}_h, q_h) = 0$ for arbitrary $q_h \in Y_h$ to the left-hand side of the error equation. Decomposing the error into

$$oldsymbol{u} - oldsymbol{u}_h = (oldsymbol{u} - ilde{oldsymbol{u}}_h) - (oldsymbol{u}_h - ilde{oldsymbol{u}}_h) =: oldsymbol{\eta} - oldsymbol{\phi}_h$$

for arbitrary $\tilde{\boldsymbol{u}}_h \in \boldsymbol{X}_{h,\mathrm{div}}$, inserting this decomposition into (3.4), and taking as test function $\boldsymbol{v}_h = \boldsymbol{\phi}_h$ yields

$$\nu \|\nabla \phi_h\|_{L^2(\Omega)}^2 = \nu(\nabla \eta, \nabla \phi_h) - (\nabla \cdot \phi_h, p - q_h) \quad \forall \ q_h \in Y_h.$$

The terms on the right-hand side are estimated by the Cauchy–Schwarz inequality and the estimate $\|\nabla \cdot \phi_h\|_{L^2(\Omega)} \le \|\nabla \phi_h\|_{L^2(\Omega)}$ (which holds with constant 1 for functions with homogeneous Dirichlet boundary conditions). Dividing by $\nu \|\nabla \phi_h\|_{L^2(\Omega)} \ne 0$ (the other case is trivial), one obtains

$$\|\nabla \phi_h\|_{L^2(\Omega)} \le \|\nabla \eta\|_{L^2(\Omega)} + \nu^{-1} \|p - q_h\|_{L^2(\Omega)} \quad \forall \ q_h \in Y_h.$$

Finally, one obtains with the triangle inequality

$$(3.5) \|\nabla(\boldsymbol{u} - \boldsymbol{u}_h)\|_{L^2(\Omega)} \le 2 \inf_{\tilde{\boldsymbol{u}}_h \in \boldsymbol{X}_{h,\text{div}}} \|\nabla(\boldsymbol{u} - \tilde{\boldsymbol{u}}_h)\|_{L^2(\Omega)} + \nu^{-1} \inf_{q_h \in Y_h} \|p - q_h\|_{L^2(\Omega)}.$$

The error estimate (3.5) shows that the bound for the velocity error $\|\nabla(u - u_h)\|_{L^2(\Omega)}$ depends on the best approximation error of the pressure, which is scaled with the inverse of the viscosity. This term becomes large if ν is small or if the best approximation error is large. Estimating the best approximation error with some interpolation error, one obtains a bound which contains the norm of the pressure in some Sobolev space. Examples 1.1–1.3 have already shown that the bound obtained in this way is sharp in the sense that large norms of the pressure dominate the velocity error and the error scales the same way as the pressure does.

Remark 3.1. It is useful to summarize the different meanings of a function being "divergence-free" that have been introduced so far. In the strong form of the Navier–Stokes equations (1.1) classical derivatives are used and \boldsymbol{u} is pointwise divergence-free. The property that a vector field is weakly divergence-free is given in (2.2). For functions $\boldsymbol{v} \in \boldsymbol{X}$, this property is equivalent to $\|\nabla \cdot \boldsymbol{v}\|_{L^2(\Omega)} = 0$; see (2.3) for g = 0. Finally, (conforming) discretely divergence-free vector fields are defined in (3.3). Clearly, a pointwise divergence-free field is weakly and discretely divergence-free. Also, a weakly divergence-free field from \boldsymbol{X} is discretely divergence-free. However, a discretely divergence-free field is usually neither pointwise nor weakly divergence-free.

Remark 3.2. Since discretely divergence-free vector fields are generally not weakly divergence-free, the question of the error in the divergence arises. From $\|\nabla \cdot (\boldsymbol{u} - \boldsymbol{u}_h)\|_{L^2(\Omega)} \le \|\nabla (\boldsymbol{u} - \boldsymbol{u}_h)\|_{L^2(\Omega)}$ one finds that this error is bounded with the same order as the error of the gradient of the velocity.

In particular, for g = 0, this estimate means $\|\nabla \cdot \boldsymbol{u}_h\|_{L^2(\Omega)} \leq \|\nabla(\boldsymbol{u} - \boldsymbol{u}_h)\|_{L^2(\Omega)}$. In numerical simulations one finds that both sides of this estimate in fact possess generally the same order of convergence. Thus, large errors $\|\nabla(\boldsymbol{u} - \boldsymbol{u}_h)\|_{L^2(\Omega)}$ usually induce a bad (local) conservation of mass.

Remark 3.3. Consider the case g=0. Then one obtains from the divergence theorem that

(3.6)
$$0 = \int_{\partial\Omega} \mathbf{u}_h \cdot \mathbf{n} \ d\mathbf{s} = \int_{\Omega} \nabla \cdot \mathbf{u}_h \ d\mathbf{x},$$

such that mass is conserved in this global sense.

If discontinuous pressure spaces $Y_h \subset Y$ are used, one has an even more local mass conservation. Since the piecewise constant functions are usually a subspace of a discontinuous pressure finite element space, one obtains from (2.1b) that

(3.7)
$$0 = \sum_{T \in \mathcal{T}_h} \int_T (\nabla \cdot \boldsymbol{u}_h) q_h \ d\boldsymbol{x} = \sum_{T \in \mathcal{T}_h} q_h \int_T \nabla \cdot \boldsymbol{u}_h \ d\boldsymbol{x}$$

for all $q_h \in \mathcal{P}_0$. Consider an arbitrary mesh cell T_1 and another arbitrary mesh cell $T_2 \neq T_1$. Then one can choose

$$q_h = \begin{cases} 1 & \text{in } T_1, \\ -\frac{|T_1|}{|T_2|} & \text{in } T_2, \\ 0 & \text{elsewhere.} \end{cases}$$

With this choice, $q_h \in Y_h$. One finds with (3.7) that

$$\int_{T_2} \nabla \cdot \boldsymbol{u}_h \ d\boldsymbol{x} = \frac{|T_2|}{|T_1|} \int_{T_1} \nabla \cdot \boldsymbol{u}_h \ d\boldsymbol{x} \quad \forall \ T_2 \in \mathfrak{T}_h.$$

It follows that

(3.8)
$$\int_{\Omega} \nabla \cdot \boldsymbol{u}_h \ d\boldsymbol{x} = \sum_{T \in \mathcal{T}_h} \int_{T} \nabla \cdot \boldsymbol{u}_h \ d\boldsymbol{x} = \sum_{T \in \mathcal{T}_h} \frac{|T|}{|T_1|} \int_{T_1} \nabla \cdot \boldsymbol{u}_h \ d\boldsymbol{x}$$
$$= \frac{1}{|T_1|} \int_{T_1} \nabla \cdot \boldsymbol{u}_h \ d\boldsymbol{x} \sum_{T \in \mathcal{T}_h} |T| = \frac{|\Omega|}{|T_1|} \int_{T_1} \nabla \cdot \boldsymbol{u}_h \ d\boldsymbol{x}.$$

From (3.6) one concludes that the last factor on the right-hand side of (3.8) vanishes. Since T_1 was chosen to be arbitrary, one obtains the local mass conservation

(3.9)
$$\int_{T} \nabla \cdot \boldsymbol{u}_{h} \, d\boldsymbol{x} = 0 \quad \forall \, T \in \mathcal{T}_{h}.$$

Note that the local mass conservation (3.9) does not necessarily imply that the error $\|\nabla \cdot \boldsymbol{u}_h\|_{L^2(\Omega)}$ is smaller in comparison with methods which use a continuous space Y_h .

4. Pressure-Robustness of Weakly Divergence-Free Mixed Finite Element Methods.

4.1. Stability and Accuracy of Pressure-Robust Mixed Methods for the Stokes Equations. In this section, mixed finite element error estimates for the discrete incompressible Stokes equations (3.1) are derived for inf-sup stable conforming element pairs $X_h \subset X$, $Y_h \subset Y$ that satisfy $\nabla \cdot X_h \subset Y_h$. It will be shown that the condition $\nabla \cdot X_h \subset Y_h$ ensures pressure-robustness in the sense that the discrete velocity error does not depend on the pressure. Due to this condition it holds that $X_{h,\mathrm{div}} \subset X_{\mathrm{div}}$. The inf-sup stability of the element pair (X_h, Y_h) ensures the existence of a so-called Fortin operator $\pi_F: X \to X_h$ such that for all $v \in X$ and for all $v \in Y_h$, $v \in Y_h$, v

Remark 4.1. Standard reasoning shows that discrete inf-sup stability is indeed equivalent to the existence of a stable Fortin interpolator with stability constant C_F and that $C_F \leq 1/\beta_h$. The precise value of the stability constant C_F is important since it enters the a priori velocity error estimate in Lemma 4.4. Classical textbooks emphasizing the convergence rates usually apply the estimate $C_F \leq 1/\beta_h$, which can lead to pessimistic estimates [55, 78]. Note that, e.g., in the case of conforming mixed finite elements, the limit inferior of a sequence of discrete inf-sup constants can be estimated by the continuous inf-sup constant, i.e., $\lim_{h \to \infty} \beta_h \leq \beta$ (cf. [23, 78]). Indeed, the continuous inf-sup constants can be very small in channel-like stretched domains. For those domains, the estimate $C_F \leq 1/\beta_h$ is pessimistic, since C_F can be of order O(1) (see, e.g., [55]), while $1/\beta_h$ can be very large. An explicit example is given in [23], where it is shown that in a rectangular domain with side lengths $0 < l_1 < l_2$ the continuous inf-sup constant β is proportional to l_1/l_2 , i.e.,

$$\beta \le \frac{\pi}{2\sqrt{3}} \frac{l_1}{l_2}.$$

Consequently, in a long stretched channel-like domain with $l_1 \ll l_2$, β and β_h are very small. In this case, estimates containing the stability constant C_F are much sharper [78], and will be preferred in what follows.

In perfect analogy to the continuous case, one obtains for the discrete solution of (3.1) the following results.

LEMMA 4.2. Let the finite element spaces $X_h \subset X$ and $Y_h \subset Y$ satisfy the discrete inf-sup stability (3.2) and let $\nabla \cdot X_h \subset Y_h$. Then, for $f \in L^2(\Omega)$ and $g \in Y$, the Stokes problem (3.1) has a unique discrete solution for which the following stability estimates hold:

(4.1a)
$$\|\nabla \boldsymbol{u}_h\|_{L^2(\Omega)} \le \frac{C_P}{\nu} \|\mathbb{P}(\boldsymbol{f})\|_{L^2(\Omega)} + \frac{1}{\beta_h} \|g\|_{L^2(\Omega)},$$

(4.1b)
$$||p_h||_{L^2(\Omega)} \le \frac{C_P}{\beta_h} ||\boldsymbol{f}||_{L^2(\Omega)} + \frac{\nu}{\beta_h^2} ||g||_{L^2(\Omega)}.$$

Proof. The proof is line by line the same as in Lemma 2.8, i.e., replace X by X_h , change the words "continuous inf-sup condition" (with stability constant β) to "discrete inf-sup condition" (with stability constant β_h), and note that $X_{h,\text{div}} \subset X_{\text{div}}$ holds. The discrete space $X_{h,\text{div}}^{\perp}$ is defined by a-orthogonality in the space X_h .

LEMMA 4.3. Let the finite element spaces $X_h \subset X$ and $Y_h \subset Y$ fulfill the discrete inf-sup stability (3.2) and $\nabla \cdot X_h \subset Y_h$. Then for all $w \in X$ with $w \in X_{\text{div}}(g)$,

$$(4.2) \qquad \inf_{\boldsymbol{w}_h \in \boldsymbol{X}_{h,\operatorname{div}}(g)} \|\nabla(\boldsymbol{w} - \boldsymbol{w}_h)\|_{L^2(\Omega)} \le (1 + C_F) \inf_{\boldsymbol{v}_h \in \boldsymbol{X}_h} \|\nabla(\boldsymbol{w} - \boldsymbol{v}_h)\|_{L^2(\Omega)}.$$

Proof. Let $\boldsymbol{v}_h \in \boldsymbol{X}_h$ be arbitrary and define $\boldsymbol{z}_h := \pi_F(\boldsymbol{w} - \boldsymbol{v}_h) \in \boldsymbol{X}_h$. Due to the properties of the Fortin interpolant one has $\|\nabla \boldsymbol{z}_h\|_{L^2(\Omega)} \leq C_F \|\nabla (\boldsymbol{w} - \boldsymbol{v}_h)\|_{L^2(\Omega)}$ and $(\nabla \cdot \boldsymbol{z}_h, q_h) = (\nabla \cdot (\boldsymbol{w} - \boldsymbol{v}_h), q_h)$ for all $q_h \in Y_h$. Then $\boldsymbol{w}_h := \boldsymbol{z}_h + \boldsymbol{v}_h \in \boldsymbol{X}_{h, \text{div}}(g)$, since

$$(\nabla \cdot \boldsymbol{w}_h, q_h) = (\nabla \cdot \boldsymbol{z}_h, q_h) + (\nabla \cdot \boldsymbol{v}_h, q_h) = (\nabla \cdot (\boldsymbol{w} - \boldsymbol{v}_h), q_h) + (\nabla \cdot \boldsymbol{v}_h, q_h)$$
$$= -(q, q_h) \quad \forall \ q_h \in Y_h.$$

Finally, the triangle inequality gives

$$\|\nabla(\boldsymbol{w} - \boldsymbol{w}_h)\|_{L^2(\Omega)} \le \|\nabla(\boldsymbol{w} - \boldsymbol{v}_h)\|_{L^2(\Omega)} + \|\nabla \boldsymbol{z}_h\|_{L^2(\Omega)}$$

$$\le (1 + C_F)\|\nabla(\boldsymbol{w} - \boldsymbol{v}_h)\|_{L^2(\Omega)}.$$

LEMMA 4.4. Let the finite element spaces $\mathbf{X}_h \subset \mathbf{X}$ and $Y_h \subset Y$ satisfy the discrete inf-sup stability (3.2) with $\nabla \cdot \mathbf{X}_h \subset Y_h$, and let $\pi_{Y_h} p \in Y_h$ be the L^2 -projection of p defined by

$$(p - \pi_{Y_h} p, q_h) = 0 \quad \forall \ q_h \in Y_h.$$

Then, for the unique discrete solution (\mathbf{u}_h, p_h) of (3.1), the following a priori error estimates hold:

$$(4.3a) \|\nabla(\boldsymbol{u} - \boldsymbol{u}_h)\|_{L^2(\Omega)} \leq 2 \inf_{\boldsymbol{w}_h \in \boldsymbol{X}_{h, \text{div}}(g)} \|\nabla(\boldsymbol{u} - \boldsymbol{w}_h)\|_{L^2(\Omega)}$$

$$\leq 2(1 + C_F) \inf_{\boldsymbol{w}_h \in \boldsymbol{X}_h} \|\nabla(\boldsymbol{u} - \boldsymbol{w}_h)\|_{L^2(\Omega)},$$

(4.3b)
$$\|\pi_{Y_h} p - p_h\|_{L^2(\Omega)} \le \frac{\nu}{\beta_h} \|\nabla(\boldsymbol{u} - \boldsymbol{u}_h)\|_{L^2(\Omega)},$$

(4.3c)
$$||p - p_h||_{L^2(\Omega)} \le ||p - \pi_{Y_h} p||_{L^2(\Omega)} + \frac{\nu}{\beta_h} ||\nabla (\boldsymbol{u} - \boldsymbol{u}_h)||_{L^2(\Omega)}.$$

Proof. For an arbitrary $\mathbf{w}_h \in \mathbf{X}_{h,\text{div}}(g)$ it holds that $\mathbf{v}_h^0 := \mathbf{u}_h - \mathbf{w}_h \in \mathbf{X}_{h,\text{div}}$. Using the Galerkin orthogonality and the Cauchy–Schwarz inequality yields

$$\nu \|\nabla \boldsymbol{v}_h^0\|_{L^2(\Omega)}^2 = a(\boldsymbol{v}_h^0, \boldsymbol{v}_h^0) = a(\boldsymbol{u}_h - \boldsymbol{w}_h, \boldsymbol{v}_h^0) = a(\boldsymbol{u} - \boldsymbol{w}_h, \boldsymbol{v}_h^0)
\leq \nu \|\nabla (\boldsymbol{u} - \boldsymbol{w}_h)\|_{L^2(\Omega)} \|\nabla \boldsymbol{v}_h^0\|_{L^2(\Omega)} \Longrightarrow \|\nabla \boldsymbol{v}_h^0\|_{L^2(\Omega)}
\leq \|\nabla (\boldsymbol{u} - \boldsymbol{w}_h)\|_{L^2(\Omega)}.$$

Now, the triangle inequality gives

$$\|\nabla(\boldsymbol{u} - \boldsymbol{u}_h)\|_{L^2(\Omega)} \le \|\nabla(\boldsymbol{u} - \boldsymbol{w}_h)\|_{L^2(\Omega)} + \|\nabla \boldsymbol{v}_h^0\|_{L^2(\Omega)} \le 2\|\nabla(\boldsymbol{u} - \boldsymbol{w}_h)\|_{L^2(\Omega)},$$

which proves the first inequality of (4.3a), since $\mathbf{w}_h \in \mathbf{X}_{h,\text{div}}(g)$ was chosen arbitrarily. The second inequality is a direct consequence of Lemma 4.3.

The proof for (4.3b) exploits the assumption $\nabla \cdot \boldsymbol{X}_h \subset Y_h$. Hence, one obtains for all $\boldsymbol{v}_h \in \boldsymbol{X}_h$

$$(4.4) \quad (\pi_{Y_h}p - p_h, \nabla \cdot \boldsymbol{v}_h) = (\pi_{Y_h}p - p_h, q_h) = (p - p_h, q_h) = \nu(\nabla(\boldsymbol{u} - \boldsymbol{u}_h), \nabla \boldsymbol{v}_h),$$

where the last step uses the definitions of the continuous and discrete Stokes problems (2.1) and (3.1), respectively. Using the discrete inf-sup condition (3.2), (4.4), and the Cauchy–Schwarz inequality yields

$$\|\pi_{Y_h} p - p_h\|_{L^2(\Omega)} \leq \frac{1}{\beta_h} \sup_{\boldsymbol{v}_h \in \boldsymbol{X}_h \setminus \{0\}} \frac{(\pi_{Y_h} p - p_h, \nabla \cdot \boldsymbol{v}_h)}{\|\nabla \boldsymbol{v}_h\|_{L^2(\Omega)}}$$

$$\leq \frac{1}{\beta_h} \sup_{\boldsymbol{v}_h \in \boldsymbol{X}_h \setminus \{0\}} \frac{\nu \|\nabla (\boldsymbol{u} - \boldsymbol{u}_h)\|_{L^2(\Omega)} \|\nabla \boldsymbol{v}_h\|_{L^2(\Omega)}}{\|\nabla \boldsymbol{v}_h\|_{L^2(\Omega)}}$$

$$= \frac{\nu}{\beta_h} \|\nabla (\boldsymbol{u} - \boldsymbol{u}_h)\|_{L^2(\Omega)}.$$

Statement (4.3b) follows with the triangle inequality.

Remark 4.5. The error estimates in Lemma 4.4 show that the discrete velocity converges with an asymptotically optimal order to the continuous velocity (in the case of sufficiently regular velocity), and that the velocity error is pressure-independent. This remarkable feature distinguishes pressure-robust mixed methods from classical mixed methods. Interestingly, something similar can be observed for the discrete pressure. According to (4.3b), the discrete pressure is the best approximation of the continuous pressure in $L^2(\Omega)$ up to an additive error that is only velocity-dependent. This property has been rarely emphasized so far in the context of mixed finite element methods for the (Navier-)Stokes equations. Moreover, the inverse of the discrete infsup constant β_h enters only the pressure estimates. In addition, it occurs only in the part of the error bound which is scaled by ν and therefore this term is usually small. In the velocity estimates, the constant C_F for an appropriate Fortin interpolant replaces the classical constant $1/\beta_h$.

The error estimates show that for pressure-robust mixed methods there holds an invariance principle, similar to the continuous problem; see Lemma 2.10.

LEMMA 4.6. Let the finite element spaces $\mathbf{X}_h \subset \mathbf{X}$ and $Y_h \subset Y$ fulfill the discrete inf-sup stability (3.2) and $\nabla \cdot \mathbf{X}_h \subset Y_h$. Then, for the unique discrete solution (\mathbf{u}_h, p_h) of (3.1) the following discrete fundamental invariance property holds: changing the right-hand side $\mathbf{f} \to \mathbf{f} + \nabla \psi$ with $\mathbf{f} \in \mathbf{L}^2(\Omega)$ and $\psi \in H^1(\Omega)/\mathbb{R}$ leads to a change in the discrete solution of the form $(\mathbf{u}_h, p_h) \to (\mathbf{u}_h, p_h + \pi_{Y_h} \psi)$.

Proof. The continuous and discrete solution operators $(\boldsymbol{f},g) \to (\boldsymbol{u},p)$ and $(\boldsymbol{f},g) \to (\boldsymbol{u}_h,p_h)$ are linear. Hence, it suffices to study (2.1) and (3.1) for the right-hand side $(\nabla \psi,0)$. The solutions of these special continuous and discrete problems are also denoted by (\boldsymbol{u},p) and (\boldsymbol{u}_h,p_h) . Due to Corollary 2.9 it holds that $\mathbb{P}(\nabla \psi) \equiv \mathbf{0}$, and the stability estimates from Lemmas 2.8 and 4.2 yield $\boldsymbol{u} \equiv \mathbf{0}$ and $\boldsymbol{u}_h \equiv \mathbf{0}$. Moreover, the continuous fundamental invariance property from Lemma 2.10 gives $(\boldsymbol{u},p)=(\mathbf{0},\psi)$. Since $\|\nabla(\boldsymbol{u}-\boldsymbol{u}_h)\|_{L^2(\Omega)}=0$, estimate (4.3b) allows us to conclude that $(\boldsymbol{u}_h,p_h)=(\mathbf{0},\pi_{Y_h}\psi)$, and the discrete fundamental invariance property is proven.

In summary, it has been shown in this section that pressure-robust mixed methods possess a number of attractive properties.

4.2. The Formal and the Discrete Vorticity Equations. It has been shown that testing with a divergence-free test function in the continuous setting (2.9) or testing with a discretely divergence-free function in the discrete setting (3.4) allows one to derive elliptic problems that determine the velocity solution. Next, it will be argued that these elliptic problems indeed represent a formal vorticity equation and a discrete vorticity equation which characterize the difference between classical mixed methods and pressure-robust mixed methods.

The Formal Vorticity Equation in the Continuous Setting. Here, the case d=3 will be discussed; the two-dimensional case follows similar arguments. For an arbitrary divergence-free vector field $\mathbf{v} \in \mathbf{X}_{\mathrm{div}} \cap \mathbf{C}_0^{\infty}(\Omega)$, there exists a vector potential $\boldsymbol{\xi} \in \mathbf{C}_0^{\infty}(\Omega)$ with $\mathbf{v} = \nabla \times \boldsymbol{\xi}$. Testing the momentum balance of (1.2) with \mathbf{v} , assuming that $(\mathbf{u}, p) \in \mathbf{H}^3(\Omega) \cap H^1(\Omega)$ and $\nabla \times \mathbf{f} \in \mathbf{L}^2(\Omega)$, and applying integration by parts yields

$$(-\nu\Delta u, \nabla \times \boldsymbol{\xi}) + (\nabla p, \nabla \times \boldsymbol{\xi}) = (\boldsymbol{f}, \nabla \times \boldsymbol{\xi}) \iff (-\nu\Delta \omega, \boldsymbol{\xi}) = (\nabla \times \boldsymbol{f}, \boldsymbol{\xi}),$$

where the notation $\omega := \nabla \times \boldsymbol{u}$ for the vorticity is used and the identity $\nabla \times (\nabla p) \equiv \boldsymbol{0}$ is applied. This equation shows that the vorticity satisfies formally, i.e., assuming sufficient regularity, the diffusion equation

$$(4.5) - \nu \Delta \boldsymbol{\omega} = \nabla \times \boldsymbol{f}.$$

Note that the formal vorticity equation is derived from the strong form that corresponds to the weak velocity equation

(4.6)
$$a(\boldsymbol{u}, \boldsymbol{v}) = (\boldsymbol{f}, \boldsymbol{v}) = (\mathbb{P}(\boldsymbol{f}), \boldsymbol{v}) \quad \forall \ \boldsymbol{v} \in \boldsymbol{X}_{\mathrm{div}},$$

which defines \boldsymbol{u} (together with the statement $-\nabla \cdot \boldsymbol{u} = g$) uniquely. This formal vorticity equation reflects perfectly the fundamental invariance property (1.4), since for the two forcings \boldsymbol{f} and $\boldsymbol{f} + \nabla \phi$ the same vorticity equation arises due to

$$\nabla \times (\mathbf{f} + \nabla \phi) = \nabla \times \mathbf{f}.$$

Therefore, the velocity \boldsymbol{u} and its vorticity $\boldsymbol{\omega}$ do not change, and the additional forcing $\nabla \phi$ only affects the pressure. In fact, the appearance of the Helmholtz projector $\mathbb{P}(\boldsymbol{f})$ in (4.6) corresponds to the dependence of the formal vorticity equation (4.5) on $\nabla \times \boldsymbol{f}$ (and not on \boldsymbol{f}). It should be noted that similar formal vorticity equations can also be derived for the time-dependent Navier–Stokes equations by testing with divergence-free vector fields.

Remark 4.7. The L^2 -orthogonality of gradient fields and divergence-free vector fields with compact support is equivalent to the vector calculus statements "gradient fields are irrotational" and "curl fields are divergence-free." Indeed, for $\boldsymbol{v} = \nabla \times \boldsymbol{\xi} \in \boldsymbol{X}_{\mathrm{div}} \cap \boldsymbol{C}_0^{\infty}(\Omega)$, integration by parts shows

$$0 = \int_{\Omega} \nabla \phi \cdot \boldsymbol{v} \, d\boldsymbol{x} = \int_{\Omega} \nabla \phi \cdot \nabla \times \boldsymbol{\xi} \, d\boldsymbol{x} = \int_{\Omega} (\underbrace{\nabla \times \nabla \phi}_{=0}) \cdot \boldsymbol{\xi} \, d\boldsymbol{x} = -\int_{\Omega} \phi (\underbrace{\nabla \cdot (\nabla \times \boldsymbol{\xi})}_{=0}) \, d\boldsymbol{x}.$$

In classical mixed methods the L^2 -orthogonality between gradient fields and discretely divergence-free test functions is relaxed. This property is equivalent to a relaxation of "gradient fields are irrotational."

Remark 4.8. The importance of the two operators divergence and curl for characterizing vector fields will be illustrated further with the following theorem from [8]: For a simply-connected bounded region $\Omega \subset \mathbb{R}^3$ with a surface $\partial\Omega$ consisting of a union of a finite number of disjoint closed C^2 surfaces, there is a uniquely defined vector field $\mathbf{v} \in \mathbf{L}^2(\Omega)$, which fulfills

$$\nabla \cdot \boldsymbol{v} = g \text{ in } \Omega, \qquad \nabla \times \boldsymbol{v} = \boldsymbol{\omega} \text{ in } \Omega, \qquad \boldsymbol{v} \cdot \boldsymbol{n} = 0 \text{ in } \partial \Omega,$$

for given $g \in L_0^2(\Omega)$ and $\omega \in \mathbb{C}^1(\Omega)$ with $\nabla \cdot \omega = 0$. The main message of this theorem is that information on the divergence and the curl of a vector field, together with some boundary data, determines the vector field completely. This result emphasizes the significance of the formal vorticity equation, since divergence and boundary data are always prescribed for the Navier–Stokes equations and only the curl of the velocity field is unknown.

Discrete Vorticity Equations for Classical and Pressure-Robust Mixed Methods. In (conforming) mixed finite element methods for the Stokes equations, the discrete velocity solution is determined by

$$a(\boldsymbol{u}_h, \boldsymbol{v}_h) = (\boldsymbol{f}, \boldsymbol{v}_h)$$

for all $v_h \in X_{h,\text{div}}$. Introducing a discrete Helmholtz projector $\mathbb{P}_h : L^2(\Omega) \to X_{h,\text{div}}$, defined as the L^2 -projection onto $X_{h,\text{div}}$, this formulation can be written as

(4.7)
$$a(\boldsymbol{u}_h, \boldsymbol{v}_h) = (\mathbb{P}_h(\boldsymbol{f}), \boldsymbol{v}_h)$$

for all $v_h \in X_{h,\text{div}}$. Similarly to the continuous setting, cf. Remark 4.7, where (4.6) is understood as a formal weak vorticity equation, testing with a (discretely) divergence-free vector field is considered as a weak application of a curl operator, which yields the discrete vorticity equation (4.7).

In the case of pressure-robust methods with $X_{h,\text{div}} \subset X_{\text{div}}$ there obviously holds $\mathbb{P}_h(\nabla \phi) = \mathbf{0}$ for all $\phi \in H^1(\Omega)$, and the discrete vorticity equation

(4.8)
$$a(\boldsymbol{u}_h, \boldsymbol{v}_h) = -\nu(\Delta \boldsymbol{u}, \boldsymbol{v}_h)$$

for all $v_h \in X_{h,\text{div}}$ is pressure-independent.

In contrast, in the case of classical mixed methods with $X_{h,\mathrm{div}} \not\subset X_{\mathrm{div}}$, one has for all $v_h \in X_{h,\mathrm{div}}$

(4.9)
$$a(\boldsymbol{u}_h, \boldsymbol{v}_h) = (\mathbb{P}_h(\boldsymbol{f}), \boldsymbol{v}_h) = -\nu(\Delta \boldsymbol{u}, \boldsymbol{v}_h) + (\mathbb{P}_h(\nabla p), \boldsymbol{v}_h),$$

and one obtains with the definition of \mathbb{P}_h , integration by parts, $(\pi_{Y_h} p, \nabla \cdot v_h) = 0$, and the approximation estimate for the L^2 -projection (assuming that p is sufficiently regular),

$$|(\mathbb{P}_h(\nabla p), \boldsymbol{v}_h)| = |(\nabla p, \boldsymbol{v}_h)| = |(p, \nabla \cdot \boldsymbol{v}_h)| = |(p - \pi_{Y_h} p, \nabla \cdot \boldsymbol{v}_h)|$$

$$\leq Ch^k |p|_{H^k(\Omega)} ||\nabla \cdot \boldsymbol{v}_h||_{L^2(\Omega)}.$$

Compared with (4.8), equation (4.9) contains the additional term $(\mathbb{P}_h(\nabla p), \mathbf{v}_h)$ with $\mathbf{v}_h \in \mathbf{X}_{h,\mathrm{div}}$. It is this term that distinguishes pressure-robust mixed methods from classical mixed methods. It can be understood as a pressure-dependent consistency error of the discrete vorticity equation of classical mixed methods. Of course, this consistency error vanishes with optimal order, whenever p is regular enough. However, it can be arbitrarily large, depending on the given flow problem.

Remark 4.9. Testing a vector field \boldsymbol{w} with a smooth compactly supported divergence-free vector field $\boldsymbol{v} = \nabla \times \boldsymbol{\xi} \in \boldsymbol{X}_{\mathrm{div}}$ is equivalent to the application of a distributional curl operator $\boldsymbol{C}_0^{\infty}(\Omega) \to \mathbb{R}$ to the vector field \boldsymbol{w} ,

$$(\boldsymbol{w}, \boldsymbol{v}) = (\boldsymbol{w}, \nabla \times \boldsymbol{\xi}).$$

This distributional curl operator vanishes for all $\mathbf{w} = \nabla \phi$.

Similarly, one can define a discrete distributional curl operator $C_0^{\infty}(\Omega) \to \mathbb{R}$ by

$$(\boldsymbol{w}, \mathbb{P}_h(\nabla \times \boldsymbol{\xi})).$$

Then, the discrete distributional curl of pressure-robust mixed methods vanishes for all $\boldsymbol{w} = \nabla \phi$, while for the discrete distributional curl operator of classical mixed methods there holds

$$|(\nabla \phi, \mathbb{P}_h(\nabla \times \boldsymbol{\xi}))| \leq \mathcal{O}(h^k)|\phi|_{H^k(\Omega)}.$$

Remark 4.10. In Lemma 4.6 it was shown that pressure-robust mixed methods satisfy a fundamental invariance property, which is in perfect analogy to the continuous result from Lemma 2.10. However, for classical mixed methods there also holds a (much weaker) discrete fundamental invariance property, which is equivalent to the statement that the discrete curl operator of classical mixed methods fulfills $\nabla_h \times \nabla \phi \equiv \mathcal{O}(h^k)|\phi|_{H^k(\Omega)}$: changing $\mathbf{f} \to \mathbf{f} + \nabla \psi_h$ by some discrete $\psi_h \in Y_h$ implies that $(\mathbf{u}_h, p_h) \to (\mathbf{u}_h, p_h + \psi_h)$. For discontinuous pressure spaces Y_h , the expression $\nabla \psi_h$ is to be understood as a discrete distributional gradient $\mathbf{v}_h \to -(\psi_h, \nabla \cdot \mathbf{v}_h)$.

4.3. A Tool to Develop Divergence-Free Elements: The de Rham Complex.

During the past 30 years, the construction of de Rham subcomplexes consisting of finite element spaces has been an invaluable tool in developing stable finite element pairs for problems in porous media flow, electromagnetics, and linear elasticity [5, 6, 19, 59]. The key idea of this program is to mimic the algebraic and topological properties found at the continuous level to obtain mixed finite element spaces with enhanced stability properties which preserve physical quantities of interest. The culmination of these ideas and tools is the finite element exterior calculus framework [5, 6], where canonical finite element spaces are developed in arbitrary dimensions for the Hodge Laplacian. However, only recently have these tools and ideas been applied to the Navier–Stokes problem to obtain divergence-free finite element pairs.

To explain the main ideas, it is first recalled that the two-dimensional de Rham complex with minimal L^2 smoothness is given by the sequence of mappings

$$(4.10) \mathbb{R} \longrightarrow H^1(\Omega) \xrightarrow{\operatorname{\mathbf{curl}}} \mathbf{H}(\operatorname{div}, \Omega) \xrightarrow{\operatorname{div}} L^2(\Omega) \longrightarrow 0,$$

where $\operatorname{\mathbf{curl}} := (\partial/\partial x_2, -\partial/\partial x_1)^t$ denotes the vector curl operator. If the domain Ω is simply connected, then this complex is exact, that is, the range of each operator is the kernel of the succeeding one [36]. In particular, the exactness of the complex implies that (i) if $z \in H^1(\Omega)$ is curl-free, then z is constant; (ii) if $v \in H(\operatorname{div}, \Omega)$ is solenoidal, then $v = \operatorname{\mathbf{curl}} z$ for some $z \in H^1(\Omega)$; and (iii) the mapping $\operatorname{div} : H(\operatorname{div}, \Omega) \to L^2(\Omega)$ is a surjection.

A finite element subcomplex of (4.10) consists of finite element spaces $\Upsilon_h \subset H^1(\Omega)$, $\mathbf{W}_h \subset \mathbf{H}(\operatorname{div}, \Omega)$, and $Q_h \subset L^2(\Omega)$ satisfying the relations

$$(4.11) \mathbb{R} \longrightarrow \Upsilon_h \xrightarrow{\operatorname{curl}} W_h \xrightarrow{\operatorname{div}} Q_h \longrightarrow 0.$$

It is well known that standard conforming finite element element spaces form a discrete complex of (4.10) [6, 59]. For example, one may take Υ_h to be the Lagrange finite element space, \boldsymbol{W}_h to be either the Raviart–Thomas or the Brezzi–Douglas–Marini (BDM) finite element space, and Q_h to be the space of discontinuous piecewise polynomials [17, 69]. Similar to the continuous setting, the subcomplex (4.11) is exact provided the domain is simply connected; as a result, the finite element pairs $\Upsilon_h \times \boldsymbol{W}_h$ and $\boldsymbol{W}_h \times Q_h$ form stable finite element pairs with respect to the curl and the divergence operators, respectively. For example, the exactness property of the subcomplex implies that div: $\boldsymbol{W}_h \to Q_h$ is a surjection, and simple arguments show that this surjection has a bounded right-inverse independent of h. From this result, one easily deduces the inf-sup condition: $\sup_{\boldsymbol{w} \in \boldsymbol{W}_h} (\operatorname{div} \boldsymbol{w}, q) / \|\boldsymbol{w}\|_{H(\operatorname{div},\Omega)} \ge \beta \|q\|_{L^2(\Omega)} \, \forall \, q \in Q_h$.

While the complex (4.10) and its discrete counterpart are useful in the study of several problems, it is not suitable for the Stokes problem due to the minimal smoothness of the Hilbert spaces. Instead, a smooth de Rham complex (or Stokes complex) has been proposed [30, 39, 58]:

$$(4.12) \mathbb{R} \longrightarrow H^2(\Omega) \xrightarrow{\operatorname{\mathbf{curl}}} H^1(\Omega) \xrightarrow{\operatorname{div}} L^2(\Omega) \longrightarrow 0.$$

Again, this complex is exact provided Ω is simply connected [36]. In particular, all divergence-free $\mathbf{H}^1(\Omega)$ functions satisfy the relation $\mathbf{v} = \mathbf{curl}\,z$ for some $z \in H^2(\Omega)$, where z is often referred to as the stream-function if \mathbf{v} models an incompressible fluid. Moreover, the mapping div : $\mathbf{H}^1(\Omega) \to L^2(\Omega)$ is a surjection, implying the continuous inf-sup condition (1.3).

Similar to the previous setting, one can obtain stable finite element pairs by considering subcomplexes of (4.12) consisting of finite element spaces,

$$(4.13) \mathbb{R} \longrightarrow \Sigma_h \xrightarrow{\operatorname{\mathbf{curl}}} \boldsymbol{X}_h \xrightarrow{\operatorname{div}} Y_h \longrightarrow 0,$$

where $\Sigma_h \subset H^2(\Omega)$, $X_h \subset H^1(\Omega)$, and $Y_h \subset L^2(\Omega)$. If the discrete complex (4.13) is exact, then the finite element pair $X_h \times Y_h$ satisfies the discrete inf-sup condition provided this mapping has a bounded right-inverse. The mappings in (4.13) then imply that $\operatorname{div} X_h = W_h$, and thus, the finite element pair yields divergence-free approximations. A useful feature of this methodology is that the complex (4.13) provides a guiding tool to develop the pair $X_h \times Y_h$ satisfying these properties, in particular, the $H^2(\Omega)$ -conforming relatives that dictate the local and global properties of these spaces. As far as we are aware, every divergence-free finite element pair has an H^2 relative satisfying (4.13).

As an example of the derivation of divergence-free pairs from H^2 -conforming finite element spaces, the Hsieh–Clough–Tocher (HCT) finite element will be considered. To describe this space, let \mathcal{T}_h denote a shape regular, conforming simplicial triangulation of $\Omega \subset \mathbb{R}^2$. For a simplex $T \in \mathcal{T}_h$, let $\{K_r^{(T)}\}_{r=1}^3$ denote the three subtriangles obtained by performing a barycenter refinement on T, and set $\mathcal{M}_h := \{K_r^{(T)}: T \in \mathcal{T}_h\}$. The HCT space Σ_h^{HCT} is defined as the space of globally H^2 piecewise cubic polynomials with respect to the (refined) mesh \mathcal{M}_h . Denoting by \mathcal{V}_h and \mathcal{E}_h the set of vertices and edges in the original mesh \mathcal{T}_h , one can show that any function $z \in \Sigma_h^{HCT}$ is uniquely determined by the constraint $z|_T \in H^2(T)$ for all $T \in \mathcal{T}_h$, and the values z(a), $\nabla z(a)$, and $\int_e \frac{\partial z}{\partial \mathbf{n}_e} d\mathbf{s}$ over all $a \in \mathcal{V}_h$ and $e \in \mathcal{E}_h$ (cf. [24] and Figure 4.1, row 1). Here, $\frac{\partial z}{\partial \mathbf{n}_e} := \nabla z \cdot \mathbf{n}_e$ and \mathbf{n}_e denotes the outward unit normal of the edge e. It follows that the dimension of this space is $\dim \Sigma_h^{HCT} = 3|\mathcal{V}_h| + |\mathcal{E}_h|$, where $|\mathcal{S}|$ denotes the cardinality of a set \mathcal{S} .

The definition of the HCT space and its properties naturally leads to finite element spaces satisfying (4.13). In particular, since differentiation lowers polynomial degree and global continuity by 1, one may take \boldsymbol{X}_h^{HCT} to be the space of globally H^1 piecewise quadratic, vector-valued polynomials with respect to \mathcal{M}_h , and take Y_h^{HCT} to be the space of (discontinuous) piecewise linear polynomials with respect to \mathcal{M}_h . The inclusions $\operatorname{curl} \Sigma_h^{HCT} \subset \boldsymbol{X}_h^{HCT}$ and $\operatorname{div} \boldsymbol{X}_h^{HCT} \subset Y_h^{HCT}$ are immediate, and thus these spaces satisfy (4.13).

To verify that the finite element spaces Σ_h^{HCT} , \boldsymbol{X}_h^{HCT} , and Y_h^{HCT} inherit the exactness property, one first observes that if $\boldsymbol{v} \in \boldsymbol{X}_h^{HCT} \subset \boldsymbol{H}^1(\Omega)$ is divergence-free, then $\boldsymbol{v} = \operatorname{\mathbf{curl}} z = (\partial z/\partial x_2, -\partial z/\partial x_1)^t$ for some $z \in H^2(\Omega)$ due to the exactness property of the complex (4.12). Using the definitions of the curl operator and of \boldsymbol{X}_h^{HCT} , one deduces that both $\partial z/\partial x_1$ and $\partial z/\partial x_2$ are piecewise quadratic polynomials, and therefore z is a piecewise cubic polynomial. Moreover, the condition $\operatorname{\mathbf{curl}} z \in H^1(\Omega)$ implies that $z \in H^2(\Omega)$, and therefore $z \in \Sigma_h^{HCT}$.

Thus, to verify the exactness of the subcomplex (4.13) and to show that $X_h \times Y_h$ forms a stable finite element pair for the Stokes problem, it suffices to show that $\operatorname{div} X_h^{HCT} \to Y_h^{HCT}$ is a surjection with a bounded right-inverse. This surjection property can be achieved by a simple counting argument. Indeed, since $\operatorname{div} X_h^{HCT} \subseteq W_h^{HCT}$, it suffices to show that the dimensions of $\operatorname{div} X_h^{HCT}$ and Y_h^{HCT} are the same. Since the finite element space Y_h^{HCT} consists of piecewise linear polynomials with respect to \mathcal{M}_h , and since the dimension of the space of linear polynomials in two dimensions is 3, one has $\operatorname{dim} Y_h^{HCT} = 3|\mathcal{M}_h| = 9|\mathcal{T}_h|$. Moreover, any function $v \in X_h^{HCT}$ is uniquely determined by its values at the vertices of \mathcal{M}_h and its mean over all edges in \mathcal{M}_h [24]. Since the number of vertices in the refined mesh \mathcal{M}_h is $|\mathcal{V}_h| + |\mathcal{T}_h|$, and the number of edges in \mathcal{M}_h is $|\mathcal{E}_h| + 3|\mathcal{T}_h|$, one has $\operatorname{dim} X_h^{HCT} = 2(|\mathcal{V}_h| + |\mathcal{E}_h| + 4|\mathcal{T}_h|)$. Therefore, by the rank-nullity theorem and Euler's formula $|\mathcal{V}_h| + |\mathcal{T}_h| - |\mathcal{E}_h| = 1$, one obtains

$$\dim\left(\operatorname{div}\boldsymbol{X}_{h}^{HCT}\right) = \dim\boldsymbol{X}_{h}^{HCT} - \dim\operatorname{\mathbf{curl}}\Sigma_{h}^{HCT} = \dim\boldsymbol{X}_{h}^{HCT} - \dim\Sigma_{h}^{HCT} + 1$$

$$= 2(|\mathcal{V}_{h}| + |\mathcal{E}_{h}| + 4|\mathcal{T}_{h}|) - (3|\mathcal{V}_{h}| + |\mathcal{E}_{h}|) + (|\mathcal{V}_{h}| + |\mathcal{T}_{h}| - |\mathcal{E}_{h}|) = 9|\mathcal{T}_{h}|$$

$$= \dim Y_{h}^{HCT}.$$

Thus, the subcomplex with the finite element spaces Σ_h^{HCT} , \boldsymbol{X}_h^{HCT} , and Y_h^{HCT} is exact. Moreover, using a macroelement technique [7], one can show that the surjection div : $\boldsymbol{X}_h \to Y_h$ has a bounded right-inverse independent of h, and therefore the discrete inf-sup condition (3.2) is uniformly satisfied. For the Stokes equations, one obtains the Scott–Vogelius pair of spaces $\boldsymbol{\mathcal{P}}_2/\mathcal{P}_1^{\text{disc}} = \boldsymbol{V}_h^{HCT}/W_h^{HCT}$ [7, 71] on a barycenter-refined mesh.

The given example is not limited to the HCT element; one may start with any $H^2(\Omega)$ -conforming finite element space to derive a stable divergence-free finite element pair for the Stokes problem. Examples of $H^2(\Omega)$ spaces include the Morgan–Scott element [60], the Argyris element [24], the rational Zienkiewicz element [24], and the Bogner–Fox–Schmit rectangular element [24]. These $H^2(\Omega)$ finite element spaces were used to derive stable divergence-free finite element pairs in [30, 39, 72]; these finite element spaces and their H^2 -conforming relatives are summarized in Figure 4.1.

While the development of divergence-free, two-dimensional Stokes elements has reached a stage of maturity, the three-dimensional case is considerably more challenging, and several issues remain to be resolved. To explain the added difficulties, as

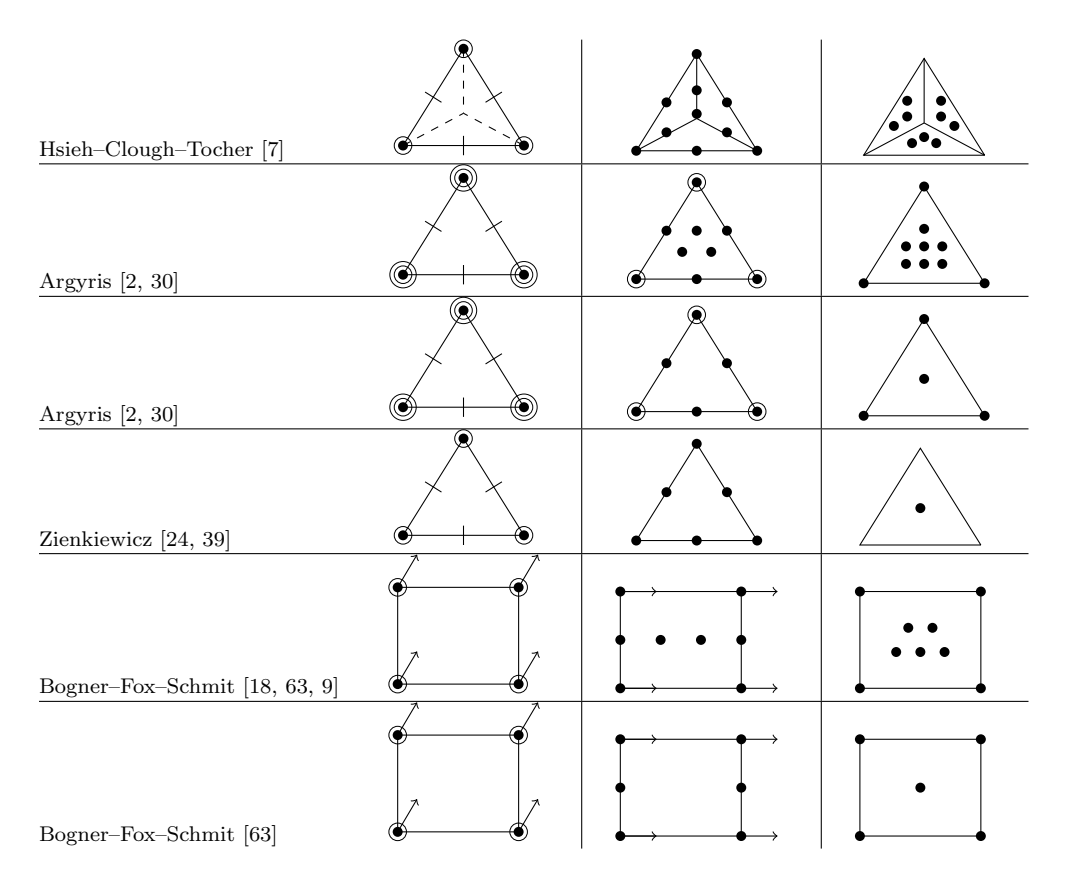


Fig. 4.1 H^2 -conforming finite element space Σ_h (left), velocity space X_h (middle), and pressure space Y_h (right) satisfying the exact complex (4.13). Small and large circles denote first and second derivative degrees of freedom (d.o.f.s), respectively, solid points denote function d.o.f.s, arrows denote directional derivative d.o.f.s, and lines without arrows denote normal derivative d.o.f.s.

before the de Rham complex with minimal L^2 smoothness is stated:

$$(4.14) \mathbb{R} \longrightarrow H^{1}(\Omega) \xrightarrow{\mathbf{grad}} \mathbf{H}(\mathbf{curl}, \Omega) \xrightarrow{\mathbf{curl}} \mathbf{H}(\mathrm{div}, \Omega) \xrightarrow{\mathrm{div}} L^{2}(\Omega) \longrightarrow 0,$$

where $H(\operatorname{curl},\Omega)$ denotes the space of square-integrable vector-valued functions whose curl is in $L^2(\Omega)$. Similar to the two-dimensional case, classical families of finite element spaces form a subcomplex of (4.14) that inherits the cohomology of the sequence.

Based on the complex (4.14) one may construct complexes with enhanced smoothness that are suitable for the Stokes problem. However, due to the additional space and the differential operator in the three-dimensional case, different Stokes complexes may be considered. For example, the complex

$$(4.15) \mathbb{R} \longrightarrow H^{2}(\Omega) \xrightarrow{\mathbf{grad}} \mathbf{H}^{1}(\mathbf{curl}; \Omega) \xrightarrow{\mathbf{curl}} \mathbf{H}^{1}(\Omega) \xrightarrow{\mathrm{div}} L^{2}(\Omega) \longrightarrow 0,$$

with $\mathbf{H}^1(\mathbf{curl};\Omega) = \{ \mathbf{v} \in \mathbf{H}^1(\Omega); \mathbf{curl} \mathbf{v} \in \mathbf{H}^1(\Omega) \}$, was proposed in [62, 73] to develop conforming and nonconforming divergence-free elements. Due to the high

regularity of the spaces, the polynomial order becomes exceedingly high. For example, the lowest degree H^2 -conforming piecewise polynomial space is 9; as a result, the lowest order velocity space based on this construction is 6 [62], which may limit the practical use of these elements. On the other hand, one could consider the quintic composite elements (also known as macroelements) documented in [46] as the H^2 -conforming finite element space. This element is most likely related to the Scott–Vogelius pair $\mathfrak{P}_3/\mathfrak{P}_2^{\mathrm{disc}}$ on barycenter-refined triangulations studied in [80]. However, the corresponding $H^1(\mathbf{curl},\Omega)$ conforming element completing the sequence (4.15) is missing in the literature.

Alternatively, the complex

$$(4.16) \mathbb{R} \longrightarrow H^1(\Omega) \xrightarrow{\mathbf{grad}} \mathbf{\Phi} \xrightarrow{\mathbf{curl}} \mathbf{H}^1(\Omega) \xrightarrow{\mathrm{div}} L^2(\Omega) \longrightarrow 0,$$

with $\Phi := \{ v \in L^2(\Omega) : \operatorname{\mathbf{curl}} v \in H^1(\Omega) \}$, was recently proposed in [29] to derive stable pairs in an isogeometric framework. On the other hand, as far as we are aware, no finite element spaces conforming to the complex (4.16) exist.

Constructions of divergence-free finite elements obtained in different ways can be found, e.g., in [81, 82].

4.4. H(div)-Conforming Finite Element Methods. Recently, to bypass the difficulty of constructing conforming, inf-sup stable, and divergence-free spaces, finite element methods for the Stokes problem that use strictly H(div)-conforming bases have been proposed [25, 38, 45, 58, 73, 76, 77, 79]. Before presenting these schemes, a criterion to ensure that a finite element space is a subspace of $H(\text{div}, \Omega)$ is reviewed.

As before, \mathcal{T}_h denotes a shape-regular triangulation of Ω . Let \mathcal{E}_h be the set of (open) edges (d=2) or faces (d=3) of the mesh. The set of boundary edges/faces is denoted by $\mathcal{E}_h^B \subset \mathcal{E}_h$, i.e., $e \in \mathcal{E}_h^B$ if $e \cap \partial \Omega \neq \emptyset$, and $\mathcal{E}_h^I := \mathcal{E}_h \backslash \mathcal{E}_h^B$ is the set of interior edges/faces.

LEMMA 4.11. Let \mathbf{W}_h denote a space of piecewise polynomials with respect to the partition \mathfrak{T}_h . Then $\mathbf{W}_h \subset \mathbf{H}(\operatorname{div},\Omega)$, provided the normal components (but not necessarily the tangential components) of functions in this space are continuous across all interelement boundaries $e \in \mathcal{E}_h^I$.

Proof. Let $\boldsymbol{w}_h \in \boldsymbol{W}_h$ and suppose that the normal component of \boldsymbol{w}_h is continuous across each $e \in \mathcal{E}_h^I$. Set $\rho_h \in L^2(\Omega)$ such that $\rho_h|_T = \nabla \cdot \boldsymbol{w}_h|_T$ for all $T \in \mathcal{T}_h$. Applying the divergence theorem elementwise yields for any $\psi \in C_0^{\infty}(\Omega)$,

$$\begin{split} -\int_{\Omega} \nabla \psi \cdot \boldsymbol{w}_h \, d\boldsymbol{x} &= -\sum_{T \in \mathfrak{T}_h} \int_{T} \nabla \psi \cdot \boldsymbol{w}_h \, d\boldsymbol{x} \\ &= \sum_{T \in \mathfrak{T}_h} \left(\int_{T \in \mathfrak{T}_h} \psi(\nabla \cdot \boldsymbol{w}_h) \, d\boldsymbol{x} - \int_{\partial T} (\boldsymbol{w}_h \cdot \mathbf{n}_T) \psi \, d\mathbf{s} \right) \\ &= \int_{\Omega} \rho_h \psi \, d\boldsymbol{x} - \sum_{T \in \mathfrak{T}_h} \int_{\partial T} (\boldsymbol{w}_h \cdot \mathbf{n}_T) \psi \, d\mathbf{s}. \end{split}$$

Since the normal component of \mathbf{w}_h is continuous, and since ψ vanishes on $\partial\Omega$, the boundary integrals vanish, and the statement of the lemma follows from Definition 2.3.

Two canonical $H(\text{div}, \Omega)$ -conforming finite element spaces satisfying this criterion include the Raviart–Thomas space of order $k \geq 0$ [61, 69],

$$(4.17a) RT_k := \{ \boldsymbol{w}_h \in \boldsymbol{H}_0(\operatorname{div}, \Omega) : \boldsymbol{w}_h|_T \in \operatorname{RT}_k(T) \ \forall \ T \in \mathfrak{T}_h \},$$

and the Brezzi-Douglas-Marini (BDM) space of degree $k \geq 1$,

(4.17b)
$$BDM_k := \{ \boldsymbol{w}_h \in \boldsymbol{H}_0(\operatorname{div}, \Omega) : \boldsymbol{w}_h|_T \in \boldsymbol{\mathcal{P}}_k(T) \ \forall \ T \in \boldsymbol{\mathcal{T}}_h \}.$$

Here, $\mathbf{H}_0(\operatorname{div},\Omega) = \{ \mathbf{v} \in \mathbf{H}(\operatorname{div},\Omega) : \mathbf{v} \cdot \mathbf{n}|_{\partial\Omega} = 0 \}$, and $\operatorname{RT}_k(T) := \mathbf{\mathcal{P}}_k(T) + \mathbf{x}\mathbf{\mathcal{P}}_k(T)$ is the local Raviart–Thomas space. Both of these spaces form inf-sup stable pairs with appropriate pressure spaces and, consequently, lead to stable discretizations for second order elliptic problems.

To make this last statement precise, denote by Q_h the space of discontinuous piecewise polynomials of degree k if $\mathbf{W}_h = \mathrm{RT}_k$, or k-1 if $\mathbf{W}_h = \mathrm{BDM}_k$, and with vanishing mean. Then the finite element pair $\mathbf{W}_h \times Q_h$ is inf-sup stable in the sense that

$$(4.18) \qquad \inf_{q_h \in Q_h \setminus \{0\}} \sup_{\boldsymbol{w}_h \in \boldsymbol{W}_h \setminus \{\mathbf{0}\}} \frac{\int_{\Omega} (\nabla \cdot \boldsymbol{w}_h) q_h \, d\boldsymbol{x}}{\|\boldsymbol{w}_h\|_{\boldsymbol{H}(\operatorname{div},\Omega)} \|q_h\|_{L^2(\Omega)}} \ge \beta_h,$$

with $\beta_h > 0$ uniformly bounded from below. Moreover, it is easy to see from their definitions that the inclusion $\nabla \cdot \boldsymbol{W}_h \subseteq Q_h$ is satisfied; as a result, the discretely divergence-free functions are weakly divergence-free, i.e., $\{\boldsymbol{w}_h \in \boldsymbol{W}_h : \int_{\Omega} (\nabla \cdot \boldsymbol{w}_h) q_h d\boldsymbol{x} = 0 \ \forall \ q_h \in Q_h\} = \{\boldsymbol{w}_h \in \boldsymbol{W}_h : \nabla \cdot \boldsymbol{w}_h \equiv 0\}.$

While these spaces are inf-sup stable with respect to the $\mathbf{H}(\operatorname{div},\Omega)$ norm and the discretely divergence-free functions are solenoidal, the spaces are not directly applicable for the Stokes problem due to their lack of smoothness. In particular, since the Raviart–Thomas and BDM spaces satisfy the noninclusion $\mathbf{W}_h \not\subset \mathbf{H}_0^1(\Omega)$, i.e., these spaces are nonconforming with respect to $\mathbf{H}_0^1(\Omega)$, the finite element method for the Stokes problem (3.1) is not well defined since the gradients of functions in \mathbf{W}_h do not exist globally. Furthermore, if the gradients in the formulation (3.1) are replaced by their piecewise defined counterpart, the resulting method, even if nonsingular, is not convergent since the method is inconsistent in the sense that

$$-\int_{\Omega} \Delta \boldsymbol{v} \cdot \boldsymbol{w}_h \, d\boldsymbol{x} \neq a(\boldsymbol{v}, \boldsymbol{w}_h)$$

for general functions $\mathbf{v} \in \mathbf{H}^2(\Omega) \cap \mathbf{H}_0^1(\Omega)$ and $\mathbf{w}_h \in \mathbf{W}_h$. As such, modifications of the method are needed to ensure that the discrete problem is stable and consistent, yet still preserves the divergence-free property. Generally speaking, this is achieved in two ways: (i) modify the bilinear forms in (3.1) or (ii) modify the $\mathbf{H}(\operatorname{div}, \Omega)$ spaces to impose tangential continuity in some weak sense.

In the first case, using techniques found in discontinuous Galerkin methods, the bilinear form $a(\cdot, \cdot)$ in (3.1) is modified to ensure that the form is consistent with the Laplace operator. Here, the symmetric interior penalty arguments given in [76, 77] are presented, although different discontinuous Galerkin techniques are available [25]. For simplicity it is assumed that $\Omega \subset \mathbb{R}^2$; however, the arguments generalize quite naturally to the three-dimensional case. Let $\boldsymbol{w}_h \in \boldsymbol{W}_h \subset \boldsymbol{H}(\operatorname{div},\Omega)$ be an arbitrary function in the Raviart-Thomas or BDM space, and assume that the velocity solution of the Stokes problem \boldsymbol{u} is sufficiently smooth. Then it follows from Green's theorem

that

$$-\int_{T} \Delta \boldsymbol{u} \cdot \boldsymbol{w}_{h} \, d\boldsymbol{x} = \int_{T} \nabla \boldsymbol{u} : \nabla \boldsymbol{w}_{h} \, d\boldsymbol{x} - \int_{\partial T} \frac{\partial \boldsymbol{u}}{\partial \mathbf{n}_{T}} \cdot \boldsymbol{w}_{h} \, ds,$$

where $\frac{\partial \boldsymbol{u}}{\partial \mathbf{n}_T} := \nabla \boldsymbol{u} \mathbf{n}_T$. Let $\boldsymbol{\tau}_T$ denote the tangential unit vector of ∂T , obtained by rotating \mathbf{n}_T by 90 degrees counterclockwise. Due to the vector identity $\boldsymbol{v} = (\boldsymbol{v} \cdot \mathbf{n}_T) \mathbf{n}_T + (\boldsymbol{v} \cdot \boldsymbol{\tau}_T) \boldsymbol{\tau}_T$ and summing over $T \in \mathcal{T}_h$, there holds

$$-\int_{\Omega} \Delta \boldsymbol{u} \cdot \boldsymbol{w}_{h} \, d\boldsymbol{x} = \int_{\Omega} \nabla_{h} \boldsymbol{u} : \nabla_{h} \boldsymbol{w}_{h} \, d\boldsymbol{x}$$

$$-\sum_{T \in \mathcal{T}_{h}} \int_{\partial T} \left(\frac{\partial (\boldsymbol{u} \cdot \mathbf{n}_{T})}{\partial \mathbf{n}_{T}} (\boldsymbol{w}_{h} \cdot \mathbf{n}_{T}) + \frac{\partial (\boldsymbol{u} \cdot \boldsymbol{\tau}_{T})}{\partial \mathbf{n}_{T}} (\boldsymbol{w}_{h} \cdot \boldsymbol{\tau}_{T}) \right) \, ds$$

$$= \int_{\Omega} \nabla_{h} \boldsymbol{u} : \nabla_{h} \boldsymbol{w}_{h} \, d\boldsymbol{x} - \sum_{T \in \mathcal{T}_{h}} \int_{\partial T} \frac{\partial (\boldsymbol{u} \cdot \boldsymbol{\tau}_{T})}{\partial \mathbf{n}_{T}} (\boldsymbol{w}_{h} \cdot \boldsymbol{\tau}_{T}) \, ds,$$

where ∇_h denotes the piecewise gradient operator and the normal continuity of \boldsymbol{w}_h was used to derive the second equality.

The sum of boundary integrals is now written as a sum of integrals over edges of the triangulation. Let $e \in \mathcal{E}_h^I$ with $e = \partial T_+ \cap \partial T_-$ and $T_\pm \in \mathcal{T}_h$. For a piecewise smooth vector-valued function \boldsymbol{w} the average and jump of \boldsymbol{w} across e, respectively, are defined as

$$\left\{\!\!\left\{\varepsilon(\boldsymbol{w})\right\}\!\!\right\}\big|_e := \frac{1}{2}\left(\frac{\partial(\boldsymbol{w}_+\cdot\boldsymbol{\tau}_{T_+})}{\partial\mathbf{n}_{T_+}} + \frac{\partial(\boldsymbol{w}_-\cdot\boldsymbol{\tau}_{T_-})}{\partial\mathbf{n}_{T_-}}\right), \quad \left[\!\!\left[\boldsymbol{w}\right]\!\!\right]_\tau\big|_e := \boldsymbol{w}_+\cdot\boldsymbol{\tau}_{T_+} + \boldsymbol{w}_-\cdot\boldsymbol{\tau}_{T_-},$$

where $\mathbf{w}_{\pm} = \mathbf{w}|_{T_{\pm}}$. For a boundary edge $e \in \mathcal{E}_h^B$ with $e = \partial T \cap \partial \Omega$ these operators are given by

$$\left.\left\{\left\{arepsilon(oldsymbol{w})
ight\}
ight|_e:=rac{\partial(oldsymbol{w}\cdotoldsymbol{ au}_T)}{\partial\mathbf{n}_T},\quad \left\|oldsymbol{w}
ight\|_{ au}\left|_e:=oldsymbol{w}\cdotoldsymbol{ au}_T.$$

Combining (4.19) with the algebraic identity $ab-cd=\frac{1}{2}(a-c)(b+d)+\frac{1}{2}(a+c)(b-d)$, and noting that the jump of \boldsymbol{u} vanishes on all edges, yields

$$-\int_{\Omega} \Delta \boldsymbol{u} \cdot \boldsymbol{w}_h \, d\boldsymbol{x} = \int_{\Omega} \nabla_h \boldsymbol{u} : \nabla_h \boldsymbol{w}_h \, d\boldsymbol{x} - \sum_{e \in \mathcal{E}_h} \int_e \{\!\!\{ \varepsilon(\boldsymbol{u}) \}\!\!\} \, [\![\boldsymbol{w}_h]\!]_{\tau} \, ds \quad \forall \, \boldsymbol{w}_h \in \boldsymbol{W}_h.$$

While the right-hand side of (4.19) induces a consistent bilinear form for the Laplace operator, it has two undesirable properties. First, the right-hand side is nonsymmetric with respect to \boldsymbol{u} and \boldsymbol{w}_h , which is in strong contrast to the self-adjoint property of the Laplacian. Second, the form induced by (4.19) restricted to $\boldsymbol{W}_h \times \boldsymbol{W}_h$ is noncoercive, again in contrast to the Laplace operator. A simple fix to address these issues is to exploit the jump-free property of \boldsymbol{u} and amend this identity with two trivial terms: (4.20)

$$-\int_{\Omega} \Delta \boldsymbol{u} \cdot \boldsymbol{w}_h \, d\boldsymbol{x} = \int_{\Omega} \nabla_h \boldsymbol{u} : \nabla_h \boldsymbol{w}_h \, d\boldsymbol{x}$$

$$-\sum_{e \in \mathcal{E}_h} \left(\int_e \{\!\{ \varepsilon(\boldsymbol{u}) \}\!\} \, [\![\boldsymbol{w}_h]\!]_{\tau} \, ds + \int_e \{\!\{\boldsymbol{w}_h\}\!\} \, [\![\boldsymbol{u}]\!]_{\tau} \, ds - \frac{\sigma}{h_e} \int_e [\![\boldsymbol{u}]\!]_{\tau} \, [\![\boldsymbol{w}_h]\!]_{\tau} \, ds \right)$$

$$=: a_h(\boldsymbol{u}, \boldsymbol{w}_h) \qquad \forall \, \boldsymbol{w}_h \in \boldsymbol{X}_h,$$

where $h_e = \text{diam}(e)$ and $\sigma > 0$ is some parameter. In the literature, the edge terms in the bilinear form $a_h(\cdot, \cdot)$, going from left to right, are commonly referred to (for obvious reasons) as consistency terms, symmetry terms, and penalization terms, respectively. The choice of the penalization parameter σ is dictated by the next lemma.

LEMMA 4.12 (see [77]). There exists $\sigma_0 > 0$ depending only on the shape regularity of \mathfrak{I}_h such that for $\sigma \geq \sigma_0$,

$$\frac{1}{2} \|\boldsymbol{w}_h\|_{1,h}^2 \le a_h(\boldsymbol{w}_h, \boldsymbol{w}_h) \qquad \forall \; \boldsymbol{w}_h \in \boldsymbol{W}_h,$$

where the discrete \mathbf{H}^1 -norm is defined as

$$\|\boldsymbol{w}\|_{1,h}^2 := \sum_{T \in \mathcal{T}_h} \|\nabla \boldsymbol{w}\|_{L^2(T)}^2 + \sum_{e \in \mathcal{E}_h} h_e \|\left\{\!\left\{\varepsilon(\boldsymbol{w})\right\}\!\right\}\|_{L^2(e)}^2 + \sum_{e \in \mathcal{E}_h} h_e^{-1} \|\left\|\boldsymbol{w}\right\|_{\tau}\|_{L^2(e)}^2.$$

Moreover, for all $\mathbf{w}_h \in \mathbf{W}_h$ and $\mathbf{v} \in \mathbf{H}^s(\Omega)$ with s > 3/2,

$$a_h(\mathbf{v}, \mathbf{w}_h) \le (1 + \sigma) \|\mathbf{v}\|_{1,h} \|\mathbf{w}_h\|_{1,h}.$$

This derivation of the bilinear form $a_h(\cdot,\cdot)$ motivates the finite element method for the Stokes problem using $\boldsymbol{H}(\operatorname{div},\Omega)$ -conforming elements: Find $(\boldsymbol{u}_h,p_h)\in \boldsymbol{W}_h\times Q_h$ satisfying

(4.21a)
$$a_h(\boldsymbol{u}_h, \boldsymbol{w}_h) + b(\boldsymbol{w}_h, p_h) = (\boldsymbol{f}, \boldsymbol{w}_h) \quad \forall \boldsymbol{w}_h \in \boldsymbol{W}_h,$$

$$(4.21b) b(\mathbf{u}_h, q_h) = (g, q_h) \forall \ q \in Q_h.$$

From the derivation of the bilinear form $a_h(\cdot, \cdot)$, one immediately sees that the method is consistent provided \boldsymbol{u} is sufficiently smooth (e.g., $\boldsymbol{u} \in \boldsymbol{H}^s(\Omega)$ with s > 3/2); in particular, if one interchanges \boldsymbol{u}_h with \boldsymbol{u} in (4.21), then the two statements are still satisfied. Furthermore, a combination of (4.18) and scaling arguments shows that the inf-sup condition is satisfied on $\boldsymbol{W}_h \times Q_h$ with respect to the discrete \boldsymbol{H}^1 -norm:

$$\inf_{q_h \in Q_h \setminus \{0\}} \sup_{\boldsymbol{w}_h \in \boldsymbol{W}_h \setminus \{\mathbf{0}\}} \frac{\int_{\Omega} (\nabla \cdot \boldsymbol{w}_h) q_h}{\|\boldsymbol{w}_h\|_{1,h} \|q_h\|_{L^2(\Omega)}} \ge \beta_h,$$

with β_h uniformly bounded. Therefore, in light of Lemma 4.12 and by slightly generalizing the framework of section 3, one concludes that if σ is sufficiently large, then there exists a unique solution to (4.21). Moreover, using the approximation properties of the finite element spaces (cf. (4.17)), and since the discretely divergence-free functions are weakly divergence-free, the errors satisfy

$$\|\boldsymbol{u} - \boldsymbol{u}_h\|_{1,h} \leq C \inf_{\boldsymbol{w}_h \in \boldsymbol{W}_h} \|\boldsymbol{u} - \boldsymbol{w}_h\|_{1,h} \leq Ch^{\ell-1} \|\boldsymbol{u}\|_{H^{\ell}(\Omega)},$$

$$\|p - p_h\|_{L^2(\Omega)} \leq C \left(\inf_{q_h \in Q_h} \|p - q_h\|_{L^2(\Omega)} + \nu \|\boldsymbol{u} - \boldsymbol{u}_h\|_{1,h}\right)$$

$$\leq C \left(h^m \|p\|_{H^m(\Omega)} + \nu h^{\ell-1} \|\boldsymbol{u}\|_{H^{\ell}(\Omega)}\right),$$

where $\ell = \min\{s, k+1\}$ and $\boldsymbol{u} \in \boldsymbol{H}^s(\Omega)$. If $p \in H^r(\Omega)$ and if $\boldsymbol{W}_h \times Q_h$ is the Raviart–Thomas pair, then $m = \min\{r, k+1\}$. If $\boldsymbol{W}_h \times Q_h$ is the BDM pair, then $m = \min\{r, k\}$.

Another class of $\mathbf{H}(\text{div}, \Omega)$ -conforming methods for the Stokes problem modifies the Raviart–Thomas and BDM spaces locally with divergence-free vector fields such that the resulting spaces possess weak tangential continuity [38, 58, 73, 79]. The reasoning behind this approach is that, if the spaces are augmented with divergence-free vector fields, then the inf-sup condition (4.18) is satisfied and discretely divergence-free functions are still weakly divergence-free. To be precise, the local spaces of these elements, in two dimensions, are of the form [38, 39]

(4.22)
$$\hat{\boldsymbol{W}}(T) = \boldsymbol{W}(T) + \operatorname{\mathbf{curl}}(b_T S(T)), \text{ with } \operatorname{\mathbf{curl}} q := \begin{pmatrix} \partial q / \partial x_2 \\ -\partial q / \partial x_1 \end{pmatrix},$$

where b_T is the cubic bubble function (i.e., the product of the three barycentric coordinates of T), S(T) is some auxiliary space, and $\mathbf{W}(T)$ is the local space of \mathbf{W}_h , that is, $\mathbf{W}(T) = \mathcal{P}_k(T)$ if \mathbf{W}_h is the BDM space or $\mathbf{W}(T) = \mathrm{RT}_k(T)$ if it is the Raviart-Thomas space. Clearly one has $\mathrm{div}\hat{\mathbf{W}}(T) = \mathrm{div}\mathbf{W}(T)$, indicating that the range of the divergence operator acting on the augmented space is preserved.

As an example, reference [58] takes $\mathbf{W}(T)$ to be the local, lowest order Raviart–Thomas space $\mathrm{RT}_0(T)$ and the auxiliary space to be the space of piecewise linear polynomials, $S(T) = \mathcal{P}_1(T)$. It is easy to see in this case that the sum in (4.22) is direct, and thus, the dimension of the local augmented space is $\dim \hat{\mathbf{W}}(T) = \dim \mathrm{RT}_0(T) + \dim \mathbf{curl}(b_T\mathcal{P}_1(T)) = \dim \mathrm{RT}_0(T) + \dim \mathcal{P}_1(T) = 3 + 3 = 6$. In addition to the property $\mathrm{div}\hat{\mathbf{W}}(T) = \mathrm{div}\mathrm{RT}_0(T) = \mathcal{P}_0(T)$, the normal component of functions in $\hat{\mathbf{W}}(T)$ are constant on the boundary of T. Indeed, if $\mathbf{w}_h = \mathbf{w}_0 + \mathbf{curl}(b_Tq_h) \in \hat{\mathbf{W}}(T)$ with $\mathbf{w}_0 \in \mathrm{RT}_0(T)$ and $q_h \in \mathcal{P}_1(T)$, then by properties of $\mathrm{RT}_0(T)$, the curl operator, and b_T ,

$$\left.oldsymbol{w}_h\cdot\mathbf{n}_e
ight|_e = oldsymbol{w}_0\cdot\mathbf{n}_e
ight|_e + \left.rac{\partial(q_hb_T)}{\partialoldsymbol{ au}_e}
ight|_e = oldsymbol{w}_0\cdot\mathbf{n}_e
ight|_e \in \mathfrak{P}_0(e).$$

On the only other hand, the tangential component is generally cubic.

In [58] it is shown that a function $\boldsymbol{w}_h \in \hat{\boldsymbol{W}}(T)$ is uniquely determined by the six values

$$\int_e \boldsymbol{w}_h \, ds, \qquad e \subset \partial T,$$

or equivalently,

(4.23)
$$\int_{e} \boldsymbol{w}_h \cdot \mathbf{n}_e \, ds, \quad \int_{e} \boldsymbol{w}_h \cdot \boldsymbol{\tau}_e \, ds, \quad e \subset \partial T.$$

The global space $\hat{\mathbf{W}}_h$ induced by the local space and degrees of freedom (4.23) is the space of L^2 -functions that are (i) locally in $\hat{\mathbf{W}}(T)$ on each $T \in \mathcal{T}_h$; (ii) continuous with respect to (4.23) on each $e \in \mathcal{E}_h^I$; and (iii) vanish on (4.23) for $e \subset \partial \Omega$.

Since the normal component of $\boldsymbol{w}_h \in \hat{\boldsymbol{W}}_h$ is constant on edges, the first set of degrees of freedom given in (4.23) implies that the normal component of \boldsymbol{w}_h is continuous across interior edges; thus, $\hat{\boldsymbol{W}}_h \subset \boldsymbol{H}(\operatorname{div},\Omega)$ (cf. Lemma 4.11) and the finite element space can be written as

$$\hat{\boldsymbol{W}}_h = \left\{ \boldsymbol{w}_h \in \boldsymbol{H}_0(\mathrm{div}; \Omega) : \ \boldsymbol{w}_h|_T \in \hat{\boldsymbol{W}}(T), \ \int_e \left[\|\boldsymbol{w}_h\|_{\tau} \ ds = 0 \ \forall \ e \in \mathcal{E}_h \right\}.$$

The pressure space is the space of discontinuous constants with vanishing mean,

$$Q_h = \{ q_h \in L_0^2(\Omega) : \ q|_T \in \mathcal{P}_0(T) \ \forall \ T \in \mathcal{T}_h \}.$$

Due to the high polynomial degree of the tangential component, the condition that $\int_e ||\boldsymbol{w}_h||_{\tau} ds = 0$ is not sufficient to ensure that $||\boldsymbol{w}_h||_{\tau} = 0$ on interior edges. As a result the global space is not \boldsymbol{H}^1 -conforming: $\hat{\boldsymbol{W}}_h \not\subset \boldsymbol{H}^1(\Omega)$; nonetheless,

$$(4.24) \qquad \qquad \int_e |\left[\left\| \boldsymbol{w}_h \right\|_{\tau} \right]^2 ds \leq C h \|\nabla_h \boldsymbol{w}_h\|_{L^2(\omega_e)}^2 \quad \forall \ \boldsymbol{w}_h \in \hat{\boldsymbol{W}}_h,$$

where ω_e denotes the set of triangles with e as an edge. One concludes from this estimate that, although the space is not globally conforming, it does possess a weak type of continuity across edges.

The finite element method for the Stokes problem utilizing these spaces has the same form as (4.21), but with \mathbf{W}_h replaced by $\hat{\mathbf{W}}_h$, and with the bilinear form $a_h(\cdot,\cdot)$ defined as

$$a_h(oldsymbol{w}, oldsymbol{v}) = \int_{\Omega}
abla_h oldsymbol{w} :
abla_h oldsymbol{v} \, doldsymbol{x}.$$

From the previous arguments, one concludes that this form is not consistent with the Laplace operator since \hat{W}_h is not globally continuous. However, one can exploit the weak continuity of \hat{W}_h to show

$$\left| - \int_{\Omega} (\Delta \boldsymbol{u}) \cdot \boldsymbol{v}_h \, d\boldsymbol{x} - a_h(\boldsymbol{u}, \boldsymbol{v}_h) \right| \le Ch \|\boldsymbol{u}\|_{H^2(\Omega)} \|\nabla_h \boldsymbol{v}_h\|_{L^2(\Omega)} \quad \forall \ \boldsymbol{v}_h \in \hat{\boldsymbol{W}}_h.$$

Using this result, it can be proved that there exists a unique solution to the finite element method and the errors satisfy

$$\|\nabla_h(\boldsymbol{u} - \boldsymbol{u}_h)\|_{L^2(\Omega)} \le Ch\|\boldsymbol{u}\|_{H^2(\Omega)},$$

$$\|p - p_h\|_{L^2(\Omega)} \le Ch(\|p\|_{H^1(\Omega)} + \nu\|\boldsymbol{u}\|_{H^2(\Omega)}).$$

5. Improving the Pressure-Robustness of Standard Mixed Finite Elements.

The (vast) majority of finite element codes contains only standard finite element methods such that the use of standard mixed methods is a straightforward option for the discretization of incompressible flow problems. Hence, approaches for improving the pressure-robustness of standard mixed methods are of great interest. There are essentially two such approaches, of which both modify the bilinear form of the momentum equation of the finite element problem. The grad-div stabilization adds a penalty with respect to the continuity equation. This method can be applied to any standard mixed method; it reduces the lack of pressure-robustness, but does not remove it. The second method chooses appropriate test functions for some terms of the finite element formulation to reestablish properties from the continuous equation in the finite element problem, e.g., the fundamental invariance property (1.4). This rather new approach is currently known to be applicable to a number of mixed methods with discontinuous pressure, and it was extended recently to the Taylor-Hood and mini-finite-element family in [49]. It leads to pressure-robust discretizations. For the sake of completeness, a postprocessing technique for low order pairs of finite element spaces that do not satisfy the discrete inf-sup condition will be briefly discussed.

5.1. Grad-div Stabilization. Grad-div stabilization is probably the most popular technique for improving the pressure-robustness of pairs of finite element spaces which do not satisfy the continuity equation in a sufficiently strong sense. In practice, it is usually applied in the case $\nabla \cdot \boldsymbol{u} = 0$ and the discussion herein will be restricted to

this case. An extension to $\nabla \cdot \boldsymbol{u} = g$ is possible with additional technical details. For g = 0, the insufficient satisfaction of the continuity equation means that the finite element solution is not divergence-free in the sense of Definition 2.3.

The grad-div stabilization arises from adding $\mathbf{0} = -\gamma \nabla (\nabla \cdot \boldsymbol{u})$ to the continuous momentum equation. Applying integration by parts in deriving the weak formulation of the equation and then replacing the infinite-dimensional spaces with finite element spaces leads to the term $\gamma(\nabla \cdot \boldsymbol{u}_h, \nabla \cdot \boldsymbol{v}_h)$ in the finite element formulation. As has been discussed throughout this article, $\nabla \cdot \boldsymbol{u}_h \neq 0$ in most common finite element choices, such as the Taylor–Hood pair of spaces, and so this "grad-div term" is nonzero and does have an effect on the discrete solution. Grad-div stabilization was first introduced in [32] and has been widely studied over the past decade.

To see the effect of grad-div stabilization, consider again the discrete Stokes system (1.2), but now with a grad-div term and with g = 0. Assuming that (X_h, Y_h) satisfies the discrete inf-sup condition (3.2), the grad-div stabilized Stokes system takes the following form: Find $u_h \in X_{h,\text{div}}$ such that

(5.1)
$$a(\boldsymbol{u}_h, \boldsymbol{v}_h) + \gamma(\nabla \cdot \boldsymbol{u}_h, \nabla \cdot \boldsymbol{v}_h) = (\boldsymbol{f}, \boldsymbol{v}_h) \quad \forall \ \boldsymbol{v}_h \in \boldsymbol{X}_{h, \text{div}},$$

where the bilinear form $a(\cdot, \cdot)$ is given in (2.1a). Since $a(\cdot, \cdot)$ is positive definite and the term $\gamma(\nabla \cdot \boldsymbol{u}_h, \nabla \cdot \boldsymbol{v}_h)$ is positive semidefinite, the existence and uniqueness of a solution of the grad-div stabilized discrete Stokes system follow directly from the lemma of Lax–Milgram.

First, it will be shown that the grad-div stabilization penalizes the divergence error. This fact can be seen immediately from an a priori estimate found by taking $v_h = u_h$ in (5.1). Applying the estimate for the dual pairing yields

$$\nu \|\nabla \boldsymbol{u}_h\|_{L^2(\Omega)}^2 + \gamma \|\nabla \cdot \boldsymbol{u}_h\|_{L^2(\Omega)}^2 = (\boldsymbol{f}, \boldsymbol{u}_h) \le \|\boldsymbol{f}\|_{H^{-1}(\Omega)} \|\nabla \boldsymbol{u}_h\|_{L^2(\Omega)} \\
\le \frac{\nu^{-1}}{2} \|\boldsymbol{f}\|_{H^{-1}(\Omega)}^2 + \frac{\nu}{2} \|\nabla \boldsymbol{u}_h\|_{L^2(\Omega)}^2.$$

Reducing this estimate gives

(5.2)
$$\nu \|\nabla \boldsymbol{u}_h\|_{L^2(\Omega)}^2 + 2\gamma \|\nabla \cdot \boldsymbol{u}_h\|_{L^2(\Omega)}^2 \le \nu^{-1} \|\boldsymbol{f}\|_{H^{-1}(\Omega)}^2.$$

Since f is given, the right-hand side is a fixed constant independent of γ . Thus, taking γ larger forces the divergence error to become smaller, since (5.2) implies that $\|\nabla \cdot \boldsymbol{u}_h\|_{L^2(\Omega)} \leq \mathfrak{O}(\gamma^{-1/2})$.

Estimate (5.2) can be refined to obtain a stronger scaling with γ , following [35]. Denote by V_h the weakly divergence-free subspace of X_h , i.e.,

$$V_h := \{ v_h \in X_h : \|\nabla \cdot v_h\|_{L^2(\Omega)} = 0 \},$$

and let V_h^{\perp} be its orthogonal complement in $X_{h,\text{div}}$ with respect to the inner product induced by $a(\cdot,\cdot)$. It is shown in [35] that for $v_h^r \in V_h^{\perp}$,

$$\|\nabla \boldsymbol{v}_h^r\|_{L^2(\Omega)} \le C(h) \|\nabla \cdot \boldsymbol{v}_h^r\|_{L^2(\Omega)},$$

with C(h) potentially depending inversely on h. However, on certain types of meshes and element degrees, it can even be independent of h [36, 56]. Orthogonally decomposing the solution into $\boldsymbol{u}_h = \boldsymbol{u}_h^0 + \boldsymbol{u}_h^r$ with $\boldsymbol{u}_h^0 \in \boldsymbol{V}_h$ and $\boldsymbol{u}_h^r \in \boldsymbol{V}_h^{\perp}$, choosing $\boldsymbol{v}_h = \boldsymbol{u}_h^r$ in (5.1), and using $a(\boldsymbol{u}_h^0, \boldsymbol{u}_h^r) = 0$ and $\nabla \cdot \boldsymbol{u}_h^0 = 0$ gives

$$\nu \|\nabla \boldsymbol{u}_h^r\|_{L^2(\Omega)}^2 + \gamma \|\nabla \cdot \boldsymbol{u}_h^r\|_{L^2(\Omega)}^2 \leq \|\boldsymbol{f}\|_{-1} \|\nabla \boldsymbol{u}_h^r\|_{L^2(\Omega)} \leq C(h) \|\boldsymbol{f}\|_{H^{-1}(\Omega)} \|\nabla \cdot \boldsymbol{u}_h^r\|_{L^2(\Omega)},$$

and consequently

$$\|\nabla \cdot \boldsymbol{u}_h\|_{L^2(\Omega)} = \|\nabla \cdot \boldsymbol{u}_h^r\|_{L^2(\Omega)} \le C(h, \boldsymbol{f})\gamma^{-1}.$$

Hence, on a fixed mesh, one can expect first order convergence to zero of the divergence error as γ^{-1} goes to zero.

It will now be discussed that the grad-div stabilization can reduce the effect of the pressure on the velocity error. The error estimate without grad-div stabilization for the Galerkin discretization is given in (3.5). It will be emphasized once more that if the pressure p is large or complex, then the second term on the right-hand side of (3.5) becomes the dominant term of the error bound. This term represents the best approximation error of the pressure scaled by ν^{-1} . Note that for the Navier–Stokes equations and other related problems, error estimates will often have this same pressure term [47], and so similar issues occur there as well.

The finite element error analysis starts by deriving an error equation for the graddiv stabilized finite element method (5.1) by subtracting the scheme from the weak form of the Stokes equation (2.1a),

$$\nu(\nabla e, \nabla v_h) + \gamma(\nabla \cdot e, \nabla \cdot v_h) = (p, \nabla \cdot v_h) = (p - q_h, \nabla \cdot v_h) \quad \forall v_h \in X_{h, \text{div}},$$

where $e = u - u_h$ and q_h is arbitrary in Y_h . For arbitrary $\tilde{u}_h \in X_{h,\text{div}}$, the error is decomposed into $e = (u - \tilde{u}_h) - (u_h - \tilde{u}_h) =: \eta - \phi_h$. Then choosing $v_h = \phi_h$ provides

$$\nu \|\nabla \phi_h\|_{L^2(\Omega)}^2 + \gamma \|\nabla \cdot \phi_h\|_{L^2(\Omega)}^2 = -(p - q_h, \nabla \cdot \phi_h) + \gamma(\nabla \cdot \eta, \nabla \cdot \phi) + \nu(\nabla \eta, \nabla \phi),$$

which immediately reduces with Cauchy-Schwarz and Young's inequalities to

$$\nu \|\nabla \phi_h\|_{L^2(\Omega)}^2 + \gamma \|\nabla \cdot \phi_h\|_{L^2(\Omega)}^2 \le 2(p - q_h, \nabla \cdot \phi_h) + \gamma \|\nabla \cdot \eta\|_{L^2(\Omega)}^2 + \nu \|\nabla \eta\|_{L^2(\Omega)}^2.$$

Next, the pressure is majorized by using again Cauchy–Schwarz and Young's inequalities,

$$2(p - q_h, \nabla \cdot \phi_h) \le 2\gamma^{-1} \|p - q_h\|_{L^2(\Omega)}^2 + \frac{\gamma}{2} \|\nabla \cdot \phi_h\|_{L^2(\Omega)}^2.$$

Absorbing the second term on the right-hand side with a corresponding term on the left-hand side is not possible for the Galerkin discretization considered in section 3. Inserting this estimate and applying the triangle inequality yields

$$(5.3) \quad \|\nabla(\boldsymbol{u} - \boldsymbol{u}_h)\|_{L^{2}(\Omega)}^{2} + \frac{\gamma}{2\nu} \|\nabla \cdot (\boldsymbol{u} - \boldsymbol{u}_h)\|_{L^{2}(\Omega)}^{2}$$

$$\leq \frac{4}{\gamma\nu} \inf_{q_h \in Y_h} \|p - q_h\|_{L^{2}(\Omega)}^{2} + \inf_{\tilde{\boldsymbol{u}}_h \in \boldsymbol{X}_{h, \text{div}}} \left(4\|\nabla(\boldsymbol{u} - \tilde{\boldsymbol{u}}_h)\|_{L^{2}(\Omega)}^{2} + \frac{3\gamma}{\nu} \|\nabla \cdot (\boldsymbol{u} - \tilde{\boldsymbol{u}}_h)\|_{L^{2}(\Omega)}^{2}\right).$$

Comparing this estimate to (3.5) and considering the choice $\gamma > \nu$, then the scaling of the velocity error (in the \boldsymbol{H}^1 norm) with the best approximation error of the pressure is reduced from ν^{-1} to $\nu^{-1/2}\gamma^{-1/2}$. Thus, if the best approximation error of the pressure is the dominant source of the velocity error, grad-div stabilization can reduce the velocity error, sometimes substantially depending on the relative size of the pressure approximation error and the velocity approximation error.

In some finite element settings, the weakly divergence-free subspace V_h of the velocity space has optimal approximation properties in the sense of

$$\inf_{\tilde{\boldsymbol{v}}_h \in \boldsymbol{V}_h} \|\nabla(\boldsymbol{v} - \tilde{\boldsymbol{v}}_h)\|_{L^2(\Omega)} \leq C \inf_{\tilde{\boldsymbol{v}}_h \in \boldsymbol{X}_h} \|\nabla(\boldsymbol{v} - \tilde{\boldsymbol{v}}_h)\|_{L^2(\Omega)}$$

holding when $\nabla \cdot \boldsymbol{v} = 0$. For example, this holds for $\boldsymbol{X}_h = \boldsymbol{\mathcal{P}}_k$ with k = d on barycenter-refined triangular/tetrahedral meshes [68, 80]. In such cases, the error analysis for the grad-div stabilized discretization can be modified by taking $\tilde{\boldsymbol{u}}_h \in \boldsymbol{V}_h$, which leads to $\|\nabla \cdot \boldsymbol{\eta}\|_{L^2(\Omega)} = 0$ and provides the modified error estimate

$$\|\nabla(\boldsymbol{u} - \boldsymbol{u}_h)\|_{L^2(\Omega)}^2 + \frac{\gamma}{\nu} \|\nabla \cdot (\boldsymbol{u} - \boldsymbol{u}_h)\|_{L^2(\Omega)}^2$$

$$\leq C \left(\frac{1}{\gamma \nu} \inf_{q_h \in Y_h} \|p - q_h\|_{L^2(\Omega)}^2 + \inf_{\tilde{\boldsymbol{u}}_h \in \boldsymbol{X}_h} \|\nabla(\boldsymbol{u} - \tilde{\boldsymbol{u}}_h)\|_{L^2(\Omega)}^2\right).$$

This estimate is better than (5.3) in the sense that one can take in (5.4) large values of γ without increasing the error bound at all. The best approximation error in $X_{h,\text{div}}$ appearing in (5.3) can be estimated with the best approximation error in X_h using (4.2). Since $V_h \subset X_{h,\text{div}}$, the constant in (5.4) will potentially be bigger than the constant which is introduced by applying (4.2) to (5.3). On the other hand, one can take γ arbitrarily large (up to where the condition number of the linear system of equations becomes prohibitively large) and essentially completely remove the impact of the pressure on the velocity error.

Proposals for the choice of the stability parameter γ in practice rely on equilibrating the terms in the error bound containing γ . For instance, if both infima on the right-hand side of (5.3) are asymptotically of the same order, then this approach leads to $\gamma \sim 1$ with respect to the mesh width. A careful study of optimal choices of γ with respect to error bounds in different norms and of the dependence of γ on norms of the solution of the Stokes problem can be found in [43]. In this paper, the analytical results were supported with comprehensive numerical studies. It turns out that for each concrete example an appropriate choice typically depends on several aspects, so a good choice is not usually a priori clear.

In summary, grad-div stabilization is a popular and simple technique for improving the pressure-robustness of any mixed method. It is now well known that it penalizes for lack of mass conservation, can improve solution accuracy for simulations of Stokes and Navier-Stokes equations by reducing the effect of the pressure on the velocity error [48, 66, 64, 65], and can improve conditioning of discrete systems [37] and convergence of iterative solvers [13, 15, 20, 40]. It has also been shown to improve solution accuracy for related coupled multiphysics problems [28, 35, 44, 57, 74]. Some recent studies have considered the optimal choice of the parameter γ . Although $\gamma \sim 1$ is often a good choice with Taylor-Hood elements, some guidelines are given in [43] for potentially better choices, depending on the pair of finite element spaces, the mesh structure, the relative size of the pressure and the size of the velocity, and whether or not the sequence of weakly divergence-free subspaces of the discrete velocity spaces has an optimal approximation property. For the time-dependent Oseen and Navier-Stokes equations, it has been shown in [3, 27] that the use of grad-div stabilization leads to error bounds for the energy norm with constants independent of inverse powers of ν . Consequently, the error bound for the L^2 norm of the velocity gradient depends explicitly on $\nu^{-1/2}$, which is a weaker dependence than for the Galerkin discretization. However, grad-div stabilization is not a complete remedy in the sense that a pressure-robust method is not constructed in this way; see also Example 6.2.

5.2. Using Appropriate Reconstructions of Test Functions. This section shows that an appropriate modification of the test functions might lead to *pressure-robust* mixed methods. This recent and quite general approach was introduced in [50, 51, 52],

and it is based on well-understood inf-sup stable mixed methods. The modifications of the standard mixed methods are not severe, and in the case of the Stokes equations, the stiffness matrix is actually unchanged.

The approach is based on the observation that test and trial functions play quite different roles. Changing the velocity test functions by using an H(div)-conforming velocity reconstruction operator, one establishes the L^2 -orthogonality between discretely divergence-free test functions and arbitrary gradient fields. In this way, one obtains the discrete counterpart of the Helmholtz-Hodge decomposition, Lemma 2.6, which is relaxed in classical mixed methods, and the fundamental invariance property (1.4) is also recovered. In addition, one obtains a discrete vorticity equation which is close to (4.8) for pressure-robust mixed methods with $X_{h,\text{div}} \subset X_{\text{div}}$. The price to pay is an additional velocity-dependent consistency error, which is, however, of sufficiently high order.

While the approach was originally presented and analyzed for the first order nonconforming Crouzeix–Raviart element, it will be presented here for the conforming pair of finite element spaces $\boldsymbol{X}_h/Y_h = \boldsymbol{\mathcal{P}}_2^{\text{bubble}}/\mathcal{P}_1^{\text{disc}}$, to enable a better comparison with the results from section 3. Besides the discrete spaces X_h and Y_h , the construction of the method needs the first order Raviart-Thomas space $\mathbf{R}_h := \mathrm{RT}_1$, which is an H(div)-conforming space (cf. section 4.4). Important properties of \mathbf{R}_h utilized for the construction of the method are:

- for all $v_h \in \mathbf{R}_h, e \subset \partial T, T \in \mathfrak{T}_h$ it holds that $v_h|_e \in \mathfrak{P}_1(e)$;
- $$\begin{split} \bullet & \text{ for all } q \in \mathcal{P}_1(e), \, \int_e q \, [|\boldsymbol{v}_h \cdot \boldsymbol{n}_e|]_\tau \, \, d\mathbf{s} = 0; \\ \bullet & \text{ for all } \boldsymbol{v}_h \in \mathbf{R}_h \text{ it holds that } \nabla \cdot \boldsymbol{v}_h \in Y_h. \end{split}$$

The construction of the method requires the definition of a velocity reconstruction operator $\Pi_h : X \to \mathbf{R}_h$ satisfying the following properties:

(5.5)
$$\int_{T} (\boldsymbol{v} - \Pi_{h} \boldsymbol{v}) d\boldsymbol{x} = 0 \qquad \forall \ \boldsymbol{v} \in \boldsymbol{X}, \forall \ T \in \mathcal{T}_{h},$$

(5.6)
$$\int (\boldsymbol{v} - \Pi_h \boldsymbol{v}) \cdot \mathbf{n}_e q_h \ d\mathbf{s} = 0 \quad \forall \ \boldsymbol{v} \in \boldsymbol{X}, \forall \ q_h \in \mathcal{P}_1(e),$$

(5.7)
$$\|\Pi_h \mathbf{v} - \mathbf{v}\|_{L^2(T)} \le C h_T^m |\mathbf{v}|_{H^m(T)}, \quad m = 1, 2,$$

with a constant C depending only on the angles of T. By this definition, the reconstruction operator is just the standard Fortin interpolator for the RT₁ element. Using the product rule, integration by parts, (5.5), (5.6), the fact that $\nabla q_h|_T$ is constant, and integration by parts again gives for $v \in X$, for all $T \in \mathcal{T}_h$, and for all $q_h \in Y_h$

$$\int_{T} \nabla \cdot \boldsymbol{v} q_{h} \, d\boldsymbol{x} = \int_{T} \nabla \cdot (\boldsymbol{v} q_{h}) \, d\boldsymbol{x} - \int_{T} \nabla q_{h} \cdot \boldsymbol{v} \, d\boldsymbol{x} = \int_{\partial T} q_{h} \boldsymbol{v} \cdot \mathbf{n}_{T} \, d\mathbf{s} - \int_{T} \nabla q_{h} \cdot \boldsymbol{v} \, d\boldsymbol{x}$$

$$= \int_{\partial T} q_{h} (\Pi_{h} \boldsymbol{v}) \cdot \mathbf{n}_{T} \, d\mathbf{s} - \int_{T} \nabla q_{h} \cdot (\Pi_{h} \boldsymbol{v}) \, d\boldsymbol{x} = \int_{T} \nabla \cdot (\Pi_{h} \boldsymbol{v}) q_{h} \, d\boldsymbol{x}.$$
(5.8)

Consequently, it holds that

(5.9)
$$\nabla \cdot (\Pi_h \mathbf{v}) = \pi_{Y_h} (\nabla \cdot \mathbf{v}).$$

In particular, for discretely divergence-free vector fields $v_h \in X_{h,\mathrm{div}}$ the left-hand side of (5.8) vanishes such that from (5.9) it follows that such fields are mapped to divergence-free fields in the sense of $\mathbf{H}(\text{div}, \Omega)$.

Now, the modified scheme reads as follows: Find $(\boldsymbol{u}_h, p_h) \in \boldsymbol{X}_h \times Y_h$ such that for all $(\boldsymbol{v}_h, q_h) \in \boldsymbol{X}_h \times Y_h$,

(5.10a)
$$a(\boldsymbol{u}_h, \boldsymbol{v}_h) + b(\boldsymbol{v}_h, p_h) = (\boldsymbol{f}, \Pi_h \boldsymbol{v}_h),$$
(5.10b)
$$b(\boldsymbol{u}_h, q_h) = (q, q_h).$$

LEMMA 5.1. Let $u \in H^3(\Omega)$ and $v \in X$; then it holds that

$$(5.11) \qquad |(\Delta \boldsymbol{u}, \Pi_h \boldsymbol{v}) + (\nabla \boldsymbol{u}, \nabla \boldsymbol{v})| \le C \sum_{T \in \mathcal{T}_h} h_T^2 |\boldsymbol{u}|_{H^3(T)} |\boldsymbol{v}|_{H^1(T)}.$$

Proof. Using integration by parts, (5.5), the Cauchy–Schwarz inequality, and interpolation estimates for both factors, e.g., (5.7), yields

$$\begin{split} (\Delta \boldsymbol{u}, \Pi_h \boldsymbol{v}) + (\nabla \boldsymbol{u}, \nabla \boldsymbol{v}) &= (\Delta \boldsymbol{u}, \Pi_h \boldsymbol{v} - \boldsymbol{v}) + (\nabla \boldsymbol{u}, \nabla \boldsymbol{v}) + (\Delta \boldsymbol{u}, \boldsymbol{v}) \\ &= (\Delta \boldsymbol{u} - \boldsymbol{\pi}_{\mathcal{P}_0(T)} \Delta \boldsymbol{u}, \Pi_h \boldsymbol{v} - \boldsymbol{v}) \\ &\leq C \sum_{T \in \mathcal{T}_h} h_T^2 \left| \boldsymbol{u} \right|_{H^3(T)} \left| \boldsymbol{v} \right|_{H^1(T)}. \end{split}$$

THEOREM 5.2. Assume that the solution of the Stokes equations (2.1) satisfies $\mathbf{u} \in \mathbf{H}^3(\Omega)$ and $p \in H^2(\Omega)$. Let the finite element problem (5.10) be discretized with $\mathfrak{P}_2^{\text{bubble}}/\mathfrak{P}_1^{\text{disc}}$; then the following error bounds hold:

(5.12)

$$\|\nabla(\boldsymbol{u} - \boldsymbol{u}_{h})\|_{L^{2}(\Omega)} \leq 2(1 + C_{F}) \inf_{\boldsymbol{w}_{h} \in \boldsymbol{X}_{h}} \|\nabla(\boldsymbol{u} - \boldsymbol{w}_{h})\|_{L^{2}(\Omega)} + Ch^{2} |\boldsymbol{u}|_{H^{3}(\Omega)},$$

$$(5.13)$$

$$\|\pi_{Y_{h}} p - p_{h}\|_{L^{2}(\Omega)} \leq \frac{\nu}{\beta_{h}} \left(2(1 + C_{F}) \inf_{\boldsymbol{w}_{h} \in \boldsymbol{X}_{h}} \|\nabla(\boldsymbol{u} - \boldsymbol{w}_{h})\|_{L^{2}(\Omega)} + Ch^{2} |\boldsymbol{u}|_{H^{3}(\Omega)} \right),$$

$$(5.14) \|p - p_{h}\|_{L^{2}(\Omega)} \leq \inf_{q_{h} \in Y_{h}} \|p - q_{h}\|_{L^{2}(\Omega)}$$

$$+ \frac{\nu}{\beta_{h}} \left(2(1 + C_{F}) \inf_{\boldsymbol{w}_{h} \in \boldsymbol{X}_{h}} \|\nabla(\boldsymbol{u} - \boldsymbol{w}_{h})\|_{L^{2}(\Omega)} + Ch^{2} |\boldsymbol{u}|_{H^{3}(\Omega)} \right).$$

Proof. Because of $\boldsymbol{u}_h \in \boldsymbol{X}_{h,\operatorname{div}}(g)$ it holds for an arbitrary $\boldsymbol{w}_h \in \boldsymbol{X}_{h,\operatorname{div}}(g)$ that $\boldsymbol{v}_h^0 := \boldsymbol{u}_h - \boldsymbol{w}_h \in \boldsymbol{X}_{h,\operatorname{div}}$. Since $\Pi_h \boldsymbol{v}_h^0 \in \boldsymbol{H}(\operatorname{div},\Omega)$ is weakly divergence-free and the homogeneous boundary condition of \boldsymbol{v}_h^0 induces that $\Pi_h \boldsymbol{v}_h^0 \cdot \mathbf{n}$ vanishes on $\partial \Omega$, one gets that $(\nabla p, \Pi_h \boldsymbol{v}_h^0) = 0$. Using this property, after applying (5.10a), gives

$$\begin{split} \nu \| \nabla \boldsymbol{v}_h^0 \|_{L^2(\Omega)}^2 &= a(\boldsymbol{v}_h^0, \boldsymbol{v}_h^0) = a(\boldsymbol{u}_h, \boldsymbol{v}_h^0) - a(\boldsymbol{w}_h, \boldsymbol{v}_h^0) \\ &= (-\nu \Delta \boldsymbol{u} + \nabla p, \Pi_h \boldsymbol{v}_h^0) - a(\boldsymbol{w}_h, \boldsymbol{v}_h^0) \\ &= a(\boldsymbol{u} - \boldsymbol{w}_h, \boldsymbol{v}_h^0) - \nu \left((\Delta \boldsymbol{u}, \Pi_h \boldsymbol{v}_h^0) + (\nabla \boldsymbol{u}, \nabla \boldsymbol{v}_h^0) \right). \end{split}$$

Using (5.11) and the Cauchy–Schwarz inequality yields

$$\nu \|\nabla \boldsymbol{v}_h^0\|_{L^2(\Omega)}^2 \le \nu \|\nabla (\boldsymbol{u} - \boldsymbol{w}_h)\|_{L^2(\Omega)} \|\nabla \boldsymbol{v}_h^0\|_{L^2(\Omega)} + \nu C h^2 |\boldsymbol{u}|_{H^3(\Omega)} \|\nabla \boldsymbol{v}_h^0\|_{L^2(\Omega)},$$
 such that

$$\|\nabla \boldsymbol{v}_h^0\|_{L^2(\Omega)} \leq \inf_{\boldsymbol{w}_h \in \boldsymbol{X}_{h,\operatorname{div}}(q)} \|\boldsymbol{u} - \boldsymbol{w}_h\|_{L^2(\Omega)} + Ch^2 |\boldsymbol{u}|_{H^3(\Omega)}.$$

With the triangle inequality it follows that

$$\|\nabla(\boldsymbol{u} - \boldsymbol{u}_h)\|_{L^2(\Omega)} \le \|\nabla(\boldsymbol{u} - \boldsymbol{w}_h)\|_{L^2(\Omega)} + \|\nabla \boldsymbol{v}_h^0\|_{L^2(\Omega)}.$$

Inserting now the estimate for $\|\nabla v_h^0\|_{L^2(\Omega)}$, noting that w_h was chosen to be arbitrary, and applying (4.2) finishes the proof of estimate (5.12).

To prove (5.13), consider an arbitrary function $v_h \in X_h$. Then $\nabla \cdot \Pi_h v_h \in Y_h$ and from the definition of the L^2 -projection and (5.8) it follows that

$$(5.15) (p, \nabla \cdot \Pi_h \boldsymbol{v}_h) = (\pi_{Y_h} p, \nabla \cdot \Pi_h \boldsymbol{v}_h) = (\pi_{Y_h} p, \nabla \cdot \boldsymbol{v}_h).$$

Using (5.10a), integration by parts, and (5.15) now yields

$$(\pi_{Y_h}p - p_h, \nabla \cdot \boldsymbol{v}_h) = (\pi_{Y_h}p, \nabla \cdot \boldsymbol{v}_h) + (\boldsymbol{f}, \Pi_h \boldsymbol{v}_h) - a(\boldsymbol{u}_h, \boldsymbol{v}_h)$$

$$= (\pi_{Y_h}p, \nabla \cdot \boldsymbol{v}_h) + (\nabla p, \Pi_h \boldsymbol{v}_h) - (\nu \Delta \boldsymbol{u}, \Pi_h \boldsymbol{v}_h) - a(\boldsymbol{u}_h, \boldsymbol{v}_h)$$

$$= (\pi_{Y_h}p, \nabla \cdot \boldsymbol{v}_h) - (p, \nabla \cdot \Pi_h \boldsymbol{v}_h) - (\nu \Delta \boldsymbol{u}, \Pi_h \boldsymbol{v}_h) - a(\boldsymbol{u}_h, \boldsymbol{v}_h)$$

$$= -(\nu \Delta \boldsymbol{u}, \Pi_h \boldsymbol{v}_h) - a(\boldsymbol{u}_h, \boldsymbol{v}_h)$$

$$= -(\nu \Delta \boldsymbol{u}, \Pi_h \boldsymbol{v}_h) - a(\boldsymbol{u}, \boldsymbol{v}_h) - a(\boldsymbol{u}_h - \boldsymbol{u}, \boldsymbol{v}_h).$$

Inserting this expression in the discrete inf-sup condition (3.2) and applying the triangle and Cauchy–Schwarz inequalities and (5.11) gives

$$\|\pi_{Y_h} p - p_h\| \leq \frac{\nu}{\beta_h} \left(\|\nabla(\boldsymbol{u} - \boldsymbol{u}_h)\|_{L^2(\Omega)} + \sup_{\boldsymbol{0} \neq \boldsymbol{v}_h \in \boldsymbol{X}_h} \frac{|(\Delta \boldsymbol{u}, \Pi_h \boldsymbol{v}_h) + (\nabla \boldsymbol{u}, \nabla \boldsymbol{v}_h)|}{\|\nabla \boldsymbol{v}_h\|_{L^2(\Omega)}} \right)$$
$$\leq \frac{\nu}{\beta_h} \left(\|\nabla(\boldsymbol{u} - \boldsymbol{u}_h)\|_{L^2(\Omega)} + Ch^2 |\boldsymbol{u}|_{H^3(\Omega)} \right).$$

The proof of (5.13) is finished by inserting (5.12).

Estimate (5.14) is a direct consequence of the triangle inequality

$$||p-p_h||_{L^2(\Omega)} \le ||p-\pi_{Y_h}p||_{L^2(\Omega)} + ||\pi_{Y_h}p-p_h||_{L^2(\Omega)},$$

estimate (5.13), and the observation that the L^2 -projection is the best approximation in the $L^2(\Omega)$ norm.

The error estimates above show that, to achieve pressure-robustness, the inclusion $X_{h,\text{div}} \subset X_{\text{div}}$ is not needed. In fact, for the incompressible Stokes equations a lack of pressure-robustness can only evolve in the discretization of the right-hand side term (f, v_h) . The key idea is to repair the L^2 scalar product, in order to ensure that discretely divergence-free vector fields become orthogonal to gradient fields. For more complex flows than the incompressible Stokes equations, one has to repair this kind of L^2 -orthogonality in every term of the discrete weak formulation, where some force is tested in the L^2 sense with a test function v_h . This issue also concerns the nonlinear convection term $(u_h \cdot \nabla)u_h$ and the Coriolis force term; see [51, 53]. So far, the approach has been generalized to mixed discretizations of arbitrarily high order on triangles, tetrahedra, squares, and cuboids, if the discrete pressures are discontinuous [52]. Extensions for conforming mixed methods with continuous pressure are presented in [49].

Remark 5.3. Instead of $\mathbf{R}_h = \mathrm{RT}_1$ one can also use $\mathbf{R}_h := \mathrm{BDM}_2$ and its standard Fortin interpolator Π_h . This approach has the advantage of a possibly smaller consistency error and it leaves quadratic test functions untouched. In other words,

only the nonquadratic bubble functions have to be modified. This version of the reconstruction was used in the numerical examples below. Similarly, the test functions of the lowest order Bernardi–Raugel element were reconstructed into $\mathbf{R}_h := \mathrm{BDM}_1$ with the associated standard Fortin interpolator, which only affects the normal-weighted face bubbles.

- 5.3. Postprocessing of Low Order Velocity Fields Computed with Non-inf-sup Stable Methods. An approach for postprocessing a finite element solution in such a way that one obtains a divergence-free solution in $H(\operatorname{div},\Omega)$ was proposed for certain stabilized discretizations in [10, 11, 12]. In these papers, two-dimensional problems were considered which were discretized with \mathcal{P}_1 finite elements for the velocity and \mathcal{P}_0 or \mathcal{P}_1 finite elements for the pressure. The stabilization with respect to the discrete inf-sup condition is based on jumps of ∇u_h or p_h across the edges of the mesh cells. The basic idea of this approach consists of adding a correction from $\mathrm{RT}_0(\mathcal{T}_h)$ to u_h so that the resulting discrete velocity is divergence-free. The concrete form of the correction depends on the stabilization used. It can be shown that the divergence-free velocity field converges with optimal order in appropriate norms.
- **6. Numerical Studies.** This section presents a couple of examples which illustrate situations in which the methods discussed in the previous sections are beneficial, and also situations where standard methods work equally well.

Example 6.1. Examples 1.1–1.3 with appropriate reconstructions of test functions. In Examples 1.1–1.3 the dependence of the velocity error on the viscosity for the standard nonconforming Crouzeix–Raviart finite element discretization $\mathcal{P}_1^{\text{CR}}/\mathcal{P}_0$ was clearly seen. As mentioned at the beginning of section 5.2, a reconstruction of the test function can be applied for this pair of finite element spaces; see [51]. In the case of the Stokes equations, this reconstruction is performed only on the right-hand side. For the Navier–Stokes equations, the test function in the convective term and, if present, also the term with the Coriolis force, have to be reconstructed; see [16]. For the Crouzeix–Raviart finite element, the reconstructed test function is a projection onto a Raviart–Thomas function of order zero (RT₀). Applying this reconstruction, one obtains the results presented in Figure 6.1. One can see that in all cases the velocity fields are recovered up to round-off errors.

Example 6.2. Grad-div stabilization. The effect of using the grad-div stabilization described in section 5.1 will be illustrated for the Stokes equations with the prescribed solution

$$\boldsymbol{u} = 200 \begin{pmatrix} x^2 (1-x)^2 y (1-y) (1-2y) \\ -x (1-x) (1-2x) y^2 (1-y)^2 \end{pmatrix}, \ p = 10 \left(\left(x - \frac{1}{2}\right)^3 y^2 + (1-x)^3 \left(y - \frac{1}{2}\right)^3 \right);$$

see Figure 6.2. The velocity field has the form of a large vortex. Note that for the flow problem from Example 1.1, the second infimum in the error bound (5.3) vanishes such that $\gamma \to \infty$ leads to the ideal computed velocity field. This situation is not representative for the general case.

Here, only a few results will be presented. The simulations were performed with the Taylor–Hood pair of spaces $\mathcal{P}_2/\mathcal{P}_1$. The unstructured initial grid depicted in Figure 6.2 was refined four times leading to 36,546 degrees of freedom (d.o.f.s) for the velocity and 4,688 d.o.f.s for the pressure. In this situation, the error estimate (5.3) for $\|\nabla(\boldsymbol{u}-\boldsymbol{u}_h)\|_{L^2(\Omega)}^2$ applies. Both infima in the error bound are of the same order, hence their equilibration leads to the choice $\gamma \sim 1$ with respect to the mesh

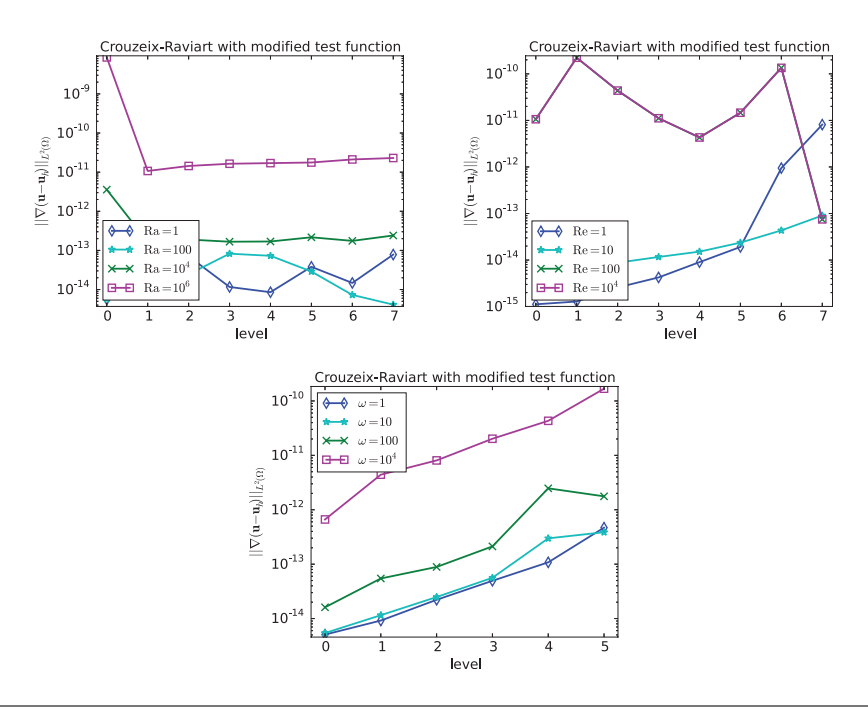


Fig. 6.1 Example 6.1. Crouzeix-Raviart pair of spaces with reconstructed test function, Examples 1.1-1.3.

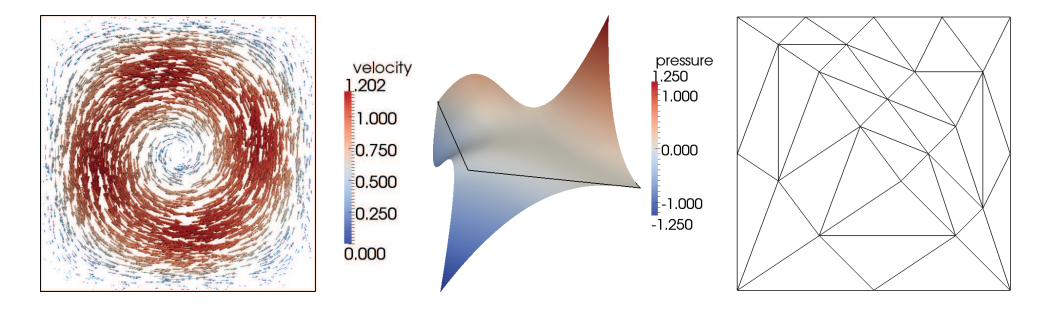
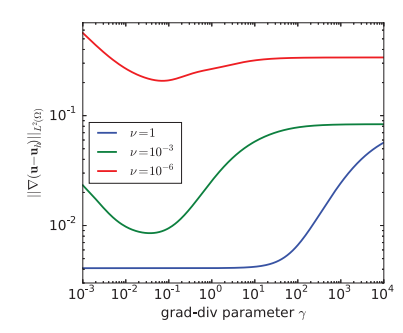


Fig. 6.2 Example 6.2. Velocity, pressure, initial grid (level 0).

width. The analysis from [43] shows that the optimal choice of γ depends on norms of the solution. Since the prescribed solution does not depend on the viscosity, the optimal stabilization parameter should be independent of ν . A representative result is presented in Figure 6.3. It can be seen that for $\nu=1$ one obtains for a wide range of γ approximately the same results. For large γ only, the divergence error decreases but at the same time $\|\nabla(\boldsymbol{u}-\boldsymbol{u}_h)\|_{L^2(\Omega)}^2$ increases. For smaller values of ν , one observes that the optimal stabilization parameter with respect to $\|\nabla(\boldsymbol{u}-\boldsymbol{u}_h)\|_{L^2(\Omega)}^2$ is contained in [0.03,0.08]. The impact on the error $\|\nabla\cdot\boldsymbol{u}_h\|_{L^2(\Omega)}^2$ is much higher for small ν . In particular, in the case $\nu=10^{-6}$, very large values of γ lead to almost divergence-free solutions with only a slightly larger velocity error compared with the optimal parameter for $\|\nabla(\boldsymbol{u}-\boldsymbol{u}_h)\|_{L^2(\Omega)}^2$. However, it shall be emphasized that large contributions of the grad-div stabilization result in linear systems of equations with large condition numbers [65].



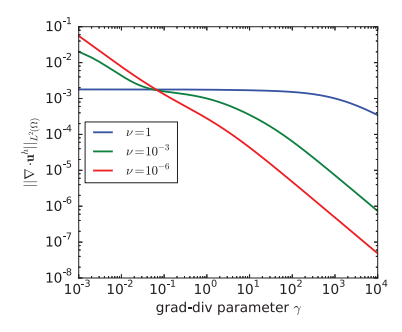


Fig. 6.3 Example 6.2. Errors for a wide range of stabilization parameters.

The presented result illustrates the final comment of section 5.1 quite well: the grad-div stabilization might improve the pressure-robustness in certain situations but it is not a remedy. For this reason, the presentation of more numerical results will be omitted here. Instead, the reader is referred to the comprehensive numerical studies in [43].

Example 6.3. Natural convection in a triangular cavity. In natural convection problems, the flow is driven by the temperature. Here, a model consisting of a coupled system of the Stokes equations and a convection-diffusion equation for the temperature will be considered:

(6.1)
$$-\Delta \boldsymbol{u} + \nabla p = \operatorname{Ra} \boldsymbol{e}_j \theta,$$

$$(6.2) \nabla \cdot \boldsymbol{u} = 0,$$

$$(6.3) -\Delta\theta + \boldsymbol{u} \cdot \nabla\theta = 0,$$

with θ representing temperature and e_j being a unit vector pointing in the direction opposite to gravity. Simulations were performed with the Rayleigh number Ra = 10^6 . Models of this type can be used for the simulation of fluids like silicon oil.

Natural convection problems defined on the unit square are standard test problems. To present a different setup, the domain Ω was chosen to be the right triangle with vertices (0,0), (1,0), and (0,1). The boundary is considered to be solid walls. Thus, homogeneous Dirichlet boundary conditions for the velocity are prescribed on the walls. For the temperature, a sinusoidal heat source is enforced on the bottom boundary with a Dirichlet condition, the left wall is set to a constant temperature of zero, and the hypotenuse wall is perfectly insulated so that a Neumann boundary condition is appropriate. The domain and the boundary conditions are shown in Figure 6.4. This figure shows also the initial triangulation (level 0) used in the simulations.

Besides presenting plots of the numerical solutions in this section, the Nusselt number defined by

$$N\mathbf{u} = \int_{\partial\Omega\cap\{y=0\}} \nabla T \cdot \mathbf{n} \, ds$$

will be studied. Extrapolating results obtained with higher order discretizations, one finds $Nu \approx 24.535$.

First, results for a low order discretization will be presented. For the Stokes equations, the Bernardi–Raugel element $\mathfrak{P}_{1}^{\mathrm{BR}}/\mathfrak{P}_{0}$ [14] was used and for the temperature,

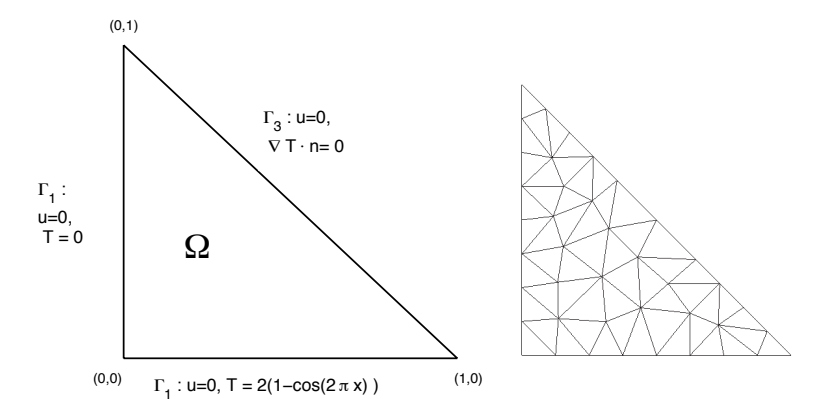


Fig. 6.4 Example 6.3. Left: domain and boundary conditions for the natural convection problem in a triangular cavity; right: initial triangulation (level 0).

the \mathcal{P}_1 finite element. The velocity space in the Bernardi–Raugel element consists of \mathcal{P}_1 functions which are enriched with edge bubble functions. For this element, a reconstruction of the test function as described in section 5.2 and Remark 5.3 can be constructed.

For the methods that use a reconstruction of the test functions, the discrete velocity fields are not weakly divergence-free. In order to enforce this property, one has to apply a projection operator which maps the discretely divergence-free velocity field to a divergence-free velocity field. To this end, the same operator Π_h can be employed that was used for reconstructing the test functions. The desired divergence-free property follows from (5.9). This reconstruction was applied to \boldsymbol{u} in (6.3).

Computed solutions obtained without and with this reconstruction are depicted in Figures 6.5–6.7. The Nusselt numbers and the divergence of the discrete velocity are given in Table 6.1. The velocity field computed using the method with reconstruction is much smoother on coarse grids; also, the temperature is somewhat smoother. The computed pressure fields look similar for both methods. With respect to the Nusselt number, the results of the method with reconstruction are generally more accurate. In summary, the use of an appropriately reconstructed test function in the Bernardi–Raugel pair of spaces led to a clear improvement of the accuracy of the computed results compared with the standard method.

As higher order discretizations, the Taylor–Hood pair $\mathcal{P}_2/\mathcal{P}_1$, the Scott–Vogelius pair $\mathcal{P}_2/\mathcal{P}_1^{\text{disc}}$ [71], and the pair $\mathcal{P}_2^{\text{bubble}}/\mathcal{P}_1^{\text{disc}}$ from [26] were considered. In the $\mathcal{P}_2^{\text{bubble}}/\mathcal{P}_1^{\text{disc}}$ finite element, the velocity space consists of \mathcal{P}_2 functions and an enrichment with mesh cell bubbles. The reconstruction of the test function for this pair is described in section 5.2 and Remark 5.3. As for the Bernardi–Raugel element with reconstruction, the reconstruction is also applied to \boldsymbol{u} in (6.3). For applying the Scott–Vogelius pair, an additional barycentric refinement of the grids was applied to guarantee the satisfaction of the discrete inf-sup condition (3.2); see [68]. Since $Y_h = \mathcal{P}_1^{\text{disc}} = \nabla \cdot \mathcal{P}_2 = \boldsymbol{X}_h$, the use of the Scott–Vogelius pair gives divergence-free velocity fields in the sense of Definition 2.3. For all higher order discretizations, the temperature was discretized with the \mathcal{P}_2 finite element.

The computed velocity fields for the higher order discretizations are presented in Figure 6.8. Only for the grids with the smallest number of degrees of freedom can small differences be observed. In this case, the velocity obtained with the Taylor—

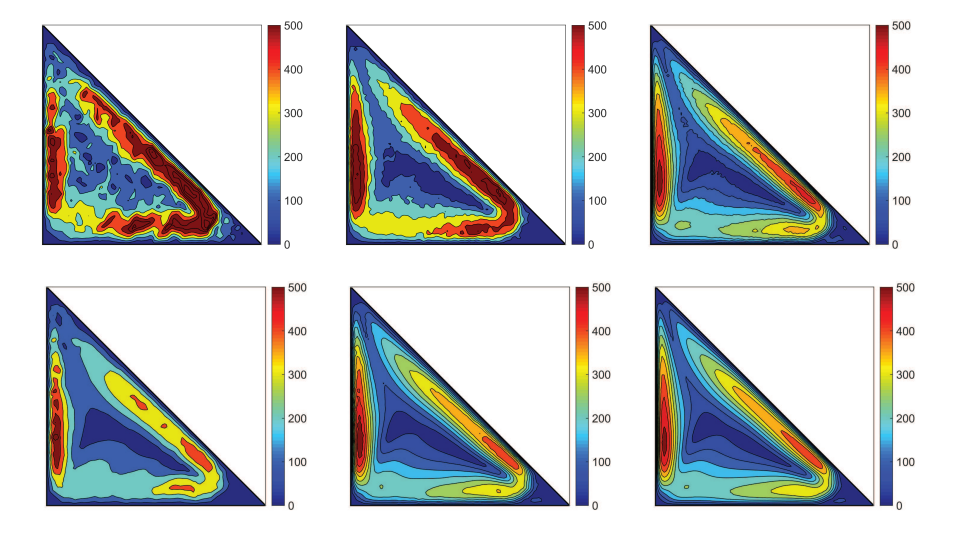


Fig. 6.5 Example 6.3. Absolute value of the velocity (speed) obtained with the Bernardi-Raugel element $\mathcal{P}_1^{\text{BR}}/\mathcal{P}_0$ on levels 1 to 3. Top: standard formulation; bottom: with reconstruction of the test function.

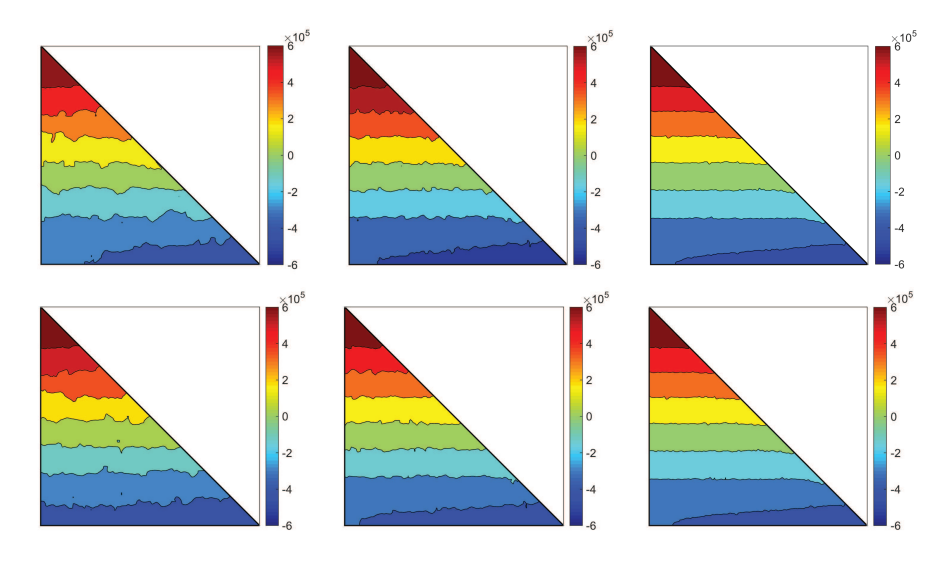


Fig. 6.6 Example 6.3. Pressure obtained with the Bernardi-Raugel element $\mathfrak{P}_1^{BR}/\mathfrak{P}_0$ on levels 1 to 3. Top: standard formulation; bottom: with reconstruction of the test function.

Hood pair seems to be the least accurate. The situation is similar for the temperature. With respect to the pressure, there are only small differences between the different methods, which is the same situation as for the low order discretizations. For the sake of brevity, the presentation of the pressures computed by the higher order methods is omitted.

To obtain a reference value for the Nusselt number, simulations with the Taylor–Hood and Scott–Vogelius finite elements were performed on very fine meshes and

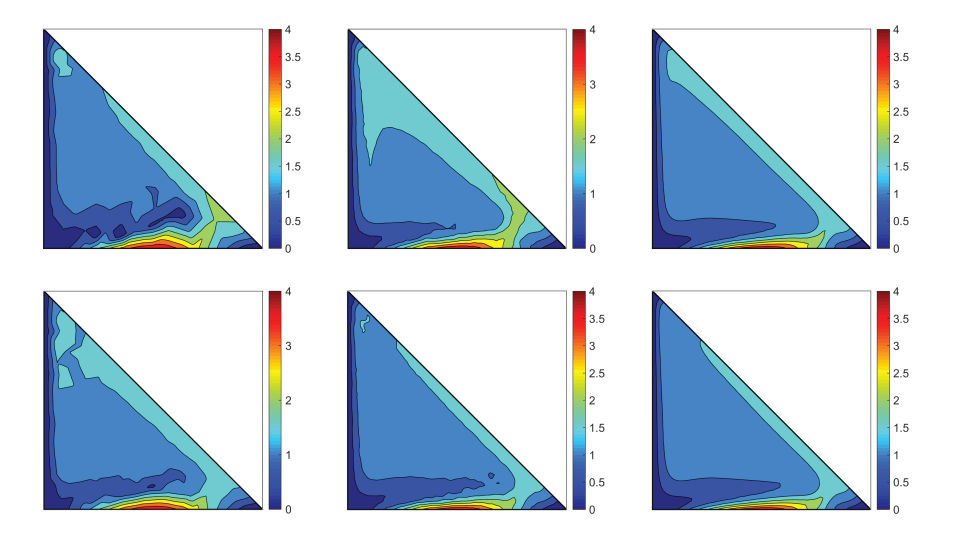


Fig. 6.7 Example 6.3. Temperature obtained with the Bernardi-Raugel element \(\Phi_1^{\text{BR}} / \Pa_0 \) on levels 1 to 3. Top: standard formulation; bottom: with reconstruction of the test function.

Table 6.1 Example 6.3. Nusselt number obtained with the Bernardi–Raugel element $\mathcal{P}_1^{BR}/\mathcal{P}_0$.

Level	d.o.f.	Standard	With reconstruction
0	271	not conv.	11.828
1	947	14.016	13.870
2	3317	17.232	20.935
3	13115	21.955	23.665
4	51697	23.664	24.238
Reference			24.535

the numbers were extrapolated by Aitken extrapolation; see Table 6.2. Both methods agree on the first two digits. For a similar number of degrees of freedom, more accurate Nusselt numbers were obtained with the Taylor–Hood pair of spaces compared with the Scott–Vogelius pair. The application of the reconstruction for $\mathcal{P}_2^{\text{bubble}}/\mathcal{P}_1^{\text{disc}}$ had only a minor effect on the computed Nusselt numbers.

In summary, with the standard Taylor–Hood pair of spaces $\mathfrak{P}_2/\mathfrak{P}_1$ good results were obtained, except on grids with very few degrees of freedom. Apart from obtaining a divergence-free solution, there is no advantage to using the Scott–Vogelius pair for this problem. There is also no advantage to applying a reconstruction of the test function for the $\mathfrak{P}_2^{\text{bubble}}/\mathfrak{P}_1^{\text{disc}}$ pair of spaces. Possibly the almost linear pressure, which can be resolved well by all discrete piecewise linear pressure spaces, is one reason why only minor differences for the higher order methods could be observed. However, it will be shown in Example 6.6 that a divergence-free solution might be very important if the scalar quantity possesses certain restrictions arising from the physics of the problem.

Example 6.4. Navier–Stokes equations for a potential flow. This example studies a problem from [54] where the potential flow $\mathbf{u} = \nabla h$, with the harmonic function $h = y^5 + 5x^4y - 10x^2y^3$, is considered for the Navier–Stokes equations on $\Omega = (-0.5, 0.5)^2$.

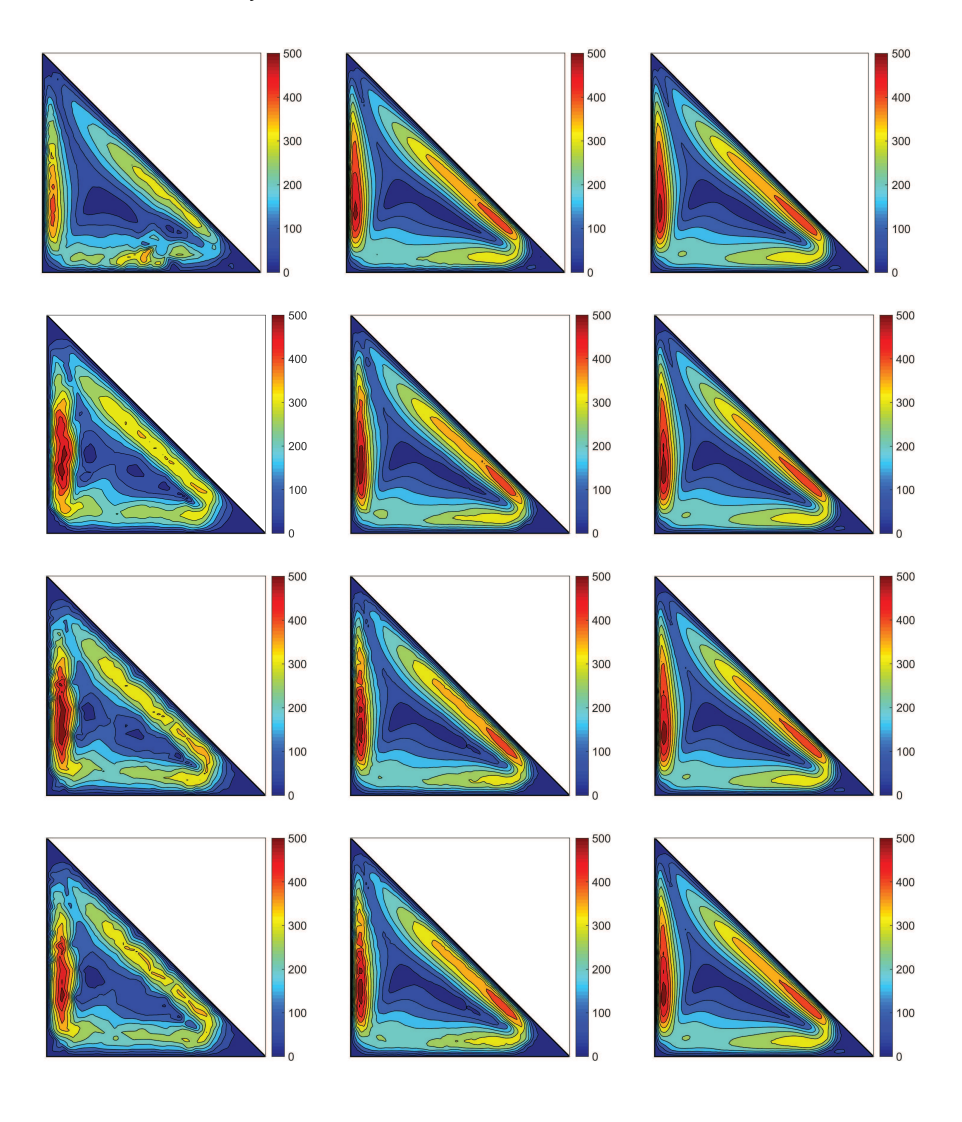


Fig. 6.8 Example 6.3. Absolute value of the velocity (speed). Top to bottom: $\mathfrak{P}_2/\mathfrak{P}_1$ (levels 1 to 3), $\mathfrak{P}_2/\mathfrak{P}_1^{\text{disc}}$ (levels 0 to 2 with barycentric refinement), $\mathfrak{P}_2^{\text{bubble}}/\mathfrak{P}_1^{\text{disc}}$ (levels 0 to 2), $\mathfrak{P}_2^{\text{bubble}}/\mathfrak{P}_1^{\text{disc}}$ with reconstructed test function (levels 0 to 2).

For potential flows, it holds that $\Delta u = 0$ and $(u \cdot \nabla)u = -\nabla(|u|^2/2)$. Hence, the pressure is solely induced by the convection term, i.e., $p = -|u|^2/2$, and the Navier–Stokes equations are satisfied with f = 0.

This example shows that the nonlinear convection term can also cause a lack of pressure-robustness. This feature will be illustrated for the $\mathcal{P}_2^{\text{bubble}}/\mathcal{P}_1^{\text{disc}}$ pair of spaces, where the nonlinear convection term in its weak form is discretized by

(6.4)
$$\int_{\Omega} ((\boldsymbol{u}_h \cdot \nabla) \boldsymbol{u}_h) \cdot \boldsymbol{v}_h \, d\boldsymbol{x}.$$

Table 6.2 Example 6.3. Nusselt number obtained with $\mathfrak{P}_2/\mathfrak{P}_1$, $\mathfrak{P}_2/\mathfrak{P}_1^{\mathrm{disc}}$, $\mathfrak{P}_2^{\mathrm{bubble}}/\mathfrak{P}_1^{\mathrm{disc}}$, $\mathfrak{P}_2^{\mathrm{bubble}}/\mathfrak{P}_1^{\mathrm{disc}}$, $\mathfrak{P}_2^{\mathrm{bubble}}/\mathfrak{P}_2^{\mathrm{disc}}$, $\mathfrak{P}_2^{\mathrm{disc}}/\mathfrak{P}_2^{\mathrm{disc}}$

	$\mathfrak{P}_2/\mathfrak{P}_1$		$\mathfrak{P}_2/\mathfrak{P}$	disc	$\mathcal{P}_2^{\text{bubble}}/\mathcal{P}_1^{\text{disc}}$ std./reco.		
Level	d.o.f.	Nu	d.o.f.	Nu	d.o.f.	Nu	Nu
0	446	0.074	1539	10.318	675	5.778	6.240
1	1551	16.105	5829	17.867	2469	13.850	13.765
2	5414	20.748	21333	21.967	8869	20.261	20.254
3	21361	23.475	86409	23.918	35561	23.460	23.461
4	84108	24.183	344685	24.333	141149	24.184	24.184
5	332757	24.427	1373127	24.471			
6	1325912	24.501					
Extrapolation 24.537		24.537		24.533			

Table 6.3 Example 6.4. L² errors of the gradient of the velocity for the classical discretization (6.4). The notation "dnc" indicates that the method did not converge.

$\nu \setminus \# \text{ d.o.f.}$	304	1200	4529	18175	71847	287593	1146124
1e+5	3.6095e+0	8.2123e-1	2.1783e-1	5.1476e-2	1.2878e-2	3.1832e-3	7.9016e-4
1e+0	3.6143e+0	8.2132e-1	2.1774e-1	5.1479e-2	1.2881e-2	3.1833e-3	7.9021e-4
1e-1	3.6670e+0	8.2534e-1	2.1753e-1	5.1732e-2	1.2961e-2	3.1998e-3	7.9470e-4
1e-2	4.9303e+0	1.1136e+0	2.6617e-1	7.2571e-2	1.8499e-2	4.6238e-3	1.1641e-3
2e-3	dnc	3.3922e+0	7.5804e-1	2.4830e-1	6.5474e-2	1.6949e-2	4.3358e-3
1e-3	dnc	dnc	1.3212e+0	4.5871e-1	1.2413e-1	3.2771e-2	8.4937e-3
2e-4	dnc	dnc	dnc	1.6678e + 0	4.9753e-1	1.3967e-1	3.8696e-2
1e-4	dnc	dnc	dnc	dnc	8.5289e-1	2.4610e-1	7.0749e-2
5e-5	dnc	dnc	dnc	dnc	dnc	dnc	1.2460 e-1

Table 6.4 Example 6.4. L² errors of the gradient of the velocity for the modified discretization (6.5). The notation "dnc" indicates that the method did not converge.

$\nu \setminus \# \text{ d.o.f.}$	304	1200	4529	18175	71847	287593	1146124
1e+5	3.6095e+0	8.2123e-1	2.1783e-1	5.1476e-2	1.2878e-2	3.1832e-3	7.9016e-4
1e+0	3.6109e+0	8.2123e-1	2.1783e-1	5.1477e-2	1.2879e-2	3.1832e-3	7.9017e-4
1e-1	3.6240e+0	8.2134e-1	2.1786e-1	5.1476e-2	1.2879e-2	3.1832e-3	7.9017e-4
1e-2	3.7743e+0	8.3142e-1	2.1925e-1	5.1567e-2	1.2891e-2	3.1837e-3	7.9020e-4
2e-3	4.3747e + 0	9.2917e-1	2.3061e-1	5.2552e-2	1.3019e-2	3.1930e-3	7.9085e-4
1e-3	dnc	1.0666e + 0	2.5486e-1	5.4077e-2	1.3213e-2	3.2124e-3	7.9252e-4
2e-4	dnc	$_{ m dnc}$	$_{ m dnc}$	7.4417e-2	1.4721e-2	3.3851e-3	8.1340e-4
1e-4	dnc	$_{ m dnc}$	$_{ m dnc}$	$_{ m dnc}$	1.7548e-2	3.6028e-3	8.4052e-4
5e-5	dnc	dnc	dnc	dnc	dnc	4.1404e-3	8.9510e-4

In the modified variant, the nonlinear convection term is discretized by

(6.5)
$$\int_{\Omega} ((\boldsymbol{u}_h \cdot \nabla) \boldsymbol{u}_h) \cdot (\Pi_h \boldsymbol{v}_h) d\boldsymbol{x}$$

with the reconstruction operator Π_h from Remark 5.3.

Tables 6.3 and 6.4 present L^2 errors of the gradient of the velocity for the classical method (6.4) and the modified method (6.5). For $\nu=10^5$, the nonlinear convection term has only little impact and both methods compute nearly the same approximation of \boldsymbol{u} . However, for decreasing values of ν , the methods behave differently. There is a much wider range of ν for which the errors of the solutions computed with the modified method stay nearly unchanged. This feature can be seen best on the finest mesh, where the L^2 errors of the velocity gradient for the modified method do not

Table 6.5	Example 6.4. Factors between the L^2 errors of the gradient of the velocity of the classical
	and modified methods using the results from Tables 6.3 and 6.4.

$\nu \setminus \# \text{ d.o.f.}$	304	1200	4529	18175	71847	287593	1146124
1e+5	1.00	1.00	1.00	1.00	1.00	1.00	1.00
1e+0	1.00	1.00	1.00	1.00	1.00	1.00	1.00
1e-1	1.01	1.00	1.00	1.00	1.01	1.01	1.01
1e-2	1.31	1.34	1.21	1.41	1.44	1.45	1.47
2e-3	-	3.65	3.29	4.72	5.03	5.31	5.48
1e-3	-	-	5.18	8.48	9.39	10.20	10.72
2e-4	-	-	-	22.41	33.80	41.26	47.57
1e-4	_	-	-	-	48.60	68.31	84.17
5e-5	-	-	-	-	-	-	139.20

increase significantly until about $\nu = 10^{-3}$, while there is already a notably larger deviation of this error for the classical method and $\nu = 10^{-1}$.

Table 6.5 lists the factors between the L^2 errors of the velocity gradient of the classical and the modified method for different values of ν and different refinement levels. A factor larger than one indicates that the error of the classical methods is larger than the error of the modified method. On finer meshes, these factors scale almost with $1/\nu$, which shows that the error in this case is dominated by the influence of the badly resolved pressure. The factors even seem to increase on finer meshes. For the smallest ν and the finest mesh in the presented study, an improvement factor of about 139 is attained. This result means that the classical method needs more than three refinement levels (under the assumption of optimal quadratic convergence) to compute an error as small as the error obtained with the modified method. In conclusion, pressure-robustness in the Navier–Stokes case also concerns the test functions of the nonlinear convection term; see [54] for more details. In a time-dependent setting, the temporal derivative of the velocity can cause a lack of pressure-robustness and can be treated similarly; compare also [54].

Example 6.5. Flow over a forward facing step with Coriolis force. As mentioned in Example 1.3, flows with strong Coriolis forces appear in several applications. The simplest model for such a flow has the form

$$-\nu\Delta \boldsymbol{u} + \nabla p + 2\boldsymbol{\omega} \times \boldsymbol{u} = \boldsymbol{f}, \quad \nabla \cdot \boldsymbol{u} = 0,$$

where ω is a constant angular velocity vector. A two-dimensional example with $\omega = (0, 0, \omega)^T$ will be considered. Since

$$\nabla \times (\boldsymbol{\omega} \times \boldsymbol{u}) = \omega \begin{pmatrix} -\partial_z u_1 \\ -\partial_z u_2 \\ \nabla \cdot \boldsymbol{u} \end{pmatrix} = \boldsymbol{0},$$

 $(\boldsymbol{\omega} \times \boldsymbol{u})$ is conservative, which implies that there is a function ϕ satisfying $\omega \nabla \phi = \boldsymbol{\omega} \times \boldsymbol{u}$. Thus, changing the magnitude ω of the Coriolis force will change only the pressure solution, i.e., $p \to p + \omega \phi$, and not the velocity solution.

This problem was considered in the domain $\Omega = (0,4) \times (0,2) \setminus [2,4] \times [0,1]$; see Figure 6.9. The inlet is situated at x = 0 and the outlet at x = 4. Dirichlet boundary conditions are prescribed on the entire boundary, where the volume preserving parabolic inflow and outflow profiles are given by

$$oldsymbol{u}_{\mathrm{in}} = egin{pmatrix} y(2-y)/2 \\ 0 \end{pmatrix}, \quad oldsymbol{u}_{\mathrm{out}} = egin{pmatrix} 4(2-y)(y-1) \\ 0 \end{pmatrix},$$

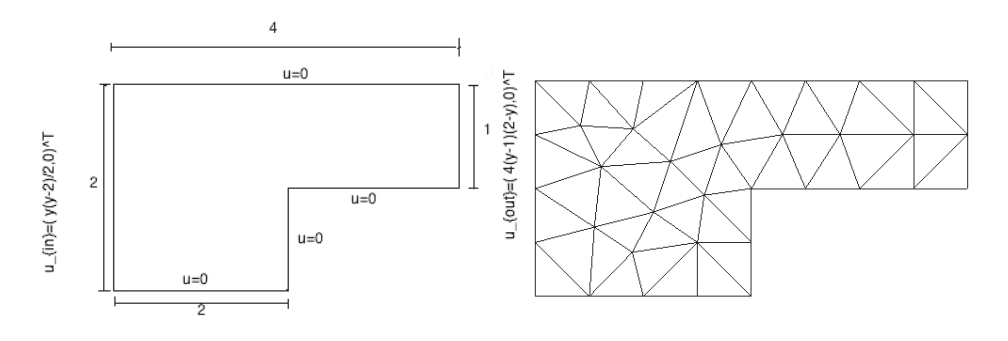


Fig. 6.9 Example 6.5. Domain and boundary conditions and coarsest mesh (level 0).

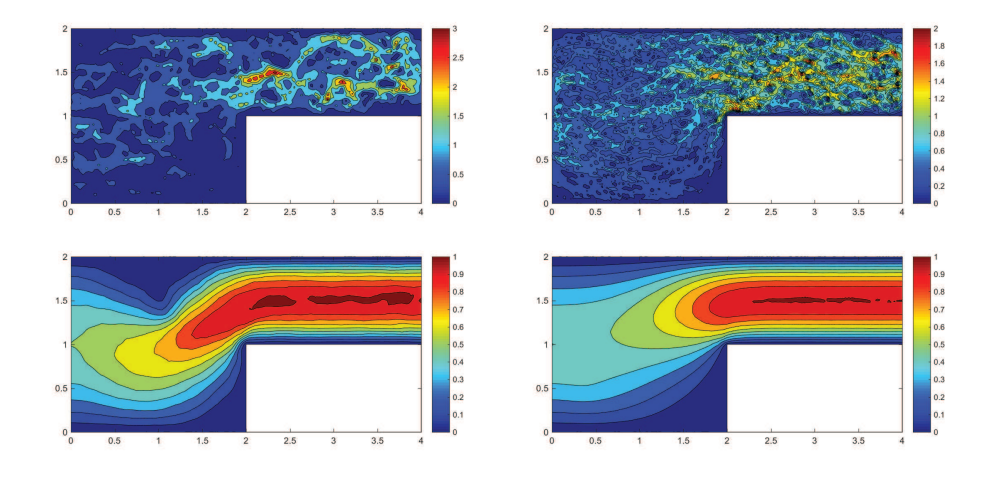
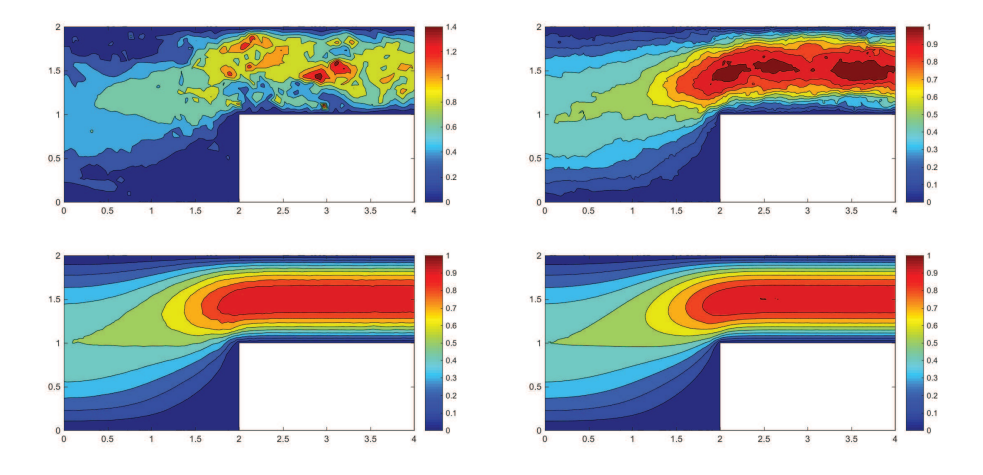


Fig. 6.10 Example 6.5. Absolute value of the velocity (speed) obtained with the Bernardi-Raugel element $\mathfrak{P}_1^{\mathrm{BR}}/\mathfrak{P}_0$ on refinement levels 2 and 3. Top: standard formulation; bottom: with reconstruction of the test function.

and no-slip conditions are used at all other parts of the boundary. Simulations were performed with $\nu=0.01$ and $\omega=100$. The initial grid is depicted in Figure 6.9. For the Scott–Vogelius pair of finite element spaces, a barycentric refinement of all grid levels was applied.

Computed solutions obtained on coarse grids are presented in Figures 6.10–6.12. The positive effect of using the formulation with reconstructed test function and Coriolis force term can be observed clearly, not only for the low order Bernardi–Raugel element $\mathcal{P}_1^{\text{BR}}/\mathcal{P}_0$, but also for the higher order $\mathcal{P}_2^{\text{bubble}}/\mathcal{P}_1^{\text{disc}}$ pair of spaces; see Figures 6.10 and 6.11. Also, the solutions computed with the divergence-free Scott–Vogelius finite element are considerably more accurate than the solutions obtained with the Taylor–Hood element on grids with a comparable number of degrees of freedom; see Figure 6.12. Note that due to the barycentric refinement, the number of degrees of freedom for the Scott–Vogelius element on level l is approximately the same as for the Taylor–Hood element on level l-1.

In summary, this example shows clearly the benefit that might be achieved if pressure-robust discretizations are used for simulations of flows with Coriolis forces.



Example 6.5. Absolute value of the velocity (speed) obtained with $\mathfrak{P}_2^{\mathrm{bubble}}/\mathfrak{P}_1^{\mathrm{disc}}$ on refinement levels 1 and 2. Top: standard formulation; bottom: with reconstruction of the test function.

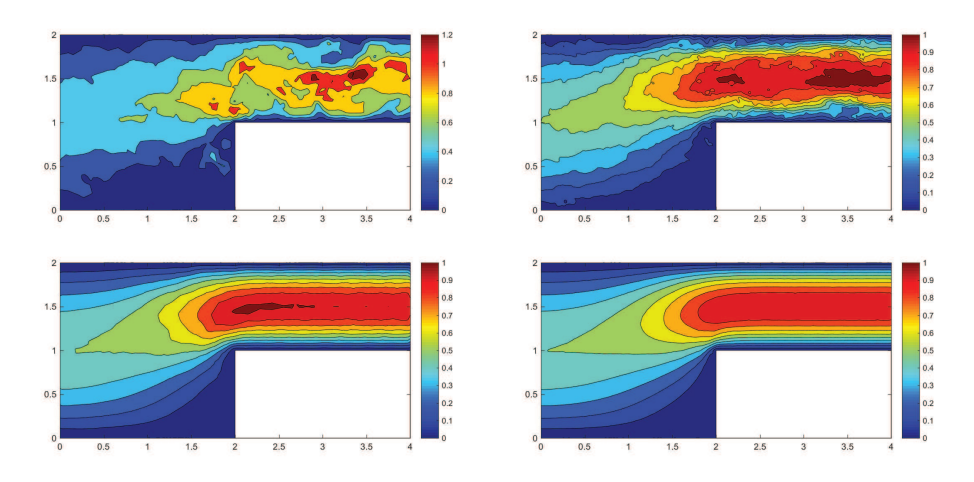


Fig. 6.12 Example 6.5. Absolute value of the velocity (speed) obtained with the Taylor-Hood element on refinement levels 1 and 2 (top) and the Scott-Vogelius element on refinement levels 0and 1 (bottom).

Example 6.6. Convection-dominated transport of a passive scalar. The final example demonstrates that divergence-free discrete velocity fields might also be of advantage in coupled problems. To this end, consider the transport of a passive scalar, e.g., temperature, through a domain with a flow field which is governed by the Stokes equations

$$(6.6) -\nu\Delta \boldsymbol{u} + \nabla p = \boldsymbol{0},$$

(6.7)
$$\nabla \cdot \mathbf{u} = 0,$$
(6.8)
$$-\varepsilon \Delta \theta + \mathbf{u} \cdot \nabla \theta = 0.$$

(6.8)
$$-\varepsilon \Delta \theta + \boldsymbol{u} \cdot \nabla \theta = 0.$$

The domain and the boundary conditions for the velocity are the same as in Exam-

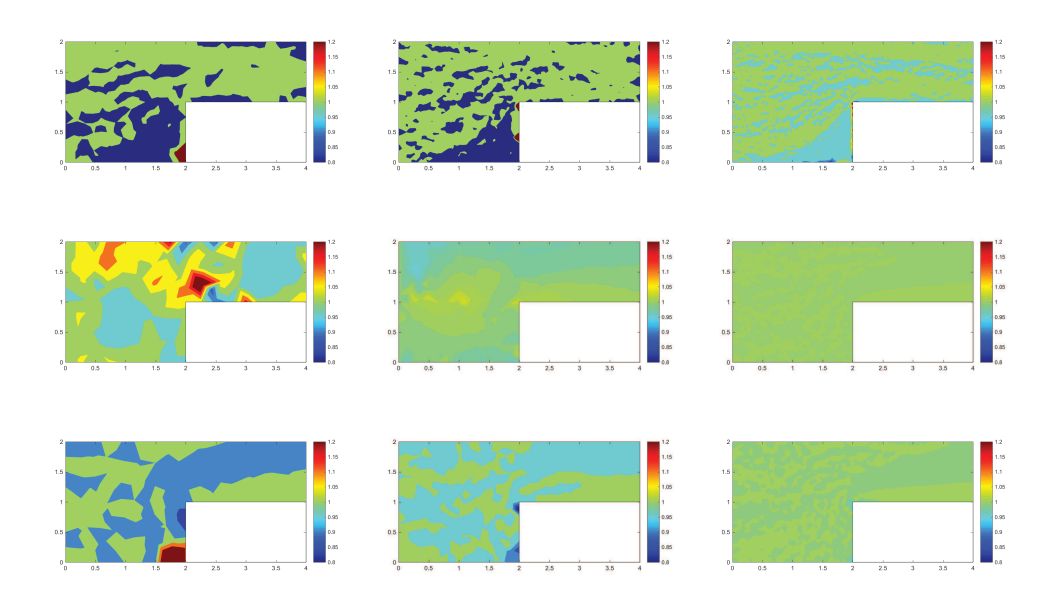


Fig. 6.13 Example 6.6. Concentration obtained with a Voronoi finite volume method and velocity fields by the Bernardi-Raugel element \(\mathbb{P}_1^{BR} / \mathbb{P}_0 \) on refinement levels 2-4 (top), the \(\mathbb{P}_2^{bubble} / \mathbb{P}_1^{disc} \) on refinement levels 1-3 (middle), and the Taylor-Hood element on refinement levels 1-3 (bottom).

ple 6.5. At the inlet, the constant temperature $\theta=1$ is prescribed and on all other boundaries, a free temperature flux $-\varepsilon\nabla\theta\cdot\mathbf{n}=0$. Together with (6.8) it follows that $\theta=1$ is the solution for the temperature field. Simulations were performed with the coefficients $\nu=0.01$ and $\varepsilon=10^{-6}$. The same initial grid was used as is presented in Figure 6.9.

The Stokes equations were discretized either by the Bernardi–Raugel element $\mathcal{P}_1^{\text{BR}}/\mathcal{P}_0$, the $\mathcal{P}_2^{\text{bubble}}/\mathcal{P}_1^{\text{disc}}$ element, or the Taylor–Hood element. Equation (6.8) for the temperature is a convection-dominated equation. It is well known that stabilizations are necessary for discretizing this type of system. There are numerous proposals; e.g., see [70]. However, there are only a few stabilized methods that satisfy a discrete maximum principle, which is an important property in many applications to guarantee that numerical solutions have meaningful physical values. One of these discretizations is the exponentially fitted Voronoi finite volume method from [33, 34]. This method satisfies the discrete maximum principle on Delaunay grids (the grids used are of this type) and for divergence-free convection fields.

The computation of weakly divergence-free fields for the methods that use a reconstruction of the test functions is described in Example 6.3.

Figure 6.13 and Table 6.6 present results of the numerical simulations. The velocity field is of the same form as in Example 6.5. Since there is no Coriolis force, visually there appear to be almost no differences in the velocity fields computed with the different discretizations (their presentation is omitted for the sake of brevity). However, the violation of the divergence constraint causes (strong) spurious oscillations of the discrete temperature in all cases where the discrete velocity fields are not divergence-free. By contrast, the methods with divergence-free velocity fields compute the temperature with exact accuracy on all grid levels.

	$\mathcal{P}_1^{\mathrm{BR}}/\mathfrak{P}_0$			e/Pdisc	$\mathfrak{P}_2/\mathfrak{P}_1$	$\mathcal{P}_2/\mathcal{P}_1^{ ext{disc}}$
Level	std.	reco.	std.	reco.		
0	0.550/1.331	1.000/1.000	0.942/2.071	1.000/1.000	0.881/1.930	1.000/1.000
1	0.273/6.343	1.000/1.000	0.875/1.319	1.000/1.000	0.828/1.640	1.000/1.000
2	0.408/2.997	1.000/1.000	0.948/1.037	1.000/1.000	0.773/1.052	1.000/1.000
3	0.582/2.761	1.000/1.000	0.993/1.005	1.000/1.000	0.955/1.030	1.000/1.000
4	0.827/1.415	1.000/1.000	0.993/1.002	1.000/1.000	0.909/1.017	1.000/1.000

 Table 6.6
 Example 6.6
 Minimal and maximal temperature.

7. Outlook. This article has provided a thorough review of state-of-the-art methods and numerical analysis used for the enforcement of the divergence constraint in mixed finite element methods for equations that model incompressible flows, with a special emphasis on the Stokes equations with possibly nonvanishing divergence of the velocity field. Although a significant amount of progress has been achieved, in particular, in the past decade, these methods have not achieved large-scale and widespread use. As discussed in section 4.3, there remain several open problems related to de Rham complexes in the three-dimensional case. Further, while the focus in this article was mainly on the Stokes equations, additional important details can arise when Coriolis forces are present, for the Navier–Stokes equations, and for multiphysics systems. This is true for all methods discussed, but especially for the pressure-robust discretizations that are only $\boldsymbol{H}(\text{div})$ -conforming and the methods that apply $\boldsymbol{H}(\text{div})$ -conforming velocity reconstructions; see section 5.2 and section 5 in [51].

Another important open problem is the development of efficient linear solvers for large-scale computations with divergence-free elements. Most linear solvers used in large-scale Navier–Stokes codes seem tailored to low order elements and are less effective when used with divergence-free elements, due to the pressure matrices being much larger. However, these larger pressure matrices are very sparse, and this can likely be exploited. Furthermore, divergence-free elements usually have a macroelement structure in the mesh, which seems to provide a natural framework for developing multigrid preconditioners.

REFERENCES

- [1] M. AINSWORTH AND W. DÖRFLER, Reliable a posteriori error control for nonconformal finite element approximation of Stokes flow, Math. Comp., 74 (2005), pp. 1599–1619. (Cited on p. 500)
- [2] J. ARGYRIS, I. FRIED, AND D. SCHARPF, The TUBA family of plate elements for the matrix displacement method, Aero. J. Roy. Aero. Soc., 72 (1968), pp. 701-709. (Cited on p. 515)
- [3] D. Arndt, H. Dallmann, and G. Lube, Local projection FEM stabilization for the timedependent incompressible Navier-Stokes problem, Numer. Methods Partial Differential Equations, 31 (2015), pp. 1224–1250, https://doi.org/10.1002/num.21944. (Cited on p. 524)
- [4] D. N. Arnold, F. Brezzi, and M. Fortin, A stable finite element for the Stokes equations, Calcolo, 21 (1984), pp. 337–344, https://doi.org/10.1007/BF02576171. (Cited on pp. 494, 504)
- [5] D. N. ARNOLD, R. S. FALK, AND R. WINTHER, Finite element exterior calculus, homological techniques, and applications, Acta Numer., 15 (2006), pp. 1–155, https://doi.org/10.1017/ S0962492906210018. (Cited on p. 512)
- [6] D. N. Arnold, R. S. Falk, and R. Winther, Finite element exterior calculus: From Hodge theory to numerical stability, Bull. Amer. Math. Soc. (N.S.), 47 (2010), pp. 281–354, https: //doi.org/10.1090/S0273-0979-10-01278-4. (Cited on pp. 512, 513)
- [7] D. N. ARNOLD AND J. QIN, Quadratic velocity/linear pressure Stokes elements, in Advances in Computer Methods for Partial Differential Equations VII, R. Vichnevetsky, D. Knight, and G. Richter, eds., IMACS, 1992, pp. 28–34. (Cited on pp. 514, 515)

- [8] G. AUCHMUTY AND J. C. ALEXANDER, L²-well-posedness of 3D div-curl boundary value problems, Quart. Appl. Math., 63 (2005), pp. 479–508, https://doi.org/10.1090/ S0033-569X-05-00972-5. (Cited on p. 511)
- T. M. AUSTIN, T. A. MANTEUFFEL, AND S. MCCORMICK, A robust multilevel approach for minimizing H(div)-dominated functionals in an H¹-conforming finite element space, Numer. Linear Algebra Appl., 11 (2004), pp. 115–140, https://doi.org/10.1002/nla.373. (Cited on p. 515)
- [10] G. R. Barrenechea and F. Valentin, Consistent local projection stabilized finite element methods, SIAM J. Numer. Anal., 48 (2010), pp. 1801–1825, https://doi.org/10.1137/ 090753334. (Cited on p. 528)
- [11] G. R. BARRENECHEA AND F. VALENTIN, A residual local projection method for the Oseen equation, Comput. Methods Appl. Mech. Engrg., 199 (2010), pp. 1906–1921, https://doi.org/10.1016/j.cma.2010.01.014. (Cited on p. 528)
- [12] G. R. BARRENECHEA AND F. VALENTIN, Beyond pressure stabilization: A low-order local projection method for the Oseen equation, Internat. J. Numer. Methods Engrg., 86 (2011), pp. 801–815, https://doi.org/10.1002/nme.3075. (Cited on p. 528)
- [13] M. Benzi and M. A. Olshanskii, An augmented Lagrangian-based approach to the Oseen problem, SIAM J. Sci. Comput., 28 (2006), pp. 2095–2113, https://doi.org/10.1137/050646421. (Cited on p. 524)
- [14] C. BERNARDI AND G. RAUGEL, Analysis of some finite elements for the Stokes problem, Math. Comp., 44 (1985), pp. 71–79, https://doi.org/10.2307/2007793. (Cited on pp. 504, 530)
- [15] S. BÖRM AND S. LE BORNE, H-LU factorization in preconditioners for augmented Lagrangian and grad-div stabilized saddle point systems, Internat. J. Numer. Methods Fluids, 68 (2012), pp. 83–98, https://doi.org/10.1002/fld.2495. (Cited on p. 524)
- [16] C. Brennecke, A. Linke, C. Merdon, and J. Schöberl, Optimal and pressure-independent L² velocity error estimates for a modified Crouzeix-Raviart Stokes element with BDM reconstructions, J. Comput. Math., 33 (2015), pp. 191–208, https://doi.org/10.4208/jcm. 1411-m4499. (Cited on p. 528)
- [17] F. Brezzi, J. Douglas, Jr., and L. D. Marini, Two families of mixed finite elements for second order elliptic problems, Numer. Math., 47 (1985), pp. 217–235, https://doi.org/10. 1007/BF01389710. (Cited on p. 513)
- [18] A. BUFFA, C. DE FALCO, AND G. SANGALLI, IsoGeometric Analysis: Stable elements for the 2D Stokes equation, Internat. J. Numer. Methods Fluids, 65 (2011), pp. 1407–1422, https://doi.org/10.1002/fld.2337. (Cited on p. 515)
- [19] A. BUFFA, J. RIVAS, G. SANGALLI, AND R. VÁZQUEZ, Isogeometric discrete differential forms in three dimensions, SIAM J. Numer. Anal., 49 (2011), pp. 818–844, https://doi.org/10. 1137/100786708. (Cited on p. 512)
- [20] Y. V. BYCHENKOV AND E. V. CHIZONKOV, Optimization of one three-parameter method of solving an algebraic system of the Stokes type, Russian J. Numer. Anal. Math. Modelling, 14 (1999), pp. 429–440, https://doi.org/10.1515/rnam.1999.14.5.429. (Cited on p. 524)
- [21] C. CARSTENSEN AND C. MERDON, Computational survey on a posteriori error estimators for the Crouzeix-Raviart nonconforming finite element method for the Stokes problem, Comput. Methods Appl. Math., 14 (2014), pp. 35–54, https://doi.org/10.1515/cmam-2013-0021. (Cited on p. 500)
- [22] M. A. CASE, V. J. ERVIN, A. LINKE, AND L. G. REBHOLZ, A connection between Scott-Vogelius and grad-div stabilized Taylor-Hood FE approximations of the Navier-Stokes equations, SIAM J. Numer. Anal., 49 (2011), pp. 1461–1481, https://doi.org/10.1137/100794250. (Cited on p. 505)
- [23] E. CHIZHONKOV AND M. OLSHANSKII, On the domain geometry dependence of the LBB condition, M2AN Math. Model. Numer. Anal., 34 (2000), pp. 935–951, https://doi.org/10.1051/m2an:2000110. (Cited on p. 507)
- [24] P. G. CIARLET, The Finite Element Method for Elliptic Problems, Stud. Math. Appl. 4, North-Holland, Amsterdam, 1978. (Cited on pp. 513, 514, 515)
- [25] B. COCKBURN, G. KANSCHAT, AND D. SCHÖTZAU, A note on discontinuous Galerkin divergencefree solutions of the Navier-Stokes equations, J. Sci. Comput., 31 (2007), pp. 61–73, https: //doi.org/10.1007/s10915-006-9107-7. (Cited on pp. 516, 517)
- [26] M. CROUZEIX AND P.-A. RAVIART, Conforming and nonconforming finite element methods for solving the stationary Stokes equations. I, Rev. Française Automat. Informat. Recherche Opérationnelle Sér. Rouge, 7 (1973), pp. 33–75. (Cited on pp. 494, 531)
- [27] J. DE FRUTOS, B. GARCÍA-ARCHILLA, V. JOHN, AND J. NOVO, Grad-div stabilization for the evolutionary Oseen problem with inf-sup stable finite elements, J. Sci. Comput., 66 (2016), pp. 991–1024, https://doi.org/10.1007/s10915-015-0052-1. (Cited on p. 524)

- [28] O. DOROK, W. GRAMBOW, AND L. TOBISKA, Aspects of finite element discretizations for solving the Boussinesq approximation of the Navier-Stokes Equations, in Numerical Fluid Mechanics: Numerical Methods for the Navier-Stokes Equations, Proceedings of the International Workshop held at Heidelberg, 1993, F.-K. Hebeker, R. Rannacher, and G. Wittum, eds., Vieweg+Teubner Verlag, Wiesbaden, 1994, pp. 50-61. (Cited on p. 524)
- [29] J. A. EVANS AND T. J. R. HUGHES, Isogeometric divergence-conforming B-splines for the steady Navier-Stokes equations, Math. Models Methods Appl. Sci., 23 (2013), pp. 1421– 1478, https://doi.org/10.1142/S0218202513500139. (Cited on p. 516)
- [30] R. S. FALK AND M. NEILAN, Stokes complexes and the construction of stable finite elements with pointwise mass conservation, SIAM J. Numer. Anal., 51 (2013), pp. 1308–1326, https://doi.org/10.1137/120888132. (Cited on pp. 513, 514, 515)
- [31] M. FORTIN, An analysis of the convergence of mixed finite element methods, RAIRO Anal. Numér., 11 (1977), pp. 341–354. (Cited on p. 507)
- [32] L. P. Franca and T. J. R. Hughes, Two classes of mixed finite element methods, Comput. Methods Appl. Mech. Engrg., 69 (1988), pp. 89–129, https://doi.org/10.1016/0045-7825(88)90168-5. (Cited on p. 522)
- [33] J. FUHRMANN, A. LINKE, AND H. LANGMACH, A numerical method for mass conservative coupling between fluid flow and solute transport, Appl. Numer. Math., 61 (2011), pp. 530–553, https://doi.org/10.1016/j.apnum.2010.11.015. (Cited on pp. 499, 539)
- [34] J. Fuhrmann, A. Linke, C. Merdon, F. Neumann, T. Streckenbach, H. Baltruschat, and M. Khodayari, Inverse modeling of thin layer flow cells for detection of solubility, transport and reaction coefficients from experimental data, Electrochimica Acta, 211 (2016), pp. 1–10. (Cited on p. 539)
- [35] K. J. GALVIN, A. LINKE, L. G. REBHOLZ, AND N. E. WILSON, Stabilizing poor mass conservation in incompressible flow problems with large irrotational forcing and application to thermal convection, Comput. Methods Appl. Mech. Engrg., 237/240 (2012), pp. 166–176, https: //doi.org/10.1016/j.cma.2012.05.008. (Cited on pp. 497, 522, 524)
- [36] V. GIRAULT AND P.-A. RAVIART, Finite Element Methods for Navier-Stokes Equations: Theory and Algorithms, Springer Ser. Comput. Math. 5, Springer-Verlag, Berlin, 1986, https: //doi.org/10.1007/978-3-642-61623-5. (Cited on pp. 502, 512, 513, 522)
- [37] R. GLOWINSKI AND P. LE TALLEC, Augmented Lagrangian and Operator-Splitting Methods in Nonlinear Mechanics, SIAM Stud. Appl. Math. 9, SIAM, Philadelphia, 1989, https://doi.org/10.1137/1.9781611970838. (Cited on p. 524)
- [38] J. GUZMÁN AND M. NEILAN, A family of nonconforming elements for the Brinkman problem, IMA J. Numer. Anal., 32 (2012), pp. 1484–1508, https://doi.org/10.1093/imanum/drr040. (Cited on pp. 516, 520)
- [39] J. GUZMÁN AND M. NEILAN, Conforming and divergence-free Stokes elements on general triangular meshes, Math. Comp., 83 (2014), pp. 15–36, https://doi.org/10.1090/S0025-5718-2013-02753-6. (Cited on pp. 513, 514, 515, 520)
- [40] T. Heister and G. Rapin, Efficient augmented Lagrangian-type preconditioning for the Oseen problem using grad-div stabilization, Internat. J. Numer. Methods Fluids, 71 (2013), pp. 118–134, https://doi.org/10.1002/fld.3654. (Cited on p. 524)
- [41] P. HOOD AND C. TAYLOR, Navier-Stokes equations using mixed interpolation, in Finite Element Methods in Flow Problems, J. T. Oden, R. H. Gallagher, O. C. Zienkiewicz, and C. Taylor, eds., University of Alabama in Huntsville Press, 1974, pp. 121–132. (Cited on p. 494)
- [42] T. J. R. HUGHES, L. P. FRANCA, AND M. BALESTRA, A new finite element formulation for computational fluid dynamics. V. Circumventing the Babuška-Brezzi condition: A stable Petrov-Galerkin formulation of the Stokes problem accommodating equal-order interpolations, Comput. Methods Appl. Mech. Engrg., 59 (1986), pp. 85–99, https://doi.org/10. 1016/0045-7825(86)90025-3. (Cited on p. 497)
- [43] E. W. JENKINS, V. JOHN, A. LINKE, AND L. G. REBHOLZ, On the parameter choice in graddiv stabilization for the Stokes equations, Adv. Comput. Math., 40 (2014), pp. 491–516, https://doi.org/10.1007/s10444-013-9316-1. (Cited on pp. 524, 529, 530)
- [44] V. JOHN AND A. KINDL, Numerical studies of finite element variational multiscale methods for turbulent flow simulations, Comput. Methods Appl. Mech. Engrg., 199 (2010), pp. 841–852, https://doi.org/10.1016/j.cma.2009.01.010. (Cited on p. 524)
- [45] G. Kanschat and N. Sharma, Divergence-conforming discontinuous Galerkin methods and C⁰ interior penalty methods, SIAM J. Numer. Anal., 52 (2014), pp. 1822–1842, https: //doi.org/10.1137/120902975. (Cited on p. 516)
- [46] M.-J. LAI AND L. L. SCHUMAKER, Spline Functions on Triangulations, Encyclopedia Math. Appl. 110, Cambridge University Press, Cambridge, 2007, https://doi.org/10.1017/ CBO9780511721588. (Cited on p. 516)

- [47] W. LAYTON, Introduction to the numerical analysis of incompressible viscous flows, Comput. Sci. Engrg. 6, SIAM, Philadelphia, 2008, https://doi.org/10.1137/1.9780898718904. (Cited on p. 523)
- [48] W. LAYTON, C. C. MANICA, M. NEDA, M. OLSHANSKII, AND L. G. REBHOLZ, On the accuracy of the rotation form in simulations of the Navier-Stokes equations, J. Comput. Phys., 228 (2009), pp. 3433–3447, https://doi.org/10.1016/j.jcp.2009.01.027. (Cited on p. 524)
- [49] P. L. LEDERER, A. LINKE, C. MERDON, AND S. SCHÖBERL, Divergence-free reconstruction operators for pressure-robust Stokes discretizations with continuous pressure finite elements, SIAM J. Numer. Anal., 55 (2017), pp. 1291–1314, https://doi.org/10.1137/16M1089964. (Cited on pp. 521, 527)
- [50] A. LINKE, A divergence-free velocity reconstruction for incompressible flows, C. R. Math. Acad. Sci. Paris, 350 (2012), pp. 837–840, https://doi.org/10.1016/j.crma.2012.10.010. (Cited on p. 524)
- [51] A. LINKE, On the role of the Helmholtz decomposition in mixed methods for incompressible flows and a new variational crime, Comput. Methods Appl. Mech. Engrg., 268 (2014), pp. 782–800, https://doi.org/10.1016/j.cma.2013.10.011. (Cited on pp. 495, 496, 524, 527, 528, 540)
- [52] A. LINKE, G. MATTHIES, AND L. TOBISKA, Robust arbitrary order mixed finite element methods for the incompressible Stokes equations with pressure independent velocity errors, ESAIM Math. Model. Numer. Anal., 50 (2016), pp. 289–309, https://doi.org/10.1051/m2an/2015044. (Cited on pp. 524, 527)
- [53] A. LINKE AND C. MERDON, On velocity errors due to irrotational forces in the Navier-Stokes momentum balance, J. Comput. Phys., 313 (2016), pp. 654-661, https://doi.org/10.1016/ j.jcp.2016.02.070. (Cited on p. 527)
- [54] A. LINKE AND C. MERDON, Pressure-robustness and discrete Helmholtz projectors in mixed finite element methods for the incompressible Navier-Stokes equations, Comput. Methods Appl. Mech. Engrg., 311 (2016), pp. 304-326. (Cited on pp. 533, 536)
- [55] A. LINKE, C. MERDON, AND W. WOLLNER, Optimal L² velocity error estimate for a modified pressure-robust Crouzeix-Raviart Stokes element, IMA J. Numer. Anal., 37 (2017), pp. 354-374, https://doi.org/10.1093/imanum/drw019. (Cited on p. 507)
- [56] A. LINKE, M. NEILAN, L. REBHOLZ, AND N. WILSON, A connection between coupled and penalty protection timestepping schemes with FE spatial discretization for the Navier-Stokes equations, J. Numer. Math., to appear. (Cited on p. 522)
- [57] C. C. MANICA, M. NEDA, M. OLSHANSKII, AND L. G. REBHOLZ, Enabling numerical accuracy of Navier-Stokes-α through deconvolution and enhanced stability, ESAIM Math. Model. Numer. Anal., 45 (2011), pp. 277–307, https://doi.org/10.1051/m2an/2010042. (Cited on p. 524)
- [58] K. A. MARDAL, X.-C. TAI, AND R. WINTHER, A robust finite element method for Darcy-Stokes flow, SIAM J. Numer. Anal., 40 (2002), pp. 1605–1631, https://doi.org/10.1137/ S0036142901383910. (Cited on pp. 513, 516, 520)
- [59] P. Monk, Finite Element Methods for Maxwell's Equations, Numerical Mathematics and Scientific Computation, Oxford University Press, New York, 2003, https://doi.org/10.1093/acprof:oso/9780198508885.001.0001. (Cited on pp. 512, 513)
- [60] J. MORGAN AND R. SCOTT, A nodal basis for C^1 piecewise polynomials of degree $n \geq 5$, Math. Comp., 29 (1975), pp. 736–740. (Cited on p. 514)
- [61] J.-C. Nédélec, Mixed finite elements in R³, Numer. Math., 35 (1980), pp. 315–341, https://doi.org/10.1007/BF01396415. (Cited on p. 517)
- [62] M. NEILAN, Discrete and conforming smooth de Rham complexes in three dimensions, Math. Comp., 84 (2015), pp. 2059–2081, https://doi.org/10.1090/S0025-5718-2015-02958-5. (Cited on pp. 515, 516)
- [63] M. Neilan and D. Sap, Stokes elements on cubic meshes yielding divergence-free approximations, Calcolo, 53 (2015), pp. 263–283, https://doi.org/10.1007/s10092-015-0148-x. (Cited on p. 515)
- [64] M. A. Olshanskii, A low order Galerkin finite element method for the Navier-Stokes equations of steady incompressible flow: A stabilization issue and iterative methods, Comput. Methods Appl. Mech. Engrg., 191 (2002), pp. 5515–5536, https://doi.org/10.1016/S0045-7825(02)00513-3. (Cited on p. 524)
- [65] M. A. OLSHANSKII, G. LUBE, T. HEISTER, AND J. LÖWE, Grad-div stabilization and subgrid pressure models for the incompressible Navier-Stokes equations, Comput. Methods Appl. Mech. Engrg., 198 (2009), pp. 3975–3988, https://doi.org/10.1016/j.cma.2009.09.005. (Cited on pp. 524, 529)

- [66] M. A. OLSHANSKII AND A. REUSKEN, Grad-div stabilization for Stokes equations, Math. Comp., 73 (2004), pp. 1699–1718, https://doi.org/10.1090/S0025-5718-03-01629-6. (Cited on p. 524)
- [67] J. Pedlosky, Geophysical Fluid Dynamics, Springer, New York, 1986. (Cited on p. 496)
- [68] J. Qin, On the Convergence of Some Low Order Mixed Finite Elements for Incompressible Fluids, Ph.D. thesis, Department of Mathematics, Pennsylvania State University, 1994. (Cited on pp. 524, 531)
- [69] P.-A. RAVIART AND J. M. THOMAS, A mixed finite element method for 2nd order elliptic problems, in Mathematical Aspects of Finite Element Methods (Proc. Conf., Consiglio Naz. delle Ricerche (C.N.R.), Rome, 1975), Lecture Notes in Math. 606, Springer, Berlin, 1977, pp. 292–315. (Cited on pp. 513, 517)
- [70] H.-G. ROOS, M. STYNES, AND L. TOBISKA, Robust Numerical Methods for Singularly Perturbed Differential Equations: Convection-Diffusion-Reaction and Flow Problems, 2nd ed., Springer Ser. Comput. Math. 24, Springer-Verlag, Berlin, 2008. (Cited on p. 539)
- [71] L. R. Scott and M. Vogelius, Conforming finite element methods for incompressible and nearly incompressible continua, in Large-Scale Computations in Fluid Mechanics, Part 2 (La Jolla, CA, 1983), Lectures in Appl. Math. 22, AMS, Providence, RI, 1985, pp. 221–244. (Cited on pp. 514, 531)
- [72] L. R. SCOTT AND M. VOGELIUS, Norm estimates for a maximal right inverse of the divergence operator in spaces of piecewise polynomials, RAIRO Modél. Math. Anal. Numér., 19 (1985), pp. 111–143. (Cited on p. 514)
- [73] X.-C. TAI AND R. WINTHER, A discrete de Rham complex with enhanced smoothness, Calcolo, 43 (2006), pp. 287–306, https://doi.org/10.1007/s10092-006-0124-6. (Cited on pp. 515, 516, 520)
- [74] L. Tobiska and R. Verfürth, Analysis of a streamline diffusion finite element method for the Stokes and Navier-Stokes equations, SIAM J. Numer. Anal., 33 (1996), pp. 107–127, https://doi.org/10.1137/0733007. (Cited on p. 524)
- [75] M. VOGELIUS, A right-inverse for the divergence operator in spaces of piecewise polynomials. Application to the p-version of the finite element method, Numer. Math., 41 (1983), pp. 19–37, https://doi.org/10.1007/BF01396303. (Cited on p. 498)
- [76] J. WANG, Y. WANG, AND X. YE, A robust numerical method for Stokes equations based on divergence-free H(div) finite element methods, SIAM J. Sci. Comput., 31 (2009), pp. 2784– 2802, https://doi.org/10.1137/080730044. (Cited on pp. 516, 517)
- [77] J. WANG AND X. YE, New finite element methods in computational fluid dynamics by H(div) elements, SIAM J. Numer. Anal., 45 (2007), pp. 1269–1286, https://doi.org/10.1137/060649227. (Cited on pp. 516, 517, 519)
- [78] M. WOHLMUTH AND M. DOBROWOLSKI, Numerical analysis of Stokes equations with improved LBB dependency, Electron. Trans. Numer. Anal., 32 (2008), pp. 173–189. (Cited on p. 507)
- [79] X. XIE, J. XU, AND G. XUE, Uniformly-stable finite element methods for Darcy-Stokes-Brinkman models, J. Comput. Math., 26 (2008), pp. 437–455. (Cited on pp. 516, 520)
- [80] S. ZHANG, A new family of stable mixed finite elements for the 3D Stokes equations, Math. Comp., 74 (2005), pp. 543–554, https://doi.org/10.1090/S0025-5718-04-01711-9. (Cited on pp. 498, 516, 524)
- [81] S. Zhang, A family of $Q_{k+1,k} \times Q_{k,k+1}$ divergence-free finite elements on rectangular grids, SIAM J. Numer. Anal., 47 (2009), pp. 2090–2107, https://doi.org/10.1137/080728949. (Cited on p. 516)
- [82] S. Zhang, Quadratic divergence-free finite elements on Powell-Sabin tetrahedral grids, Calcolo, 48 (2011), pp. 211–244, https://doi.org/10.1007/s10092-010-0035-4. (Cited on p. 516)